Fiber Reinforcement in Concrete Pavements

SPR-807
November 2026





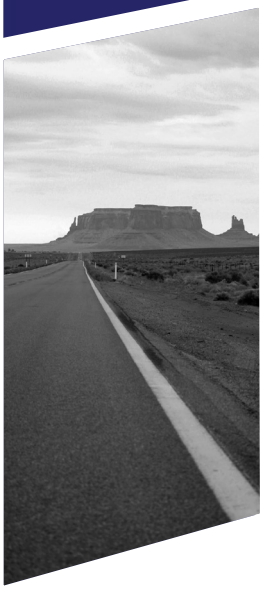

18-386

ARIZONA DEPARTMENT OF TRANSPORTATION
Arizona Department of Transportation Research Center

ARIZONA DEPARTMENT OF TRANSPORTATION

Fiber Reinforcement in Concrete Pavements

SPR-807

November 2026

Published by:
Arizona Department of Transportation
206 South 17th Avenue
Phoenix, Arizona 85007
In cooperation with
U.S. Department of Transportation
Federal Highway Administration

Disclaimer

This study was funded in part by the Federal Highway Administration, U.S. Department of Transportation. This document is disseminated under the sponsorship of the Arizona Department of Transportation and the United States Department of Transportation in the interest of information exchange. The opinions, conclusions expressed or implied, and contents of this document reflect the views of the authors, who are responsible for the facts and the accuracy of the data, and for the use or adaptation of previously published material, presented herein.

The contents do not necessarily reflect the official views or policies of the Arizona Department of Transportation or the Federal Highway Administration, U.S. Department of Transportation. The State of Arizona and the United States Government assume no liability of its contents or use thereof.

This document does not constitute a standard, specification, or regulation, nor is it intended for construction, bidding, or permit purposes. Trade or manufacturers' names that may appear herein are cited only because they are considered essential to the objectives of the report. The U.S. government and the State of Arizona do not endorse products or manufacturers.

This report is subject to the provisions of 23 USC § 407. Any intentional or inadvertent release of this material, or any data derived from its use, does not constitute a waiver of privilege pursuant to 23 USC § 407, which reads as follows:

> **23 USC § 407 — Discovery and admission as evidence of certain reports and surveys**
> Notwithstanding any other provision of law, reports, surveys, schedules, lists, or data compiled or collected for the purpose of identifying, evaluating, or planning the safety enhancement of potential accident sites, hazardous roadway conditions, or railway-highway crossings, pursuant to sections 130, 144, and 148 of this title or for the purpose of developing any highway safety construction improvement project which may be implemented utilizing Federal-aid highway funds shall not be subject to discovery or admitted into evidence in a Federal or State court proceeding or considered for other purposes in any action for damages arising from any occurrence at a location mentioned or addressed in such reports, surveys, schedules, lists, or data.

This study was conducted in accordance with Title VI of the Civil Rights Act of 1964 (78 Stat. 252.42 U.S.C. §2000d-4), Americans with Disabilities Act of 1990, and other nondiscrimination laws and authorities.

© 2026 Arizona Transportation Institute and the Arizona Department of Transportation. All rights reserved.

Technical Report Documentation Page

1. Report No. SPR-807	2. Government Accession No. none	3. Recipient's Catalog No. none
4. Title and Subtitle Fiber Reinforcement in Concrete Pavements		5. Report Date 2026 6. Performing Organization Code none
7. Authors Barzin Mobasher, ORCID: 0000-0002-7580-2855		8. Performing Organization Report No. none
9. Performing Organization Name and Address Arizona State University 300 E Lemon St Tempe, AZ, USA		10. Work Unit No. none 11. Contract or Grant No.
12. Sponsoring Agency Name and Address Arizona Department of Transportation 206 S. 17th Avenue Phoenix, AZ 85007		13. Type of Report & Period Covered Final Report 14. Sponsoring Agency Code none
15. Supplementary Notes Prepared in cooperation with the U.S. Department of Transportation, Federal Highway Administration		
16. Abstract This research identified the major gaps in the analysis and design of FRC pavements and gathered various structural-mechanics methods and solutions to various FRC-based concrete application that include: fatigue, tension stiffening, shrinkage cracking, multiple parallel cracking distribution, toughening of hybrid systems by fibers, development of tensile stress distribution across the thickness of a slab, and the moment-curvature response of a section, limit analysis of plates, as well as the load-deflection response of a slab.		
17. Key Words fiber-reinforced concrete, hybrid reinforced concrete, concrete overlays, jointed plain concrete pavement, jointed reinforced concrete pavement, nonlinear fracture mechanics, shrinkage-reducing admixtures	18. Distribution Statement Document is available to the U.S. public through the National Technical Information Service, Springfield, Virginia 22161	23. Registrant's Seal

19. Security Classification Unclassified	20. Security Classification Unclassified	21. No. of Pages 139	22. Price none

Table of Contents

Fiber Reinforcement in Concrete Pavements 2
Executive Summary 1
Introduction 3
Background 3
Project Objectives 5
Task 1: Literature Review and Roadmap 5
Task 2: Recommendations 5
Implementing FRC 6
The Serviceability of Rigid Pavements 8
Structural Applications of FRC by Utilization of Residual Tensile Strength 9
Distress Mechanisms in Concrete Pavements 12
Time-Dependent Loading 12
Stress Development Due to Volumetric Thermal and Moisture Changes 13
Plastic Shrinkage Cracking at the Pavement Surfaces 13
Fatigue Performance of FRC 14
The Nature of Repeated Load on Pavements 15
Adoptions and Gaps in FRC Applications 17
Conventional Concrete Pavement 21
Design Approaches 21
ADOT Specifications for Rigid Concrete Pavements (Based on AASHTO Empirical Method 1993) 21
AASHTO ME Rigid Pavement Approach (Software Based) 24
Fundamental Aspects of Pavement Design 26
Westergaard Approach 26
Meyerhof Approach (TR34 and ACI 360) 26
Consequences of Failure Due to Presence of Joints 29
Proposed Method of Approach 30
Case A: Plain FRC 31
Case B: Continuous Reinforced + Fibers (Hybrid RC) 32
Case C: RCC with Fibers 33
Minor Options 34

Summary of Key Aspects of FRC Pavements 35
Fiber Dosage and Structural Efficiency *35*
Curing Requirements *35*
Aggregate and Material Quality *35*
Supplementary Cementitious Materials and Cement Reduction *36*
Placement and Compaction *36*
Structural Role of Fibers *36*
Jointing Strategy *37*
Edge Support and Confinement *37*
Summary of Key Aspects of Mix Design 38
Recommended Practices for FRC Pavements *38*
Equivalent System Analysis of Plain, Fiber-Reinforced, and Hybrid Concrete in JPCP *39*
Reinforcing Steel Content in CRCP and the Role of Fibers *41*
Equivalent System Analysis of CRCP With and Without Fibers *43*
Field Checklist: FRC Pavement (ADOT) *46*
Conclusion 47
APPENDIX A: Pavement Distress as Associated with Joints 48
APPENDIX B: Field Data of Distress Mechanism in Concrete Pavements 53
Stress Developed by Shrinkage and Creep *53*
Evaluation of Plastic Shrinkage *53*
Characterization of Thermal Loading *56*
Characterization of Traffic Loading *59*
Limitations of Current Design Approaches on Dynamic Load *61*
APPENDIX C: The Performance of PP and Steel Fiber Reinforcement 62
Summary of Flexural Test Results for Polypropylene (PP) and Steel FRC in Accordance with ASTM C1609 ..... *65*
APPENDIX D: Review of Several DOT Specifications for FRC Applications 68
Applications of FRC-Based Design in Pavements by Several States *68*
APPENDIX E: Conventional Concrete Pavement Design Approaches 75
Sensitivity Analysis of ADOT Specifications for Rigid Concrete Pavements *75*
Westergaard Approach *83*
Meyerhof Approach (TR34 and ACI 360) *85*
Moment Capacity Calculation as Per British Standards TR34 ..... *87*

ACI 360 Concrete Slabs on Ground *89*
ACPA, AASHTO Approaches for Incorporating FRC in Pavements *90*
Design Procedures Using Residual Strength and Moment Capacity of FRC *92*
Software Link and User Guide *99*
APPENDIX F: The Comparison of Full-Scale Testing Results on Conventional RC and Plain Fiber Reinforced Concrete Labs 101
Load-Deflection Response of RC vs. Hybrid RC *102*
Crack Pattern at The End of The Test *104*
APPENDIX G: Specifications for Addressing Temperature and Shrinkage Requirements of FRC for Slab 109
Listing of All of the ACI Guidelines and Tools Available *110*
APPENDIX H: ASTM C1609 Testing Method and Equipment 116
Insights to Consider for ASTM C1609: Flexural Testing *117*
APPENDIX I: Tension Stiffening Model for Joint Spacing Design 121
Fiber Bridging Effect *121*
Tension-Stiffening Modeling of Cement Composite *122*
References 125

List of Figures

Figure 1. Schematic Illustration of Faulting. 3
Figure 2. MOR Stress of Plain Concrete vs. Post-Cracking Performance of FRC. 10
Figure 3. Age-Dependent Strain Changes in Concrete [25]. 12
Figure 4. Effect of Fiber Addition on Shrinkage Cracks: 14
Figure 5. Fatigue Testing of FRC and Material Characterization. 14
Figure 6. The Deformation Shape of the Slab at Different Temperature Gradients Over a Day. 15
Figure 7. Static Weight vs. Moving Loading Response. 16
Figure 8. Most Sensitivity Design Parameters for MOR. 22
Figure 9. Most Sensitivity Design Parameters for Drainage Coefficient. 23
Figure 10. Pavement Section, per ADOT [36]. 23
Figure 11. Rigid Pavement Design Strategies that Can Be Simulated with AASHTOWare Pavement ME Design [9]. 24
Figure 12. Westergaard Model of a Rigid Pavement Slab. 26
Figure 13. Cross Section of FRC. 31
Figure 14. Cross Section of FRC with Rebar Reinforcement. 32
Figure 15. Cross Section of FRC Above RCC. 33
Figure 16. Cross-Section Comparisons of Plain Concrete vs. FRC vs. Hybrid RC. 39
Figure 17. Moment and Curvature for JPCP. 40
Figure 18. Secant Flexural Stiffness and Curvature for JPCP. 41
Figure 19. Cross-Section Comparison of TxDOT's Hybrid RC vs. Proposed Method for ADOT's Use. 44
Figure 20. Moment and Curvature for CRCP. 45
Figure 21. Secant Flexural Stiffness and Curvature for CRCP. 45
Figure 22. Restrained Shrinkage-Induced Stresses in Concrete. 53
Figure 23. Humidity Profile Throughout the Thickness of the Concrete Slab Simulated by Fick's Law of Diffusion and Idealized Average Free-Shrinkage Strain Applied to the Tension-stiffening Model. 54
Figure 24. Initial Condition. 54
Figure 25. Shrinkage Effect. 54
Figure 26. Cracking Sequence. 55
Figure 27. Conceptual Stress Distribution in Concrete. 55
Figure 28. Conceptual Stress Distribution in Rebar. 55
Figure 29. Finite Element Analysis of Concrete Pavement Subjected to Thermal Loading from Ambient Air Temperature [49]. 56

Figure 30. Finite Element Analysis of Concrete Pavement Subjected to Thermal Loading from Solar Radiation [49]. 57
Figure 31. Factors Affecting Heat Transfer in Pavement Structures. 58
Figure 32. Temperature Calibration of the Thermal Model Against Experimental Data for the Characteristic Summer Cycle at Three Height Levels (Top, Center, Bottom) on the Slab [49,50]. 58
Figure 33. Concrete Strain Variation. 59
Figure 34. Concrete Strain Variation After Total Curing Period [51]. 59
Figure 35. Tensile Stress Influence Line in JPCP [52]. 60
Figure 36. Base Deflection Influence Line in JRCP Due to TADT [52]. 61
Figure 37. Comparison of Peak Flexural Strength Between Polypropylene (PP) and Steel FRC Tested Under ASTM C1609. 63
Figure 38. Comparison of Residual Strength Ratio (Re3) Between Polypropylene (PP) and Steel FRC Tested Under ASTM C1609. 63
Figure 39. Comparison of Toughness at L/150 Between Polypropylene (PP) and Steel FRC Tested Under ASTM C1609. 64
Figure 40. Comparison of Equivalent Flexural Strength (F_{e3}) Between Polypropylene (PP) and Steel FRC Tested Under ASTM C1609. 64
Figure 41. Plate on Elastic Foundation. 83
Figure 42. Westergaard's Case: Internal, Edge and Corner Loading [37]. 84
Figure 43. Slab on Foundation Cases with M_p and M_n [59]. 85
Figure 44. Difference Between M_c (left) and M_s (right) [59]. 87
Figure 45. Typical Graph of Test Load Flexural Stress vs. CMOD. 88
Figure 46. ASTM C1609 Test Response with Stress Distributions. 91
Figure 47. Quad-Linear Tension Model for High Dosage FRC (left) and the Simulated Responses (right) Using the Tension Model [70]. 93
Figure 48. Available Data of EN14651 for FRC Characterization. 94
Figure 49. Load vs. Deflection with Inverse Analysis Fit of Simulation. 94
Figure 50. Stress Distribution Measured Using Inverse Analysis of the EN14651 Data at Strain Value of 0.017 at the Beam Bottom. 95
Figure 51. Extracted Tension Model from Inverse Analysis. 95
Figure 52. Extracted Compression Model from Inverse Analysis. 96
Figure 53. Cross Section of the Designed Slab Section of 210 mm (per unit length). 96
Figure 54. Full Moment-Curvature Relation from ACI 544.8R Approach. 97
Figure 55. Beam Cross-Section of Hybrid Reinforcement. 98
Figure 56. Hybrid Case Using ACI 544.8R Approach. 98

Figure 57. Title Page of the “HRC Designer Software User Guide.” 99
Figure 58. Hybrid Beam Designer..... 100
Figure 59. Testing Configuration. 101
Figure 60. Load-Deflection Response RC and Hybrid RC Panels Effect of Fiber in SLS at 0.5 in..... 103
Figure 61. Effect of Fiber at Ultimate Limit State (ULS)..... 104
Figure 62. Bottom Crack. 104
Figure 63. Bottom Crack. 105
Figure 64. Top Crack. 105
Figure 65. Schematic of a Slab Subjected to a Point Load Exhibiting Fan Pattern Cracking. 106
Figure 66. The Simulation of Load-Deflection Response..... 108
Figure 67. Title Page for ACI Spec 544.12-23. 109
Figure 68. Report on Design and Construction of Fiber-Reinforced Precast Concrete Tunnel Segments. 111
Figure 69. Report on Design and Construction of Steel Fiber-Reinforced Concrete Elevated Slabs..... 112
Figure 70. Report on Measuring Mechanical Properties of Hardened Fiber-Reinforced Concrete. 113
Figure 71. Report on Indirect Method to Obtain Stress-Strain Response of Fiber-Reinforced Concrete (FRC). 114
Figure 72. Fiber Effect on Reducing the Permeability of Cracked Concrete Structures. 115
Figure 73. An Available Testing System for Closed-Loop Testing of FRC Developed by GCTS, Tempe, AZ. 116
Figure 74. ASTM C1609 Test Setup for Four-Point Bending Test. 117
Figure 75. Scatter Plot of All Data with Mean Curve and Box-and-Whisker Plot of Flexural Response of Individual Data for 28-day Specimens [73]. 118
Figure 76. Coefficient Determination Between Residual and First Crack Flexural Strength Parameters [74]. 119
Figure 77. Analysis for Back-Calculated Stress Ratio [74]..... 120
Figure 78. Typical Example of Conventional RC. 121
Figure 79. Typical Examples of Hybrid RC. 122
Figure 80. Mechanical Behavior of a Cracked Fabric Reinforced Cement Composite: (a) Matrix Strength for Cracking Criterion, (b) Bond-Slip Model, (c) Longitudinal Yarn Stress-Strain Model, (d) Nonlinear Spring Model Simulating Anchorage Strength at Cross Yarn Junction [48]. 123
Figure 81. (a) Cracking Mechanisms Including Matrix Cracking, Fiber Bridging in Terms of Stress-Crack Width Relation, Interface Bonding Stress-Slip Model and Tensile Stress-Strain Relationship of Longitudinal Reinforcement; (b) Stress Distribution in Matrix at Cracked State. 124

List of Tables

Table 1. Design Specifications by Other DOTs..... 19
Table 2. Summary Table for AASHTOWare Pavement ME Design: Key Features and Limitations. 25
Table 3. Summary of Reinforcements' Constructability..... 43
Table 4. Characteristics of Polypropylene Fiber..... 65
Table 5. Characteristics of Steel Fiber..... 67
Table 6. Required Hardened FRC Properties..... 74
Table 7. The Load Performance of Conventional RC and Hybrid RC Panels. 103
Table 8. Material Parameters of Conventional RC and Hybrid RC Panels. 107
Table 9. Tension Parameters of Conventional RC and Hybrid RC Panels. 107
Table 10. Compression Parameters of Conventional RC and Hybrid RC Panels. 108
Table 11. The Ultimate Load Capacities..... 108
Table 12. ACI 544-12R "Equivalent Flexural Residual Strength for Temperature and Shrinkage Reinforcement Based on ACI 544.4R."..... 110
Table 13. Testing Procedure Used in the MTS Station Manager to Control the Test (C1609)..... 118

Acronyms, Abbreviations, and Symbols

AADT	average annual daily traffic
AASHTO	American Association of State Highway and Transportation Officials
ACI	American Concrete Institute
ACPA	American Concrete Pavement Association
ADOT	Arizona Department of Transportation
ALDOT	Alabama Department of Transportation
ASTM	American Society for Testing and Materials
ASU	Arizona State University
BCOA	bonded concrete overlay of asphalt
CMOD	crack mouth opening displacement
COA	concrete overlays, typically four to six inches thick, mainly concrete-on-asphalt
COC	concrete-on-concrete
CRCP	continuously reinforced concrete pavement
CTE	coefficient of thermal expansion
DD	directional distribution
DL	lane distribution
DOT	department of transportation
ESAL	equivalent single axle loads
FHWA	Federal Highway Administration
FRC	fiber-reinforced concrete
GM	global maximum
HMA	hot mix asphalt
HRC	hybrid reinforced concrete
HRWR	high-range water reducers
HRWRA	high-range water-reducing admixtures
IDOT	Illinois Department of Transportation
IHRB	Iowa Highway Research Board
JPCP	jointed plain concrete pavement
JRCP	jointed reinforced concrete pavement

LTD	longitudinal, transverse, and diagonal
LTE	load-transfer efficiency
LVDT	linear variable differential transformer
ME	mechanistic-empirical
MEPDG	Mechanistic-Empirical Pavement Design Guide
MoDOT	Missouri Department of Transportation
MOE	modulus of elasticity
MOR	modulus of rupture
MR	resilient modulus
NCHRP	National Cooperative Highway Research Program
NLFM	nonlinear fracture mechanics
NTIS	National Technical Information Service
PCC	portland cement concrete
PE	polyethylene
PP	polypropylene
PVA	polyvinyl alcohol
QPL	Qualified Product List
RC	reinforced concrete
RCC	roller-compacted concrete
SCM	supplementary cementitious materials
SFRC	steel fiber reinforced concrete
SI	International System
SLS	serviceability limit state
SRA	shrinkage-reducing admixtures
TADT	tandem axle dual tire
TTCC	Technology Transfer Concrete Consortium
TxDOT	Texas Department of Transportation
ULS	ultimate limit state
UTW	ultra-thin whitetopping

Executive Summary

Concrete pavements are subject to various types of distress that affect their performance, cost, and service life. Identifying the sources of distress and understanding the sequence of events leading to failure are crucial for effective pavement management and design. The primary category of distress in pavements is cracking, which is also associated with the interaction of the joints in the pavements. This report addresses several forms of pavement distress, primarily those associated with construction and the design of jointed concrete pavements.

Joints may be intentionally placed in concrete to control the location of shrinkage, but cracks may cause their failure. Further, failure in a two-way slab is often due to various mechanisms of settlement, corner stresses, and/or water penetration through the joint, compromising the functionality of the subgrade. The brittleness of concrete allows for distress failures—such as faulting, cracking, spalling, and punchouts—to take place. Fiber-reinforced concrete (FRC) has been widely used as a structural reinforcement strategy to address the brittleness challenges found in various concrete applications, including slabs, shotcrete, jointed concrete pavements, and thin-bonded overlays.

The problem with widespread adoption of FRC is the necessary identification of the gaps in the knowledge of applying fiber concrete to pavements, which must happen prior to widespread FRC utilization. This project capitalizes on the enhanced residual strength provided by fibers as the primary reinforcement design component for advancing pavement design. Therefore, the goal is not to have a very high cement content; rather, the design is adjusted to provide concrete with the successful post-cracking ductility needed to handle permanent cyclic and environmental loads. Depending on the fiber type, dosage, shape, and length, the use of FRC is generally effective in reducing plastic shrinkage cracking and increasing strain capacity and toughness. However, current rigid pavement design methods are based on mechanistic-empirical (ME) principles that consider fatigue and thermal cracking as failure modes, but do not rely on separating the mechanisms of the crack-growth resistance of fibers used with the intent of reducing fatigue/prolonging life or that make the concrete more ductile. The modulus of rupture (MOR) is used as the most important metric in rigid pavement design, with the implicit assumption that the concrete may remain uncracked due to a high strength value. The residual tensile capacity that occurs after the cracking can enhance crack tolerance and increase the service life of the pavement by controlling how the cracking is distributed.

This research identified the major gaps in the analysis and design of FRC pavements and gathered various structural-mechanics methods and solutions to various FRC-based concrete application that include: fatigue, tension stiffening, shrinkage cracking, multiple parallel cracking distribution, toughening of hybrid systems by fibers, development of tensile stress distribution across the thickness of a slab, and the moment-curvature response of a section, limit analysis of plates, as well as the load-deflection response of a slab.

The objective is to increase the residual post-cracking strength sufficiently so that it becomes the primary reinforcement method. This approach has not been proposed before. Based on the combination of the analysis of the tools listed above (which are standard structural engineering tools), computational

work will propose solutions that adjust the geometry with fiber content, modes of loading (thermal, fatigue, traffic, support loss, etc.). Using a load- and resistance factor design approach, the resistance offered by the structure should be adjusted to withstand the sources of residual or applied loads from various potential modes of failure.

Suggestions include three areas with the highest chance of success:

- Increasing the fiber content throughout the volume of slab so that the effective thickness can be reduced by 15–20 percent compared to the methods practiced today.
- Using a multilayer concrete section with a roller-compacted porous concrete layer topped with a FRC layer.
- Use of fibers as a partial rebar substitution in the continuously reinforced concrete pavement (CRCP) application since the synergy of interaction between the rebar macro reinforcement and fibers enhances the performance.

The proposed method recognizes that Arizona's extreme climate demands solutions beyond traditional pavement construction. FRC is introduced to redistribute stresses after cracking, improve toughness, and extend service life. The approach emphasizes performance-based testing using ASTM C1609 residual strength parameters (f_{150}, f_{300}, f_{600}) and optimized fiber dosage, with steel or macro-polymeric fibers enhancing post-cracking strength and shrinkage resistance. Special attention is given to shrinkage, creep, and joint spacing, where fibers help control crack widths and reduce maintenance needs.

Three application cases are identified have cost savings from different sources: plain FRC, which can replace conventional reinforcement, or saw cutting joints in remote locations; hybrid CRCP (rebar + fibers), balances reinforcement ratios with fiber content to improve ductility, increase joint spacing, and load capacity while reducing the cost compared to conventional concrete; and two-layer roller-compacted concrete (RCC) with fibers, enabling rapid, large-scale construction with added crack resistance placed at the top of the slab to reduce the cost. Together, these strategies provide a framework for integrating FRC into ADOT pavement specifications, ensuring more durable and cost-effective infrastructure.

Introduction

Background

Concrete pavements are adopted for highways because of their potential for increased ride quality, minimal maintenance, and extended service life [1]. However, concrete pavements, including CRCP, undergo forms of distress such as faulting, cracking, spalling, punchouts, etc., that lead to early repairs and even full failure. These failures can result from factors including under-design, incorrect material characterization, poor construction materials, or behavior such as excessive settlement of base supports, loss of foundation and edge support, excessive crack width, high cyclic thermal strains during and after construction, etc. [1].

The ME design approach is a prominent method for designing new pavements and rehabilitating existing ones. It combines principles of mechanics and physics to calculate pavement responses such as stresses, strains, and deflections under given loads and environmental conditions [9, 10]. These calculated responses are then used in conjunction with empirical transfer functions or performance models, which are calibrated based on field performance data, to predict pavement distress and performance over time [11]. Common predicted distresses include fatigue cracking and faulting. Under repeated traffic loading, tensile stresses develop at the bottom of the concrete slab. Even when these stresses are lower than the flexural strength of the concrete, the cumulative effect of millions of load repetitions can lead to progressive microcracking and eventual fatigue cracking. Figure 1 shows the formation of surface from slab curling and faulting as described in [12] and its combined effect with fatigue loading.

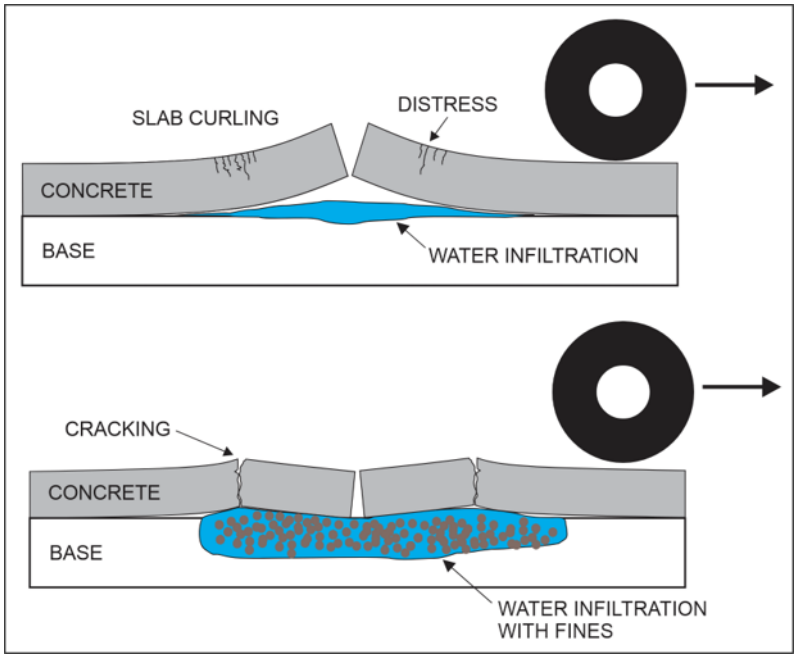

Figure 1. Schematic Illustration of Faulting.

The ME design method provides a rational framework, but it is constrained by the assumptions tied to conventional concrete and base conditions. It does not fully capture localized failures or evolving damage under variable support. Moreover, the framework offers little flexibility for incorporating novel materials such as FRC.

Reinforcement with short, discrete fibers has the potential to address some of these challenges and improve concrete pavement performance [2,3]. FRC has been widely used in various concrete applications, including slabs, shotcrete, jointed concrete pavements, and thin-bonded overlays [4–6]. FRC is understood to be effective in reducing plastic shrinkage cracking [7] and increasing toughness [8]. Depending on the fiber type, dosage, shape, and length, additional benefits may also be obtained.

Project Objectives

The mechanisms of distress and failure in concrete pavements are complex, primarily due to undefined boundary conditions at the slab–base interface and the combined effects of environmental exposure and repeated traffic loading. These interactions often lead to damage mechanisms that are not fully accounted for in traditional design approaches. This report first outlines the current methodologies used in the design of concrete pavements, then examines critical distress behaviors that are often neglected or insufficiently addressed. It proceeds to list the underlying mechanics of failure based on first principles and concludes by proposing a framework for incorporating discrete fibers into the design. This integration aims to improve the ability of pavement to resist both internal cracking and surface deterioration.

To achieve these objectives, this project is divided into two primary tasks, each with its own corresponding subtasks:

Task 1: Literature Review and Roadmap

Establish the state of the practice and identify knowledge gaps. This involves compiling internal knowledge and developing a roadmap (Section 2), conducting a comprehensive literature review (Sections 3–5), and examining FRC applications both within state departments of transportation (DOTs) and in the broader concrete industry (Section 6).

Task 2: Recommendations

Build upon the conclusions of Task 1 by focusing on the implementation of recommended strategies. The first step is to define the material properties of FRC as they relate to specific pavement applications (Section 7), followed by exploring design approaches that ensure serviceability (Section 7). Finally, utilize appropriate test methods and validation procedures to establish design and quality control (Sections

8–9), enabling the practical adoption of FRC in structural applications as a supplementary reinforcement system. The three proposed implementation methods for Arizona Department of Transportation (ADOT) pavement are discussed in Section 10.

Through this approach, the project aims to document the performance benefits of FRC and develop a pathway for its systematic adoption in rigid pavement design. The ultimate objective is to provide ADOT with a decision framework with enhanced post-cracking performance of rigid pavements, a process that is non-existent in the current design standards but which promises to extend pavements' service life while reducing maintenance costs.

Implementing FRC

Concrete pavements are subject to various types of distress that affect their performance and service life. Identifying the sources of distress and understanding the corresponding sequence of events is crucial for effective pavement management and design [13]. The primary categories of distress in pavements are the various types of cracking, which may also be caused by the interaction of joints within the pavements.

Appendix A includes several forms of pavement distress that are mostly associated with the construction and proper design of jointed concrete pavements. The joints that are intentionally placed in concrete reduce the ability of the slab to function as a two-dimensional slab, and quite often the failure is due to various mechanisms of water and other chemicals that penetrate through the joint and alter the functionality of the subgrade. Also, the loss of load-transfer capability, pressure build-up under the section, and creation of a free boundary condition at the joint increase the magnitude of the stresses applied by the external loads, which contribute to the failure mechanisms shown in Appendix A.

Significant knowledge gaps remain regarding the long-term performance of FRC in various pavement types under different climatic and traffic conditions. Optimization of fiber types and dosages for specific applications allows for the development of widely accepted design standards that leverage the costs and benefits of fibers across all pavement types. The full impact of fibers on large-scale construction practices, especially when fibers significantly reduce the use of continuous rebar, can only be measured by observing long-term changes in the cost of materials and labor as well as the costs of repair due to user traffic.

Experimental characterizations of quantitative fracture, bending, thermal, and fatigue response of FRC are important aspects of developing the thickness-based design of ordinary concrete. The interactions among these failure criteria overlap, which then creates gaps in the design process and thus prevents a universal implementation of FRC in pavements. Specific areas of focus might include:

- **Material and Structural Design:** Develop a rational, mechanics-based design method to address the effect of material properties on the flexural, punching shear, thermal expansion, and restrained shrinkage cracking types as a function of fiber dosage, such that the structural contribution of fibers can be utilized.
- **Construction Aspects of Fiber Concrete:** Develop a field casting, finishing, and curing plan for the construction of the concrete pavements in different lifts or layers. Address the additional cost of fibers to the overall mix design.
- **Long-Term Field Performance Monitoring:** There is a need for trial FRC pavement sections to be established and monitored. These sections may be placed to account for Arizona's various climates so that long-term performance data on distress development can be collected (cracking, spalling, faulting, punchouts, etc.) under typical traffic loading.

- **Correlation of Lab and Field Performance:** Develop robust correlations between laboratory-measured FRC properties (toughness, residual strength, early-age tensile strength, creep effect, fatigue performance, and shrinkage cracking reduction) and observed field performance in ADOT applications (CRCP, overlays, slabs-on-grade).
- **Optimization of FRC Mixes for Constructability and Performance:** Conduct studies on the implementation costs of various fiber types (steel, synthetic, hybrid), as well as on their effects (of fiber types and dosages) on the workability, placement, and finishing of concrete mixes used in ADOT's pavement-construction practices, balancing improved hardened properties with cost and constructability requirements.
- **Development of ADOT-Specific FRC Design Guidelines:** Based on the collected long-term performance data and verified lab–field correlations, develop or refine ME design procedures that explicitly incorporate the benefits of FRC for specific ADOT pavement types (e.g., CRCP, ultra-thin whitetopping [UTW]) and conditions. This should include guidance on selecting appropriate fiber types and dosages based on design life, traffic, and desired performance outcomes.
- **Economic Analysis:** Conduct comprehensive life-cycle cost analyses comparing conventional concrete pavements/repairs to FRC alternatives in ADOT-specific contexts, considering initial construction costs, long-term maintenance, and extended service life benefits.

Addressing these research areas may provide ADOT with the necessary data and tools to confidently incorporate fiber reinforcement into their pavement design and construction specifications, leading to more durable, cost-effective, and sustainable transportation infrastructure.

Fiber reinforcement holds significant promise for improving the performance and extending the service life of concrete pavement slabs. While its benefits in terms of cracking control and toughness are well-documented in the lab and utilized in some thin overlay design procedures, focused research is essential to fully understand and quantify its long-term performance benefits, optimize its use across various pavement types, and integrate into standard design practices for agencies like ADOT. The proposed research plan outlines key areas of investigation necessary to bridge the existing knowledge gaps and provide ADOT with the necessary technical basis for implementing FRC effectively in their future infrastructure projects.

The Serviceability of Rigid Pavements

The design of pavement systems is governed by the pavement's ability to meet the design requirements in terms of providing a safe and effective riding surface for the duration of its intended life. Accounting for future and potential maintenance issues is an important aspect of the design process that requires a routine set of standards—based on the characteristics of aged pavement—to measure and quantify appropriate performance metrics. This approach allows for the classification of the two principal categories of pavement failure modes (as described by Yoder and Witczak [14]): structural failure and functional failure.

Structural failure occurs when at least one pavement component deteriorates to the point that the pavement can no longer carry intended loads without excessive distress. Functional failure refers to the loss of serviceability. The pavement may still support traffic structurally, but it no longer provides a safe or comfortable riding surface, often due to excessive roughness, surface defects, or cracking patterns that pose hazards to drivers. Structural failures often lead to functional failures.

Structural failure in pavements is typically a progressive process, developing over time under the combined effects of repeated traffic loading and the time-dependent behavior of concrete. Concrete undergoes changes in its mechanical properties with the duration of service due to creep and shrinkage, both of which induce strains that alter internal stresses and influence crack development. Traffic loading enhances these effects by repeatedly applying stresses over the service life of pavement and is defined as a fatigue process. Therefore, a comprehensive understanding of pavement deterioration must consider both the gradual material property changes and the cumulative impact of external loading.

Structural Applications of FRC by Utilization of Residual Tensile Strength

FRC is utilized to improve certain properties of concrete, particularly its post-cracking behavior, which can help address many of these distresses [15]. Fibers work by bridging cracks that form, providing resistance to crack opening and propagation [16].

Specific benefits of fibers identified in the sources include:

- **Reducing Crack Growth:** Fibers are effective in reducing the growth rate of plastic shrinkage and drying shrinkage cracking, which are types of non-load-related cracking [15]. They also help control and reduce the crack width, which is critical for maintaining load transfer across cracks and joints [17]. Controlling crack width can also reduce the infiltration of water and solutions that contribute to issues like corrosion, alkali-silica reactions, durability cracking, and pumping [17].
- **Increasing Toughness and Residual Strength:** Toughness describes the ability of concrete to dissipate energy by means of frictional fiber pullout to resist fracture after cracking [1]. Fibers significantly improve flexural toughness and provide residual strength, meaning that the concrete continues to carry loads after the first crack forms. This post-cracking load capacity is crucial for the structural performance of FRC pavements, allowing them to deform and carry load even when cracked. Flexural toughness is considered a key parameter for quantifying the benefit of fibers.
- **Improving Fatigue Performance:** Fibers can increase resistance to fatigue loads. By controlling crack propagation and providing residual strength, FRC can withstand more load cycles before reaching a failure state compared to plain concrete [18,19].
- **Addressing Spalling and Punchouts:** By increasing toughness and controlling crack width, fibers can potentially mitigate spalling, which is often related to stresses at joints and cracks. Improved load-transfer efficiency resulting from narrower cracks can also help reduce punchouts in CRCP. Research in Texas specifically investigated the use of fibers to reduce or prevent spalling in CRCP.
- **Enhancing Durability:** The ability to limit crack width and improve post-cracking performance contributes to the overall durability and resilience of the pavement structure by a direct increase in sectional properties such as the moment-curvature response [20].

The basis for design with FRC is summarized in Figure 2. For plain concrete, the flexural behavior is governed by two parameters: elastic modulus, E, and the flexural strength, MOR. Technically, MOR is not a material property for a FRC system that exhibits stable crack growth. With fiber use, the pavement gains a marginal increase in its flexural strength; however, the most important benefit of fibers is in

what happens after the peak load is reached by providing a continuous residual strength curve similar to a yield plateau that covers the tensile zone during the entire loading history and crack-opening process. This tensile stress can be used to obtain the equivalent bending moment capacity. The American Concrete Institute (ACI) 544 documents (Appendix G) provide examples, technical information, and support for these methods.

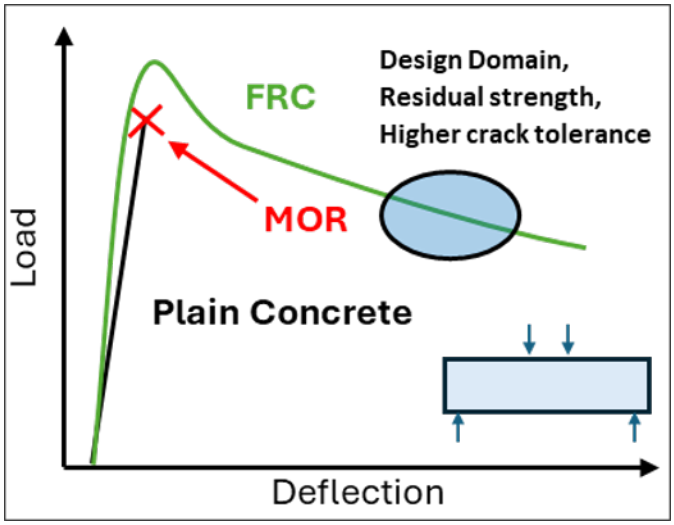

Figure 2. MOR Stress of Plain Concrete vs. Post-Cracking Performance of FRC.

FRC's damage tolerance when undergoing large displacements is also a significant contribution. The MOR in plain concrete is indicative of a brittle failure at maximum tensile strain values that are about 100 microstrains. In a well-designed FRC with a high-enough fiber content to be useful for structural applications, the load bearing at large deflection values of 0.1–0.3 inch in a cracked beam can be as much as 50–60 percent of the maximum load (refer to Appendix C). These data have been proven to work in the case of hybrid reinforcement, where more than 60 percent of the rebars can be completely replaced by using less than 0.5 percent by volume of steel fibers, or equivalent polypropylene (PP) macrofibers [21]. This level of stress distribution cannot be obtained by means of standard MOR calculations since the material is not mistakenly assumed to be elastic. However, this stress level can be used in an equivalent elastic-plastic response for a ductile section, and that is the primary aim of this project. The goal is to find the level of fiber reinforcement that can reduce the need for more than 50 percent of the rebars in a structural concrete section and thus determine the most economic solution.

While it has been difficult to introduce fibers into specifications and design standards due to challenges in the quantification of their effects, both ACI 544 [16] and *fib* model code [22] have made progress in developing design procedures that account for the benefits of fibers in concrete, particularly in the areas of precast tunnel lining, industrial floor applications, and elevated slabs. These procedures can be directly applied to pavements and thin concrete overlays, even if the condition of the underlying soil is poor enough that it cannot provide any support to the pavement. In the case of expansive soils, fibers may contribute through the large-scale deformation capacity of restraining the imposed deformations. An appropriate selection of fiber type and dosage is required for their application. There are two types of fibers recommended for structural concrete pavement applications:

- **Steel Fibers:** In transportation applications, steel fibers are discussed frequently in the context of thin-bonded overlays, pavements, and bridge decks. They are also the primary means of structural reinforcement for the geotechnical applications in the design of traffic and metro tunnel segments [23]. Steel fibers are associated with improved tensile performance and can reduce the volume of conventional steel reinforcement, allow for longer spans, increase the joint spacing, and reduce slab thickness. Studies have shown steel fibers to be excellent supplements to concrete pavements—particularly in thin-bonded overlays, ultra-high performance concrete, and industrial floor applications—due to a significant reduction in the labor force required in construction.
- **Macro-Synthetic Fibers:** These include monofilament polymeric fibers such as PP, polyethylene (PE), and polyvinyl alcohol (PVA) fibers.
    - **Polypropylene Fibers:** Macro monofilament PP fibers have been developed to compete with steel fibers. They have also been used in hybrid applications for reducing the rebars in floor and slab applications. Micro-synthetic fibers are primarily used at low-dosage rates (e.g., 0.1 percent by volume) to control plastic shrinkage cracking [1].
    - **Polyvinyl Alcohol Fibers:** PVA fibers have been used to improve the high-tensile-strain capacity, toughness, and structural integrity of pavement overlays [24]. Basalt fiber reinforcement is referenced regarding crack behavior in asphalt composite CRCP alongside the inclusion of PVA fibers. Thermal degradation of PVA is a concern for the Arizona climate.

In both these cases, the amount of fiber used should be sufficiently high to provide a significant level of post-cracking residual capacity. However, any method of determining this quantity has not yet been addressed by any of the rigid pavement researchers to provide a significant moment capacity and crack distribution due to the tension-stiffening effects of the fibers (as discussed in Appendix C). In the case of steel, the concrete would require at least 0.4 percent volume fraction (50 pounds per cubic yard) steel fibers by volume, and in the case of polymeric, a volume fraction of 0.6 percent is typically required to utilize the contribution of fibers (nine pounds per cubic yard).

Distress Mechanisms in Concrete Pavements

Time-Dependent Loading

The time-dependent loading is governed by the inducing deformations that exceed the strain capacity of concrete, which is governed by the combined effects of shrinkage, creep, and recovery phenomena (Figure 3). Shrinkage strain (ε_{sh}) begins immediately after the preparation of the concrete mixture (t_s), and this process continues over the lifespan of the material due to moisture loss and hydration reactions. The shrinkage is therefore a continuous function of time that gradually decreases with age as internal moisture is lost. The moment that the road opens to traffic, the structure is subjected to vehicular load (t_0), and an instantaneous elastic strain (ε_m) develops. This strain represents the immediate deformation response of concrete to external loading.

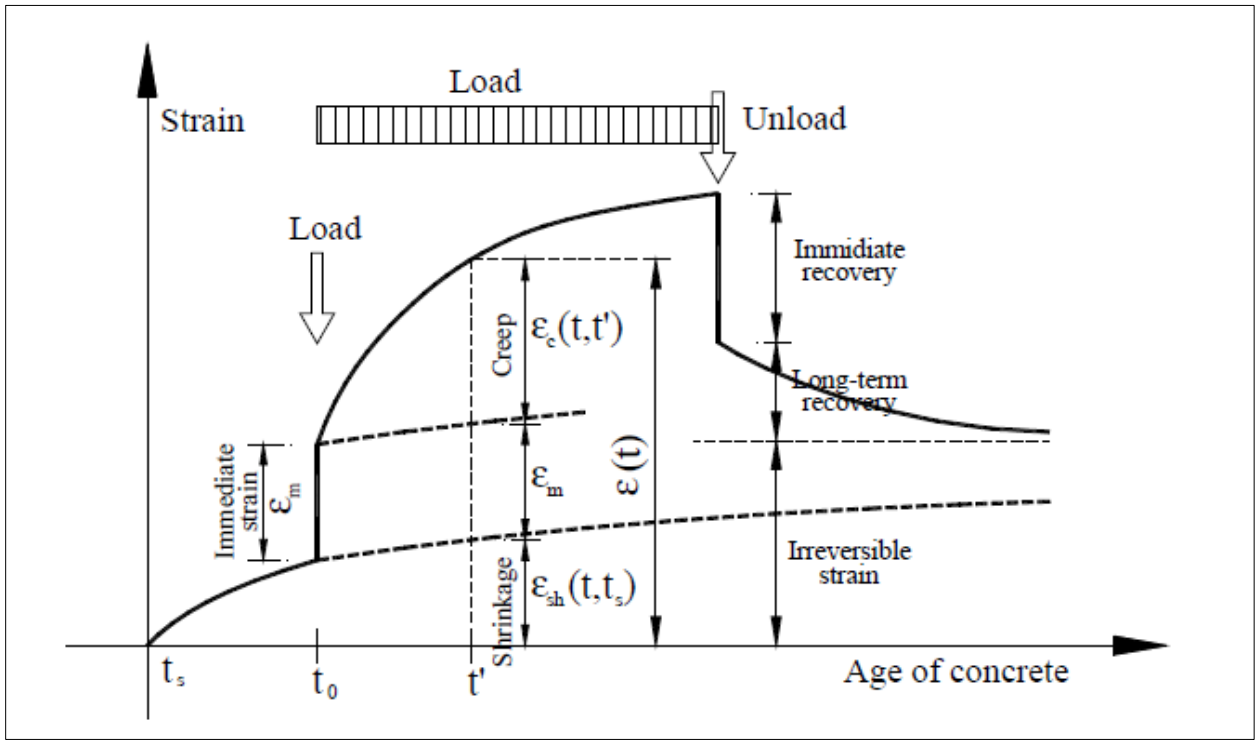

Figure 3. Age-Dependent Strain Changes in Concrete [25].

Following the initial loading, the concrete undergoes creep, which is the addition of strain defined as a time-dependent viscoelastic deformation under sustained load. This creep strain (ε_c) accumulates gradually and diminishes in rate over time as the material continues to age (t'). The total strain at any time consists of the superimposed effects of elastic strain, creep, and shrinkage. Upon unloading, the concrete exhibits partial strain recovery. A portion of this recovery is immediate due to elastic unloading, while another portion is recovered more gradually over time, reflecting the viscoelastic nature of the creep mechanism.

However, a significant part of the accumulated strain remains permanent, termed irreversible strain, which arises from inelastic microstructural changes such as microcracking or plastic deformation within the concrete matrix. These changes are intrinsic to the long-term behavior of concrete. Therefore, understanding and quantifying these strain components is essential for accurate long-term deformation prediction and durability assessments in concrete design. The modeling approach for plastic shrinkage evaluation in continuously reinforced pavements is discussed in Appendix C.

Stress Development Due to Volumetric Thermal and Moisture Changes

According to Hooke's Law, the stress-strain relationship describes how restraining a slab from shrinkage deformation generates internal tensile forces that act to cause cracking and exacerbate its opening. When the resultant tensile stress exceeds the concrete tensile strength, cracking will initiate and propagate; however, this is the exact moment that fibers are activated, and they transfer a major portion of the force generated through a small and finite opening imposed. In restrained conditions, such as pavement slabs bonded by friction to a subbase, shrinkage-induced stresses develop rapidly during early ages. However, creep-induced relaxation can help lower early-age shrinkage stresses, often by 30–70 percent. Experimental studies [26–28] have also demonstrated that incorporating fibers, particularly steel fibers, into the concrete matrix significantly reduces the overall shrinkage strain. This reduction is attributed to the fibers creating bridges across the microcracks, redistributing tensile stresses, and limiting the crack' opening, making them an effective method for enhancing dimensional stability and shrinkage resistance in concrete structures. This mechanism allows for reducing the number of joints in the pavement, as instead of a few large joints being damaged, many small microcracks form that would not affect the surface riding characteristics or slab curling (Appendix C).

Plastic Shrinkage Cracking at the Pavement Surfaces

When slab surfaces dry, tensile stresses develop in the restrained layer, potentially exceeding the tensile capacity of the fresh mix. If uncontrolled, these initiate cracking that can serve as a direct ingress path for unfavorable substances (e.g., chlorides, oxygen). This is one of the major issues compromising the long-term performance of concrete pavements. The purpose of fibers is to hinder the microcracking and not allow for the joining of the microcracks into macrocracks. Figure 4 illustrates the outcome of shrinkage cracks in pavements both with and without fiber additions.

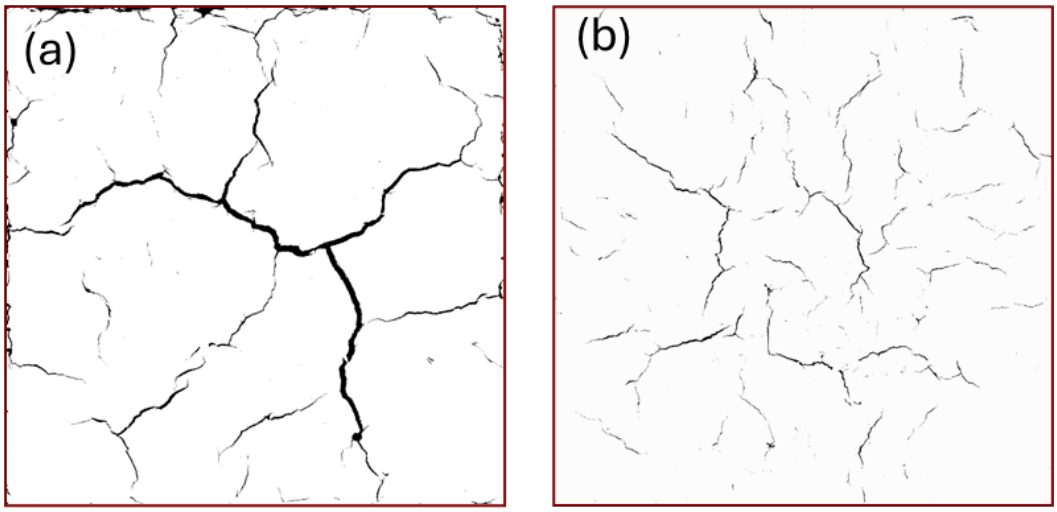

Figure 4. Effect of Fiber Addition on Shrinkage Cracks:

Fatigue Performance of FRC

Pavement fibers serve to bridge cracks and provide residual tensile strength under repeated traffic and thermal loading. Once a crack forms, the fibers engage through pullout and debonding, which redistributes stress and delays further crack propagation. This increases the number of load cycles the pavement can sustain before failure when compared to plain concrete, where cracking leads to the rapid loss of stiffness. Steel fibers improve flexural fatigue resistance by maintaining load transfer across cracks, while synthetic fibers reduce early-age shrinkage and control microcrack development, which would otherwise accelerate fatigue damage. Incorporating residual strength parameters (f_{150}, f_{300}, f_{600}) from ASTM International (formerly American Society for Testing and Materials) C1609 into the pavement design allows the quantification of these benefits and enables the design of pavements with reduced thickness or extended joint spacing while maintaining comparable service life. Figure 5 shows the characterization of the fatigue response of FRC using the standard beam test.

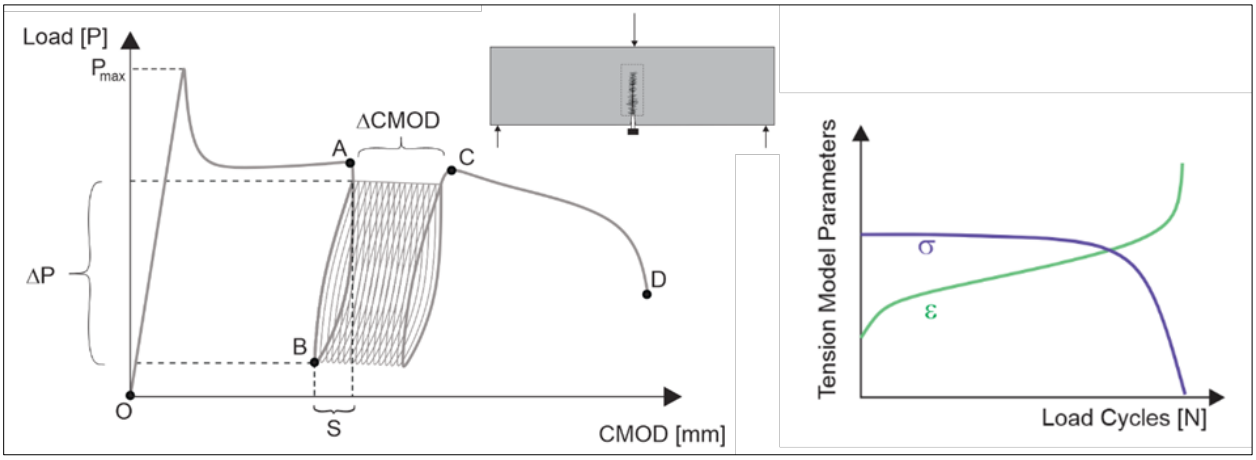

Figure 5. Fatigue Testing of FRC and Material Characterization.

The Nature of Repeated Load on Pavements

Thermal Loading

Thermal loading of concrete pavements refers to the stresses and movements caused by temperature changes. The magnitude and distribution of these thermally induced stresses are governed by the coefficient of thermal expansion (CTE) of the concrete, the degree of restraint provided by the subgrade and adjacent slabs, and the temperature gradient magnitude across the slab thickness. Temperature differentials between the pavement surface and bottom create non-uniform volumetric changes that manifest as slab curling and warping deformations. These cyclic deformations subject the pavement to repeated stress reversals, contributing significantly to fatigue crack initiation and propagation. For typical concrete pavement mixtures, the CTE ranges from 8–12 × 10^{-6}/°C (4.4–6.7 × 10^{-6}/°F). The specific value of 9.9 × 10^{-6}/°C (5.5 × 10^{-6}/°F) cited represents a commonly used design value for concrete pavements with moderate cement content and mixed aggregate sources. The characteristics of thermal loading obtained from field data are presented in Appendix B.

The deformed configuration is directly related to the temperature gradient profile through the slab depth. During positive temperature gradients (ΔT > 0), where the surface temperature exceeds the bottom temperature, differential thermal expansion generates upward curling, as shown in Figure 6. Conversely, negative temperature gradients (ΔT < 0) develop during cooling periods, when radiative heat loss and convective cooling create surface temperatures lower than the slab interior. This condition induces downward curling (convex deformation), with the slab edges and corners lifting from the foundation, also shown in Figure 6.

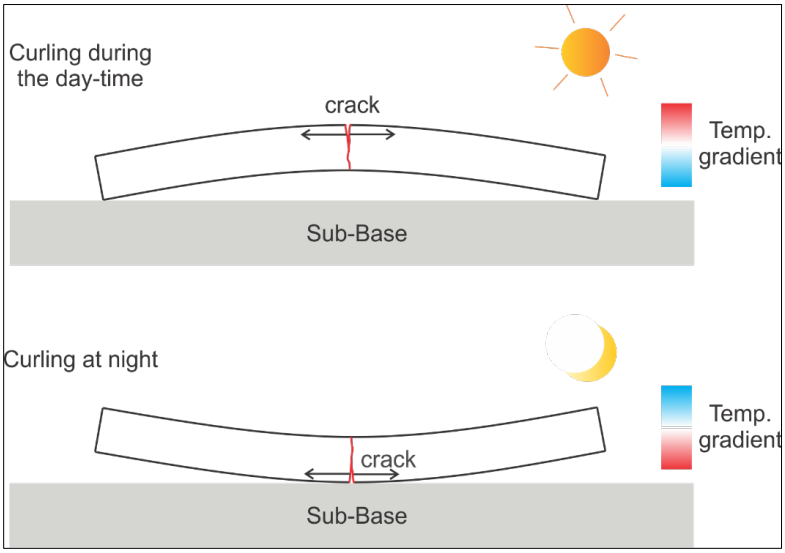

Figure 6. The Deformation Shape of the Slab at Different Temperature Gradients Over a Day.

Traffic Loading

Traffic loading presents unique design challenges for concrete pavements that differ significantly from concrete building design. Unlike buildings, where loads are primarily static, pavement design must account for traffic as one of the major load components that concrete must carry throughout its service life. Traffic means that every element on the pavement will experience maximum stress as vehicles pass over different locations. The dynamic response of the concrete pavement potentially leads to different amplified deflections, stresses, and strains that exceed those predicted by static analysis (Figure 7). Appendix B presents the traffic load patterns obtained from full-scale pavement testing.

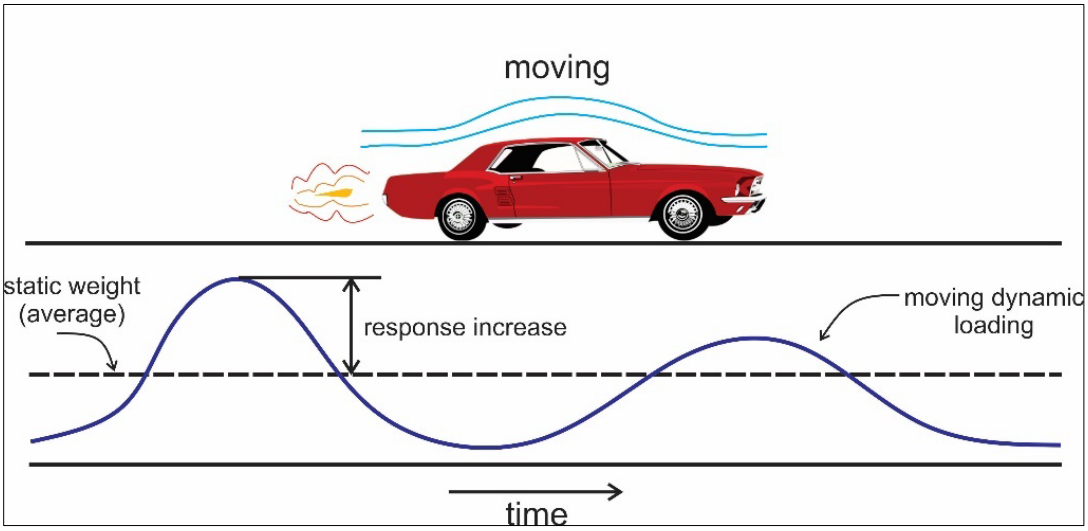

Figure 7. Static Weight vs. Moving Loading Response.

Adoptions and Gaps in FRC Applications

A literature review on existing DOTs was conducted, and their specifications for the use of FRC were gathered and summarized in Table 1. A more detailed overview of the DOT specifications is given in Appendix D.

Identified gaps in the literature include:

- Continued monitoring of existing field test sections to understand the long-term effects of fibers on distresses such as longitudinal cracking, transverse cracking, and spalling.
- Correlation of field data with design variables to isolate the role of fibers in reducing or eliminating types of pavement distress such. Correlation of the initial cement content and curing protocol with the damage states is an important aspect of long-term cracking potential.
- Research on newer fiber types—such as monofilament macro-polypropylene fibers, which were developed to behave like steel fibers—is needed, especially considering the various climatic conditions that Arizona highways can experience.
- The necessity of building a larger, more diverse database of long-term field performance data for pavement applications with various fiber types and dosages to derive reliable mathematical correlations between lab data and field performance.
- Further studies to better understand the impact of fiber type and dosage on construction and finishing practices to overcome challenges related to constructability and rideability.
- Economic evaluations, such as the inclusion of the user cost in the reduction of construction time, are essential for developing firm guidelines and recommendations for using fibers.
- Use of a mechanics-based approach to address FRC's individual and incremental benefits.
- Quantifying the benefits of fibers by incorporating their properties in the standardized design specifications.
- The full response of the load-deflection results needs to be used for proper analysis of the data—the reporting of the residual strength, or an effective MOR, by means of ASTM C1609 is insufficient for proper design.
- Use of an effective MOR as promoted by American Concrete Pavement Association (ACPA) [31] is erroneous and leads to a significant overestimation of concrete capabilities by more than 70 percent.
- Challenge of incorporating the role of fibers within the ME design approach, as embodied in AASHTOWare™ Pavement ME Design®, since the model is based on a quasi-linear elastic response up to an effective residual strength parameter.
- Many fiber applications in pavements use a low fiber content to increase the residual tensile properties. Low fiber contents fail to show any tangible structural benefits of fibers to reduce labor and thickness, thus the cost.

- Current performance models primarily address plain concrete using a single parameter failure criterion [9]. The ME models may not fully capture the specific benefits of fiber reinforcement such as the sustained load-carrying capacity after cracking; thus, new models must be developed.
- The direct test results of load-deformation from ASTM C1609, EN14651, and JCI-SF4 establish a robust link between the material properties and pavement distress prediction within the ME framework and can be used to gain insight into fatigue cracking as a characteristic limit state of a single-parameter design. Empirical tests, like ASTM C1018 and ASTM C1399, have severe limitations in correlating indices to actual field pavement performance and have become obsolete.
- Advanced mechanics-based approaches—such as nonlinear fracture mechanics (NLFM) or elastic-plastic analysis based on limit states—are suited for materials like FRC that exhibit strain-softening behavior after cracking [20,32]. These methods have been simplified by several new approaches to achieve simplified designs for slabs. These simplified methods are presented in the ACI 544 documentation

Table 1. Design Specifications by Other DOTs.

Title	Author(s)	Agency	Fiber Type	Dosage	Final Design Specifications and Other Data
FHWA/TX-07/0-4392-2: Fiber in CRCP	K. Folliard, D. Sutfin, R. Turner, D.P. Whitney	TxDOT[1]	Synthetic & steel	Not specified	Fibers reduced spalling. Steel > synthetic in toughness/residual strength. Thickness 8–15 inches, crack width ≤0.025 inches, longitudinal steel 0.5–0.8%, Class P concrete specs.
Structural Fibers in Thin Overlays	B. Hansen, M. Barman, T.U. Rahman	Minnesota DOT	Macro-synthetic (Tuf-Strand SF™, Strux® 90/40)	3–7.5 lb/yd³	Recommendation based on other DOT (example) GA DOT: Tuf-Strand SF™, Strux® 90/40; IL DOT: Strux® 90/40; IA DOT: 1–3 lb/yd³.
FHWA/TX-07/0-4392-2: Ultra-Thin Whitetopping	J. Roesler et al.	Illinois DOT	Structural fibers (general)	Performance-based (R_{150} ≥20%)	Required ≤4 inches, recommended 4–6-inch slabs. MOR ≥550 psi @14d; mean design MOR 750 psi @90d.
Residual Strength Estimator for FRC Overlays	J.R. Roesler et al.	CP Road Map	Synthetic & steel	0.19–0.5% vol. (≈4–8 lb/yd³ synthetic; 25 lb/yd³ steel)	Effective flexural strength: f_{eff} = MOR + f_{150}. Residual strength typical f_{150} = 100–200 psi. Performance-based spec on residual strength.
FHWA/VTRC 06-R11: FRC in Bridge Decks	C. Ozyildirim	Virginia DOT	Synthetic (PP/PE blend)	8.75 lb/yd³	Mixture: Cement 395, Slag 263, Water 286, Agg. 1830/1152. 28d compressive 5260–5570 psi. Permeability <2000 coulombs. Shrinkage exceeded limit. Freeze-thaw failed.
LTRC Report 438: Flexural Strength & Fatigue of SFRC[2]	J. Eggers, T. Rupnow	Louisiana DOTD	Steel fibers	65, 85, 95–100 lb/yd³	ASTM C-78 beams. Deck models matched original 2004 mix.
FHWA/AZ-18-705: FRC for ADOT Structures	A. Birely, P. Park, J. McMahon, X. Shi, Y. Rew	ADOT	Hooked-end steel (35 mm, AR 65, 1345 MPa), straight steel (13 mm, AR 65, 2660 MPa)	Not specified (lab trials)	Purpose: crack control, tensile/post-cracking strength. Mix: w/c=0.43, 25% fly ash. Workability issues unless central plant batching.
cmr 23-003: FRC for Bridge Deck Overlays	K. Amini, P. Vaddey, B. Birch, D. Corr	Missouri DOT	Synthetic & Steel (macro & micro)	Synthetic: 3.5–8 lb/yd³; Steel: 11–64 lb/yd³	Benefits: toughness, residual strength, crack control. Hooked-end steel best toughness. ASTM C1609/C1399/C1550 used. National survey with detailed DOT requirements.

Title	Author(s)	Agency	Fiber Type	Dosage	Final Design Specifications and Other Data
FHWA-ICT-24-009: Performance & Design of CRCP	A. Sakulneya, C. Anderson, J. Castro-Perez, J. Roesler	Illinois DOT	Not specified	N/A	Spreadsheet-based CRCP tool calibrated to Illinois. Crack spacing 3.1–33 ft. Spalling correlated with CTE ≤5.5 με/°F. Construction/material issues major distress cause.
TR-816 / InTrans 22-829: Field Performance of FRC Overlays	D. King, B. Yang, P. Taylor, H. Ceylan	Iowa DOT/IHRB[3]	Synthetic macrofibers	4 lb/yd³ (0.3% vol.) typical; 2.5–7.5 lb/yd³ range	Residual strength ≈150 psi. Typical overlays 0.2–0.5% vol. Fibers may improve long-term bond. No major effect on load transfer/smoothness.
Guide to Concrete Overlays (4th Ed.)	G. Fick, J. Gross, M.B. Snyder, D. Harrington, J. Roesler, T. Cackler	FHWA	Synthetic & steel macrofibers	Synthetic: 3–8 lb/yd³; Steel: 25–75 lb/yd³ (0.2–0.5% vol.)	Effective flexural strength: f_{eff} = MOR + f_{150}. Residual strength (f_{150}) performance spec. ASTM C1609 & C1550 used.
Synthetic Fibers for PCC[4]	—	Indiana DOT	Synthetic (Type III, ASTM C1116 / D7508)	≥4 lb/yd³	*Requirements:* Aspect ratio 70–100, Tensile ≥70 ksi, modulus of elasticity (MOE) ≥800 ksi, Length 1.5–2.25 inch *Testing:* ASTM C1609 (R_{150} ≥25%), ASTM C1579 (C_{RR} ≥85%). *Performance:* f_1 ≥600 psi before testing. Max. deflection 0.12 inch for 6×6×20-inch beams.

1: TxDOT = Texas Department of Transportation
2: SFRC = steel fiber reinforced concrete
3: IHRB - Iowa Highway Research Board
4: PCC = portland cement concrete

Conventional Concrete Pavement

Design Approaches

Design procedures have evolved over several decades by incorporating an increasing understanding of material behavior, traffic loading, local materials sources, and environmental factors [33]. Some of the procedures reviewed in detail include those from the Colorado Department of Transportation, New Jersey Department of Transportation, the ACPA, the American Association of State Highway and Transportation Officials (AASHTO), and the Federal Highway Administration (FHWA). Key focus areas concentrated on the following topics:

- A common failure criterion for concrete pavements is fatigue cracking under traffic loading [33,34].
- Empirical or mechanistic-empirical approaches such as AASHTOWare Pavement ME Design Guide [10] represent a state-of-the-art approach incorporating rigid pavement stress calculations, fatigue damage analysis, and performance prediction. This software is based on research conducted through the National Cooperative Highway Research Program (NCHRP).
- Current knowledge on CRCP design is quite useful in addressing the familiarity of the industry with these approaches [17]. Many additional factors are incorporated in terms of the failure criteria that include the potential for loss of foundation and edge support, excessive crack width and spacing, slab thickness, and cyclic thermal strains during and after construction.
- UTW with fiber applications and strength data from the Illinois Department of Transportation (IDOT) [33].

ADOT Specifications for Rigid Concrete Pavements (Based on AASHTO Empirical Method 1993)

Rigid pavement design, as outlined in the ADOT Pavement Design Manual, follows the methodology established in the 1993 AASHTO Guide for Design of Pavement Structures. The process is centered on determining an appropriate slab thickness that ensures long-term performance under traffic loads, quantified in terms of equivalent single axle loads (ESALs). The primary design equation is the same as the 1993 AASHTO design equation for rigid pavement.

The processes and guidelines for pavement design has changed significantly in the years since. The following section addresses these changes. Prior to the recent development of AASHTOWare Pavement ME Design, the 1993 AASHTO Guide for Design of Pavement Structures [35] was the standard. It used an empirical equation based on data from the AASHTO Road Test. This method estimated pavement performance using ESALs and pavement properties, assuming uniform materials and conditions. The 1993 AASHTO Rigid Pavement Design Equation (Equation 1) is as follows:

$$\log_{10}(W_{18}) = Z_R \cdot S_o + 7.35 \cdot \log_{10}(D+1) - 0.06 + \frac{\log_{10}\left(\frac{\Delta PSI}{4.5-1.5}\right)}{1+\frac{1.624\times10^7}{(D+1)^{8.46}}} + (4.22 - 0.32 \cdot p_t) \cdot \log_{10}\left(\frac{S_c' \cdot C_d \cdot (D^{0.75} - 1.132)}{215.63 \cdot J \cdot \left(D^{0.75} - \frac{18.42}{(E_c/k)^{0.25}}\right)}\right)$$

Equation 1

Where

W_{18}	Design ESALs (18-kip Equivalent Single Axle Loads)
D	Slab thickness (inches)
Z_R	Standard normal deviate for reliability (typically −1.645 for 95%)
S_o	Overall standard deviation (usually 0.35–0.45)
ΔPSI	Loss in serviceability index (typically 4.5 − 2.5 = 2.0)
p_t	Terminal serviceability index (typically 2.5 for highways)
Sc’	MOR of concrete (psi)
C_d	Drainage coefficient (0.80–1.0 based on drainage quality)
J	Load-transfer coefficient (1.0 to 3.2, depending on joint condition)
E_c	Elastic modulus of concrete (psi)
K	Modulus of subgrade reaction (psi/in)

Note that Sc’ is the MOR obtained from a flexural (bending) test, typically representing the tensile strength of concrete under third-point loading as per ASTM C1609 test.

A sensitivity analysis of the design parameters is shown in Appendix E. The results indicate the thickness is highly sensitive to two parameters, the MOR (Sc’) and the drainage coefficient (Figure 8 and Figure 9). The MOR in plain concrete occurs at the first crack, and no post-cracking performance is considered, which indicates the inefficiency in the design of rigid pavements.

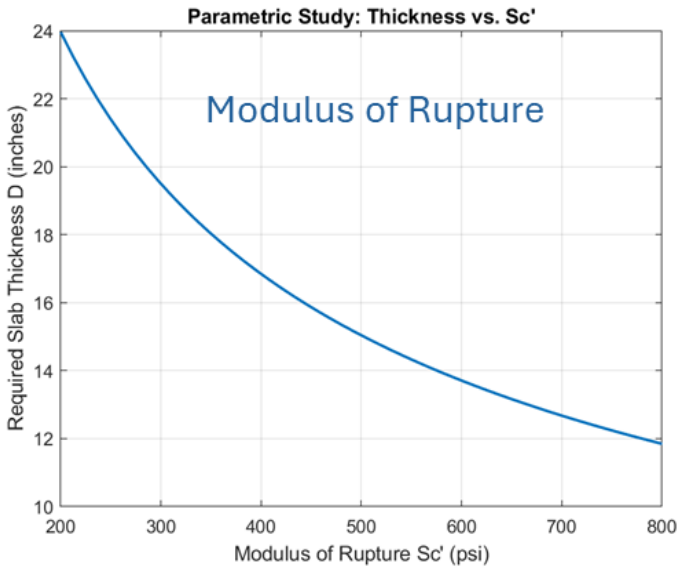

Figure 8. Most Sensitivity Design Parameters for MOR.

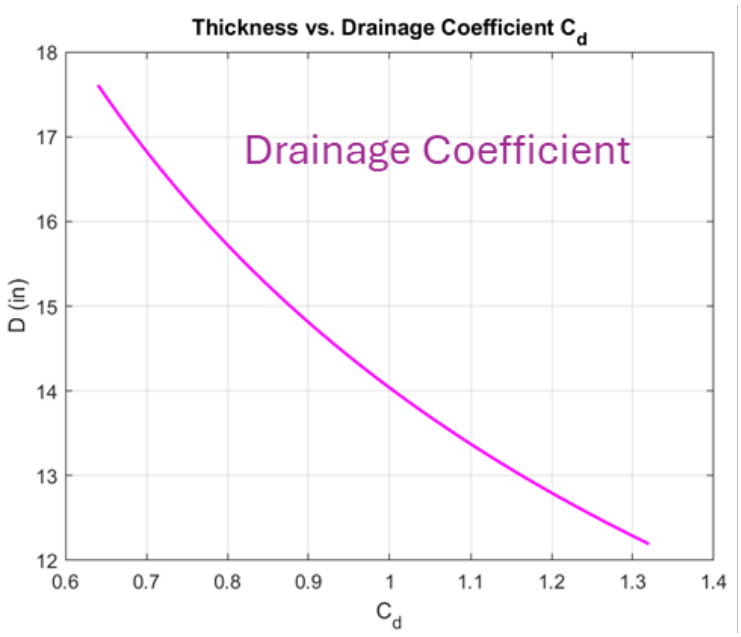

Figure 9. Most Sensitivity Design Parameters for Drainage Coefficient.

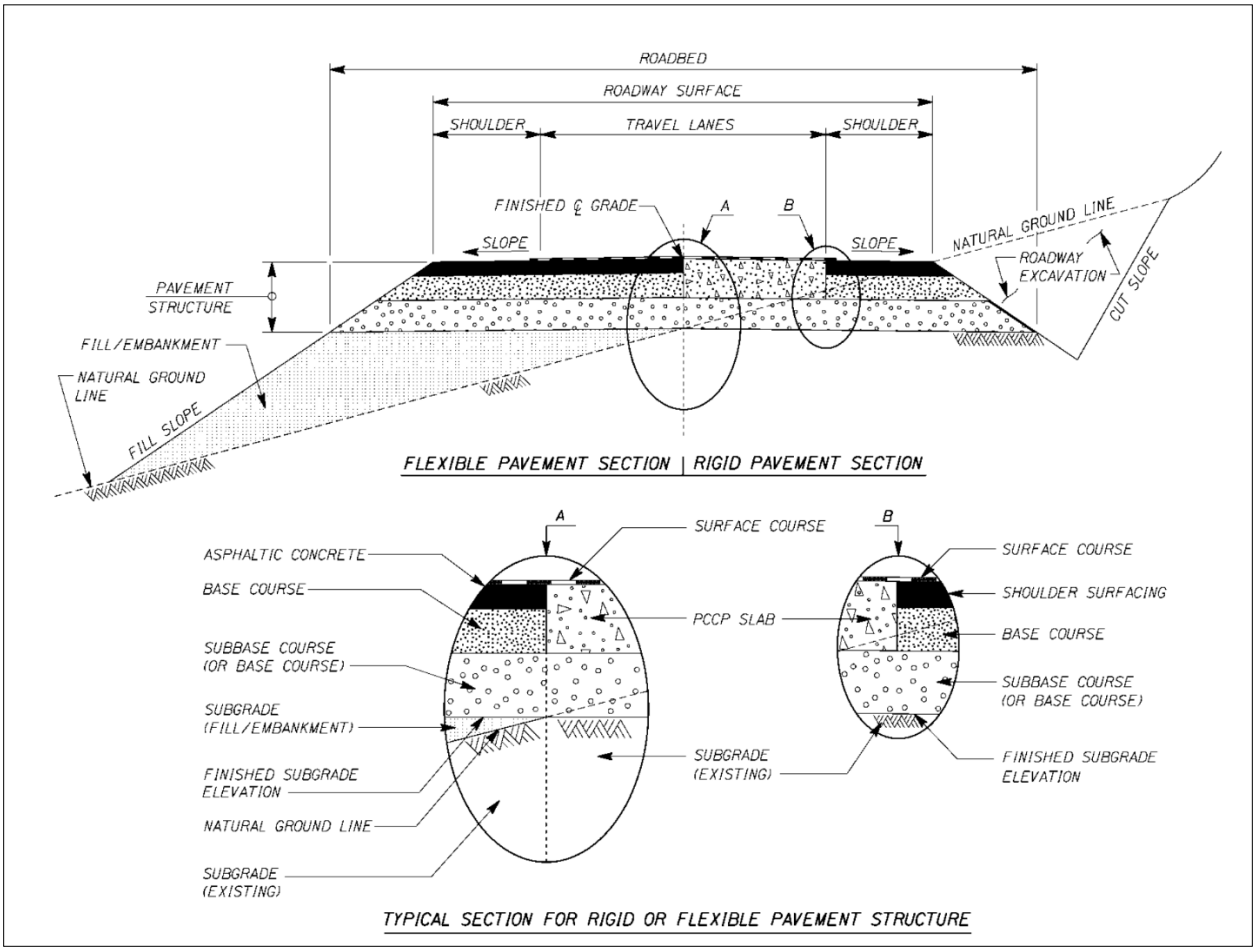

Figure 10. Pavement Section, per ADOT [36].

ADOT typically uses a reliability level of 95–99 percent and a standard deviation of 0.35 for rigid pavements. The modulus of subgrade reaction is adjusted based on support conditions and possible loss of base support, and the load-transfer coefficient reflects the presence or absence of dowels and tied shoulders. The final slab thickness is found through iterative use of the AASHTO equation, balancing structural adequacy with constructability and cost-efficiency.

AASHTO ME Rigid Pavement Approach (Software Based)

In contrast to AASHTO 1993 method, the AASHTOWare Pavement ME Design approach is simulation-based, integrating mechanistic analysis of pavement response (using layered elastic theory and finite element principles) with empirically derived distress models. Design in the ME method is performed iteratively. Trial slab thicknesses are simulated and evaluated against performance thresholds, and adjustments are made until design objectives are satisfied. This approach replaces the earlier equation-based solution with a more robust, data-driven process. The mechanism is, however, based on elastic plate theory and of a plate on an elastic foundation as proposed by Westergaard [37] discussed in later sections.

The design relies on ME principles, combining stress-strain response analysis with calibrated empirical distress models to predict long-term pavement performance. The method supports different types of concrete pavement such as jointed plain concrete pavement (JPCP) and CRCP, as well as their overlays on flexible, composite, or rigid foundations. However, several factors are not fully captured within the AASHTOWare framework, including durability-related distresses, volume change in expansive or frost-susceptible soils, and the behavior of semi-rigid or ultra-thin overlays. In such cases, users are expected to perform local calibration or supplement design using agency standards and engineering judgment.

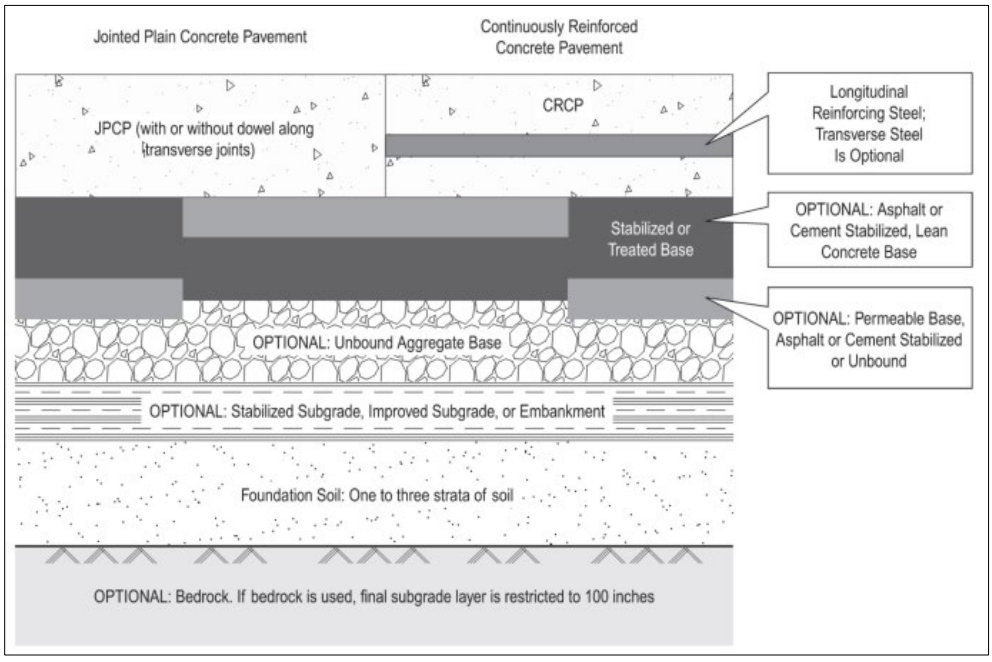

Figure 11. Rigid Pavement Design Strategies that Can Be Simulated with AASHTOWare Pavement ME Design [9].

Table 2. Summary Table for AASHTOWare Pavement ME Design: Key Features and Limitations.

Category	Description
Supported PCC Types	JPCP (≥6 in, 10–20 ft joints), CRCP (≥7 in, continuous reinforcement)
Overlay Types	JPCP/CRCP overlays on rigid, flexible, or composite pavements
Restoration Methods	Diamond grinding, dowel bar retrofit, slab replacement, spall repair, shoulder replacement
Joint Handling	JPCP: transverse + longitudinal (tied/untied); CRCP: transverse joints for construction only
Base Materials Supported	Unbound aggregate, stabilized bases (asphalt, cement, lean concrete, RAP, etc.)
Durability Modeling	ASR, D-cracking, raveling, and stripping are not modeled; joint spalling is modeled empirically
Soil Volume Change	Frost heave and expansive clay effects are not included
Skid Resistance & Noise	Not modeled; must rely on historical data or specs
Tire Types	Defaults to dual tires; super-single simulation possible
Reinforcement Materials	Geogrids and other reinforcements are not supported
ATPB Handling	Included in rigid designs; modeled with 65 ksi modulus; not calibrated for flexible pavements
Semi-Rigid Pavements	Supported but not globally calibrated; fatigue cracking functions set to 1.0
Preservation Strategies	Not directly modeled; user must adjust via local calibration
Staged Construction	Only the opening date of the final layer can be entered; no long-term staged analysis
Unsupported Pavement Types	JRCP[1] (not included), Ultra-thin overlays (min. JPCP = 6 in, CRCP = 7 in)
Traffic Opening Time	PCC cannot be opened before 28 days
Interface Friction Modeling	Customization not available for HMA-over-PCC interfaces; full bond assumed (except CTB[2] bases)

1: JRCP = jointed reinforced concrete pavement
2: CTB = cement-treated base

Fundamental Aspects of Pavement Design

Westergaard Approach

Westergaard's approach (1926) [37] for rigid pavement design forms the basis of classical slab analysis in concrete pavement engineering. It models the pavement as an elastic slab resting on a dense system of Winkler foundation, which represents the support from the subgrade. A wheel load *P* applied on the slab produces a deflection *w*, bending stresses, and tensile stresses at the bottom of the slab. The key outcome of Westergaard's theory is the relative stiffness equation, which relates slab thickness, elastic modulus, and foundation stiffness, and allows engineers to estimate critical stresses at interior, edge, and corner loading positions (refer to Figure 12). The approach assumes the slab and subgrade are perfectly elastic, the slab remains uncracked, and the foundation reaction is linearly proportional to deflection. These simplifications limit its ability to capture real pavement behavior such as cracking, nonlinear soil response, and load transfer across joints.

The ME pavement design framework continues to adopt Westergaard's solutions as its analytical foundation, using relative stiffness and stress equations to estimate critical responses. These mechanistic outputs are then linked to empirically calibrated transfer functions to predict long-term performance. Thus, while Westergaard's assumptions are restrictive, they remain embedded in ME design practice as the mechanistic basis for distress prediction. However, because these formulations inherently assume uncracked, elastic slab behavior, the mechanisms captured in ME are not sufficient to represent the post-cracking performance required for the design of FRC pavements.

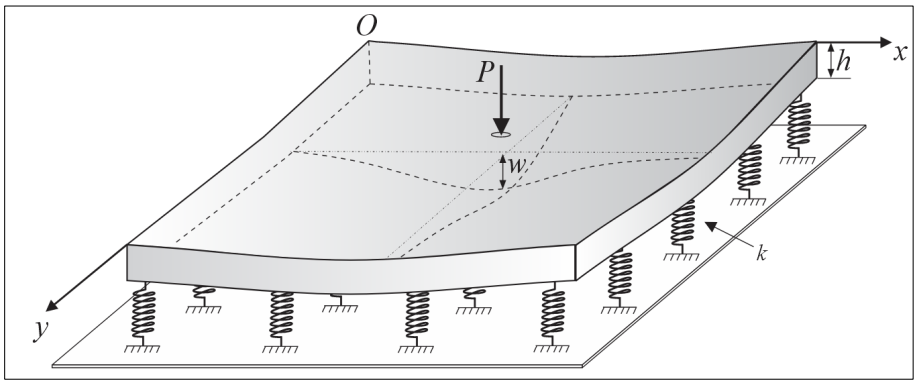

Figure 12. Westergaard Model of a Rigid Pavement Slab.

Meyerhof Approach (TR34 and ACI 360)

The Meyerhof method [38] applies yield line theory to predict the ultimate capacity of concrete pavement slabs under wheel loads. The slab is assumed to form plastic hinges along failure lines, and the collapse load is determined from equilibrium of internal and external work.

Key assumptions in the Meyerhof Approach:

- Pavement slab behaves as a rigid-plastic plate that carries load until a collapse mechanism forms.
- Subgrade is assumed to be perfectly supportive and elastic, always in full contact with the slab.
- Temperature, moisture effects, and in-plane forces are ignored; only bending governs failure.
- Concrete strength is simplified with a basic tensile cut-off model, not full biaxial behavior.
- Slab properties (thickness, material) are taken as uniform and constant up to collapse.
- Analysis assumes sufficiently large load-contact areas to avoid punching failure.
- Joint load transfer is represented by fixed percentage factors, not detailed mechanics.

These assumptions allow Meyerhof to derive closed-form expressions and simple design charts for the collapse (ultimate) load of centrally, edge-, and corner-loaded concrete slabs-on-grade, but they limit applicability where significant warping, membrane action, subgrade yielding, or complex joint behavior dominates. This approach is used in the British standard TR34 for industrial floors and ACI 360 for slab-on-ground design. The yield line-based method considers the post-elastic performance of concrete, making it suitable for slabs reinforced with fibers (FRC). It allows for quick, preliminary design calculations of ultimate capacity, providing a practical tool before moving to more detailed analyses (refer to Appendix E).

However, a more precise yield line-based design can be developed based on experimental results of hybrid and reinforced concrete (RC) slabs (refer to Appendix F).

$$\int dW_E = \int dW_I \qquad \text{(a)} \qquad \textbf{Equation 2}$$

Where

External work = $$dW_E = \left[\left(\frac{P_{ult}}{2\pi}\right)\delta\right]d\alpha = \left[\left(\frac{P_{ult}}{2\pi}\right)(R-a)\theta\right]d\alpha \qquad \text{(b)}$$

Internal work = $$dW_I = \left(M_P^+ + M_P^-\right)\delta d\alpha = \left(M_P^+ + M_P^-\right)(R-a)\theta d\alpha \qquad \text{(c)}$$

Assuming, $$\phi_r = M_P^- / M_P^+ \qquad \text{(d)}$$

then $$dW_I = \left(M_P^+ + \phi_r\right)\delta d\alpha = \left(M_P^+ + M_P^-\right)(R-a)\theta d\alpha \qquad \text{(e)}$$

Finally, substituting Equations (b) and (d) in energy Equation 2 (a), there is

$$\int_0^{2\pi} M_P^+(1+\phi_r)R\theta d\alpha = \int_0^{2\pi}\left[\frac{P_{ult}}{2\pi}(R+a)\theta\right]d\alpha \qquad \text{(f)}$$

The energy method presented in Appendix F can be combined with the nonlinear load-deflection solution for hybrid reinforced sections in Appendix E to establish a robust analytical framework for pavement design. This integrated solution is developed to predict the ultimate flexural capacity of hybrid pavements in a rational manner, moving beyond purely empirical design approaches.

For the case of concentrated point loads, the use of empirical joint-spacing or load-capacity rules often fails to capture the complex behavior of pavements reinforced with different fiber dosages or mix designs. Since these parameters significantly influence residual strength and post-cracking ductility, the resulting flexural response is highly variable and cannot be reliably addressed using conventional empirical procedures.

Accordingly, this framework provides a path toward performance-based design of hybrid pavements, where fiber dosage, mix proportions, and residual strength properties are directly integrated into the structural evaluation rather than treated as secondary empirical adjustments.

Consequences of Failure Due to Presence of Joints

There is currently no rational basis for the design of joints for concrete slabs on ground. Joint spacing is typically governed by empirical practices rather than mechanistic models, and improper spacing often leads to premature cracking, spalling, or loss of load transfer. These failures compromise serviceability, accelerate deterioration, and increase maintenance costs.

The tension-stiffening model for distributed parallel cracking in RC under uniaxial tension provides a more rational approach to joint design. This model captures the load-sharing mechanism between reinforcement and the surrounding concrete after cracking, accounting for bond-slip interactions and stress redistribution between cracks, which is described in detail in Appendix I.

By incorporating fibers in hybrid reinforced CRCP slabs, the tension-stiffening effect is enhanced through additional fiber bridging, which reduces crack spacing, limits crack width, and improves fatigue resistance. Therefore, the application of this model can directly address the potential benefits of hybrid fiber-reinforced CRCP systems, offering a mechanistic framework to interpret available field data and design slabs that minimize distress caused by poorly spaced or ineffective joints.

Proposed Method of Approach

The climate of Arizona plays a critical role in material behavior. Adopting only traditional construction methods may not be adequate to address the unique challenges posed by extreme temperature variations, rapid drying conditions, and high thermal stresses. The addition of fiber reinforcement to redistribute stress after cracking developments can be an effective solution to enhance pavement service life.

Design considerations:

- **Material Optimization:** FRC eliminates the need for conventional rebar fabrication, which is beneficial for rural or remote construction where time and logistics are challenging.
- **Performance Testing:** Residual tensile strength and post-cracking flexural capacity must be quantified using ASTM C1609. Key residual parameters:
  - f_{150} at L/150 deflection
  - f_{300} at L/300 deflection
  - f_{600} at L/600 deflection
- **Fiber Dosage and Type:**
  - Steel fiber (typically 50–70 lb/yd³) significantly improves post-cracking tensile resistance. Dosages should be optimized through trial batching to achieve the target residual strengths.
  - Macro-synthetic fibers (typically 7–14 lb/yd³) enhance crack distribution and control early-age shrinkage but contribute less to long-term flexural strength.
- **Shrinkage and Creep:** Fibers reduce plastic shrinkage cracking, but hot–dry climate in Arizona, creep relaxation may partially offset tensile stresses. Long-term monitoring of shrinkage-induced cracking is needed. The studies [29,39] in the efficiency of different fibers in mitigating restrained plastic shrinkage cracking in cementitious composites can be used as a guideline.
- **Joint Design:** Tension-stiffening modeling is a useful tool for designing joint spacing in reinforced and FRC pavements [40]. The model, based on nonlinear finite difference methods, captures tensile cracking by considering matrix strength, bond-slip behavior, and reinforcement. Results show that higher reinforcement ratios or fiber dosages reduce crack widths and cumulative cracking, allowing for wider joint spacing without compromising serviceability.

Case A: Plain FRC

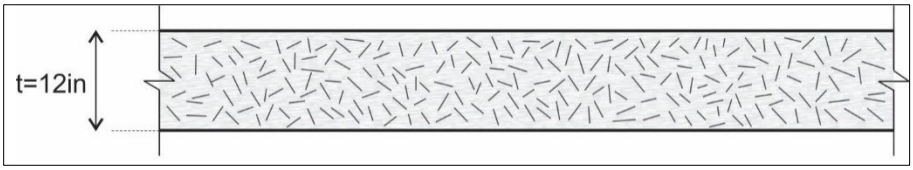

Figure 13. Cross Section of FRC.

Thickness will be based on a 14-percent reduction compared to a 12-inch plain concrete section and also increasing the allowable joint spacing.

Primary goal: Cost savings associated with materials, labor, and transportation associated with a reduced thickness,

Expected change: Thickness reduction of 20 percent given the fatigue life improvements with the use of fibers and increased joint spacing, less shrinkage cracks, and curling

Key points:

- FRC-based residual strength is used to find an effective reduced thickness design. An equivalent moment-curvature capacity curve is obtained and compared to the MOR-based flexural response using a linear elastic brittle section. The net gain is a reduction of section thickness and a significant increase in fatigue life under high loads, reaching 60–70 percent of standard MOR.
- The joint spacing can be significantly increased due to the use of fibers providing tension stiffening and resistance to cracking.
- This is particularly advantageous in rural or remote projects where the transportation cost of delivering extra concrete and staging is significantly expensive transport, fabrication, and placement are challenging.
- The performance of plain FRC is highly dependent on fiber dosage. Insufficient fiber content results in inadequate crack control and limited post-cracking strength, reducing the effectiveness of the system. Excessive fiber dosage can significantly reduce workability.
- A parametric study of the constitutive compression and tension models of plain FRC, applied to the moment-curvature response, can follow the approach of Soranakom and Mobasher (2008) [41].
- The effect of curling and shrinkage can be evaluated as a function of humidity variations and free-shrinkage strain. Acceptable uplift deflection is determined by the interaction between slab thickness, support conditions, and fiber reinforcement. The study by Destrée et al. (2016) [42][43] showed that steel fibers contribute to reducing crack opening induced by curling and shrinkage gradients, thereby improving slab serviceability and enabling larger joint-free panel sizes.

Case B: Continuous Reinforced + Fibers (Hybrid RC)

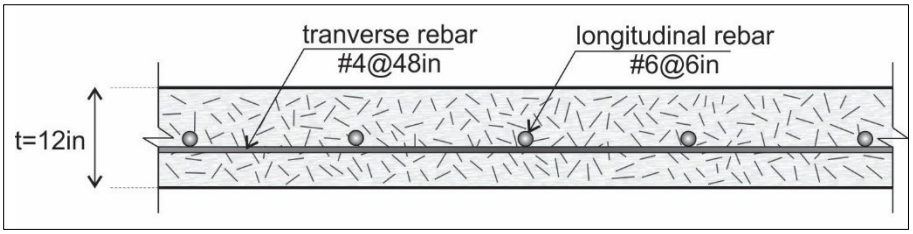

Figure 14. Cross Section of FRC with Rebar Reinforcement.

Make this about 10 inches.

Primary goal: Cost savings associated with the reduction of content materials, labor, and transportation associated with a reduced thickness of a CRCP.

Expected change: Thickness reduction by 20 percent, significant labor reduction, extended joint spacing, reduced cost compared to CRCP.

Keys points:

- A proposed new design approach for CRCP, which substitutes at least 50 percent of the rebar content with a structurally equivalent fiber dosage.
- A more detailed design analysis based on fundamental mechanics of materials is proposed. A design chart will be developed to develop an equivalent balance of reinforcement ratios with fiber dosage. The presented manuscripts [44,45] developed closed-form solutions for minimum reinforcement, balanced reinforcement, and minimum fiber parameters, which provide a framework for serviceability-based design. These solutions allow designers to optimize hybrid reinforced concrete sections to achieve higher load-carrying capacity compared to plain FRC while ensuring that ductility requirements are maintained. These calculations are available upon request for a specific design case to be planned.
- The performance of hybrid systems has been evaluated through studies combining different reinforcement ratios with varying fiber dosages. Recent work by Pleesudjai et al. (2025) [21] highlights the role of fibers in improving serviceability performance. These publications are currently in press and can be directly used for the approval process.

Case C: RCC with Fibers

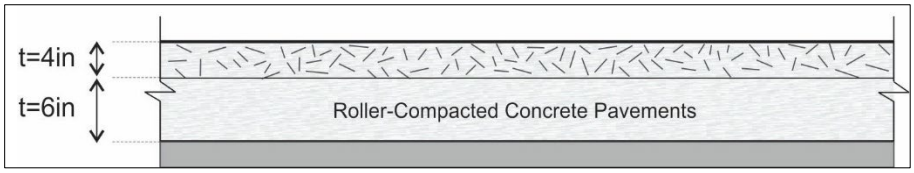

Figure 15. Cross Section of FRC Above RCC.

Primary goal: Cost savings associated with the reduction of cement content, and strength, labor, and transportation associated with a reduced thickness, uniform distribution of tensile stresses due to a functional gradient.

Expected change: Thickness reduction by 20 percent, significant labor reduction, and extended joint spacing.

Key points:

- Based on the ACI 544, ACI 360, and TR34 approach, an optimized moment-based design is suggested that utilizes a portion of the most effective top layer with high dosage FRC. The FRC serves as a thick overlay on top of RCC pavement.
- Benefits of both cases A and B and C combined with a multilayer approach. This approach combines the high compressive strength of RCC and stiffness with the post-cracking toughness of FRC for improved structural efficiency.
- Fibers in the overlay limit crack width, enhance load transfer, and reduce chloride and moisture ingress.
- Better suited for Arizona's climate by mitigating shrinkage and thermal cracking while resisting fatigue under repeated loads. Expected lower shrinkage due to the lower cement content of the base layer.
- FRC overlay further protects the subgrade by controlling crack-induced drainage paths.
- Allows rapid construction with asphalt-type paving equipment, while eliminating rebar placement simplifies logistics. Potential use of a geotextile bonding membrane.
- Fewer joints and enhanced crack control extend service life and reduce long-term maintenance.
- Design must account for dry consistency of the RCC layer with a low cement, low w/c gap graded coarse aggregates, which affects proper bond with the FRC layer, fiber dispersion in the top layer. Specialized equipment for mixing and compaction is required, however such projects have been completed elsewhere (such as Missouri DOT from Table 1).
- Residual strength testing of RCC using modified ASTM C1609 procedures is recommended to evaluate post-cracking strength and toughness at L/150 deflection.

Minor Options

Shrinkage-Reducing Admixtures

Shrinkage reducing admixtures (SRAs) function by lowering the surface tension of pore water, reducing capillary stresses that drive drying shrinkage cracking. Studies such as [46] have shown that SRAs can reduce drying shrinkage strains which is particularly beneficial hot–dry environment where rapid moisture loss is a distress factor. When combined with fibers, SRAs help maintain tighter crack widths and improve dimensional stability, reducing the probability of early-age cracking. This represents a supplemental strategy to enhance crack resistance where FRC alone may not be sufficient.

Extended Curing Time

Curing practices are critical in ensuring proper hydration and controlling early-age shrinkage. Continuous water curing, curing compounds, or membrane coverings can significantly improve tensile strength and reduce shrinkage-induced cracking. Extending curing beyond the standard 7-day period to 14–21 days can reduce cracking risk and improve resistance to chloride penetration. In Arizona's climate, rapid evaporation and high temperatures accelerate moisture loss, making extended curing an important strength factor. Although extended curing increases initial construction time and may pose logistic challenges, the reduced maintenance demand and improved durability justify its consideration.

Use of Expansive Agents for Reduction of Tensile Cracking

Expansive agents counteract tensile stresses from shrinkage, helping maintain compressive stress states that delay or prevent cracking. When dosed appropriately, expansive agents can significantly reduce transverse and longitudinal cracking in pavements and bridge decks. However, performance is highly sensitive to mix proportioning and curing conditions; excessive expansion can cause warping or localized distress. For ADOT, limited use of expansive agents may be considered in projects where shrinkage and thermal gradients are critical drivers of distress, particularly in continuous reinforced or thin overlay systems.

Summary of Key Aspects of FRC Pavements

Fiber Dosage and Structural Efficiency

The proposed design approach incorporates a much higher fiber content than conventionally practiced so that the structural contribution of fibers in a cracked section can be reliably utilized. The approach is to increase from the common 3–6 lb/yd³ (1.8–3.6 kg/m³) to 9–12 lb/yd³ (5.2–7.12 kg/m³) for polypropylene fibers and as much as 40–75 lb/yd³ (24–45 kg/m3) for steel fibers. Although these dosages are more costly on a per-unit basis, their tensile contribution can be justified by the potential to achieve at least 10–15 percent reduction in slab thickness based on residual tensile capacity and MOR performance. When evaluating cost-effectiveness, the analysis should consider life-cycle costs, including reduced initial construction, maintenance, and extended service life, to ensure that design decisions affect the overall economic and performance benefits. The higher dosage allows fibers to fully replace conventional temperature and shrinkage additives and also improves minimum reinforcement. Experiments and simulations on RC sections shows that this level of fiber dosage can reduce the amount of steel reinforcement in CRCP by as much as 50 percent while the thickness is also reduced. This approach provides enhanced crack control, improved load transfer at the joints, and greater stiffness in the serviceability range.

Using fibers directly improves a pavement's resistance to fatigue failure, joint movement, dowels, edge-related cracking, and free-edge boundaries. Additional laboratory testing and modeling with representative samples are required to correlate the performance of a given traffic load. Analytical models based on closed-form solutions in Appendix E have already been developed to incorporate fiber residual strength into ME pavement design for individual projects as long as the analysis focuses on the serviceability of the section due to its stiffness retention.

Curing Requirements

To achieve the desired performance, extended covered wet curing for up to two weeks is recommended. This practice minimizes early-age shrinkage cracking, enhances hydration, and ensures long-term durability of thin slabs. When wet curing is not feasible, curing compounds may be considered, but extended moist curing remains the benchmark for ensuring uniform strength gain and maximizing fiber effectiveness.

Aggregate and Material Quality

Durability and performance depend on careful control of aggregates and fines. Specifications should emphasize crushed rock with a well-graded sand-gravel curve, while maintaining tight control over the minus No. 200 sieve content to prevent excessive shrinkage or weak paste zones. High-quality

aggregates contribute to improved interlock and reduced susceptibility to distress. Proper distribution and sieve analysis of the aggregates should meet the guidelines in accordance with the methods developed in the ADOT Final Report SPR-745 “Developing Ultra High-Performance Concrete Mix Designs for Arizona Bridge Element Connections.”

Supplementary Cementitious Materials and Cement Reduction

The mixture design emphasizes sustainability and durability through the use of fly ash and slag cements, reduced total Portland cement content, and coarser-ground cements. A lower water-to-cementitious materials ratio—between 0.40–0.45 (w/cm)—combined with supplementary cementitious materials (SCMs), improves long-term strength while lowering shrinkage and mitigating alkali-silica reactivity. This approach aligns with performance-engineered mixtures, reducing carbon footprint while enhancing service life. ADOT Final Report SPR-780 “Sources and Substitutes for Fly Ash in ADOT Concrete Mixes” provides a significant set of guidelines and selection strategies for the use of SCMs and provides a good reference when performing this work.

Placement and Compaction

Placement should employ paver-type equipment with roller compaction methods, producing a condensed, zero-slump or very low-slump mix (1–2 inches). The resulting dense concrete ensures durability and effective fiber dispersion, even at high dosages. High-range water reducers (HRWRs) should be used instead of additional water to maintain workability, ensuring uniform fiber distribution and minimizing balling. Fiber distribution and orientation has been significantly addressed by measuring the mechanical response of the samples through ASTM C1609, and an average value based on the flexural tests conducted on the sections will be used in accordance with the standardized procedures. Mix designs will be validated using performance-based specifications for the residual strength defined through ACI 544-12R report.

Structural Role of Fibers

Fibers serve a triple enhancement role:

- Primary reinforcement for temperature and shrinkage stresses, meeting or exceeding the minimum reinforcement ratio specified in design codes.
- Enhancing post-cracking performance, wider joint spacing, reduced reliance on conventional rebars, WWF, dowels, and improved fatigue resistance under repetitive traffic loading.
- Reducing the crack widths to significantly smaller sizes would inherently increase the aggregate interlock, shear fracture resistance, moisture loss and transmission, and slab curling. The longer a crack, the more difficult it is to open, so additional cracks form, allowing for a homogenization of stiffness throughout the volume. Dowelling mechanisms would not be necessary if the fibers were distributed throughout the cracks and joints.

Jointing Strategy

Integrating FRC permits a reduction in the number of saw-cut joints through increased joint spacing. Wider panels decrease maintenance requirements while fibers maintain crack width control and joint LTE. Proper timing of saw cuts and attention to curing practices are often critical to ensure controlled crack development. Simulations: Use of fibers and proper curing eliminates any guesswork in the number, mobilization, and timing of saw cuts. Simulations will be conducted to correlate the effect of residual strength and the joint spacing, opening, and curling potentials.

Edge Support and Confinement

The design of shoulder region is important since it must provide adequate support, reinforcement, and confinement for the slab, reducing the potential for curling, faulting, and base erosion. Unlike ordinary RC, FRC does not require a sacrificial cover thickness, which is significantly useful since the cracking of the unreinforced concrete cover is the initiation of potential damage problems. Well-compacted shoulders with tied connections improve the overall performance of the slab system, especially when combined with extended joint spacing and high fiber dosage.

Summary of Key Aspects of Mix Design

Recommended Practices for FRC Pavements

General

Placing, finishing, and curing FRC pavements in accordance with the details shown on the plans are important aspects of specifications. The information and recommendations contained herein are for general guidance and not intended for direct use without ADOT review and approval. The authors of this document assume no responsibility or liability for the use/misuse of this information. Practicing engineers conduct the required evaluations (refer to Appendix J) to verify the suitability of specific fiber types, dosages, and mixture designs for the intended application.

Materials

- Cementitious Materials: Use Type II/V or Type IL cement, with 25–40 percent fly ash and/or slag to improve durability and reduce cement demand.
- Aggregates: Conform to ADOT Construction Manual Section 1006, with well-graded fine and coarse aggregates and a maximum of 3.0 percent passing the #200 sieve to limit fines. Consult the ADOT Final Report SPR-745 in the mix proportioning and particle size distribution.
- Fibers: ASTM C1116 Type III. Specify synthetic fibers at 9–12 lb/yd³ (5.2–7.1 kg/m³) or alternate hooked-end steel fibers at 40–75 lb/yd³ (24–45 kg/m³). Residual flexural strength fD_{150} shall be in accordance with guidelines of ACI544-12R per ASTM C1609.
- Admixtures: HRWRA per ASTM C494 for workability; air entrainment provided as required for durability.

Mix Design

The job mix formula shall be submitted 30 days prior to construction, with a water-to-cementitious materials ratio (w/cm) not greater than 0.45 and not less than 0.40, a maximum cementitious content of 560 lbs/yd³, a minimum compressive strength ($f'c$) of 4,000 psi at 28 days and a residual flexural strength f^{D}_{150} based on ASTM C1609 as discussed above.

Construction Requirements

- Placement: Concrete can be placed using a slipform paver equipped with internal vibration. Slump shall be 0–3 inches, verified at the point of placement. No water shall be added at the site beyond that established in the approved job mix formula.
- Fiber Dispersion: Fibers shall be uniformly distributed throughout the mixture. To prevent balling or clumping, pre-blending with aggregates or other approved methods shall be used. The effect of fiber dispersion can be addressed by the analysis of a minimum set of flexural mechanical tests to determine the allowable design values.

- Jointing: Saw cuts per plans. Joint spacing may be increased when LTE ≥ 80 percent by falling weight deflectometer. Saw cuts two to eight hours after placement.
- The finished surface shall be given a transverse tine or broom texture as specified in the project documents, producing a uniform, skid-resistant finish.

Curing

Fourteen days continuous wet curing (burlap, blankets, or approved methods) is ideal. If infeasible, cure the compound at 1.25× rate + ≥ 7 days wet cure. Protect against premature drying.

Equivalent System Analysis of Plain, Fiber-Reinforced, and Hybrid Concrete in JPCP

The design of JPCP and its advanced variants increasingly focuses on achieving equivalent structural performance with reduced slab thickness. This approach aligns with ADOT's goals of lowering material consumption, extending service life, and improving sustainability. In this section, the flexural behavior of three representative systems is compared:

- Plain Concrete Slab (t = 14 inches)
- FRC Slab (t = 12 inches) with f^D_{150} = 500 psi
- Hybrid Reinforced Concrete (HRC) Slab (t = 10 inches) with f^D_{150} = 500 psi, longitudinal reinforcement (#6 at 6 inches), and transverse reinforcement (#4 at 48 inches)

All sections are designed with a compressive strength of 4000 psi, representing a typical pavement-grade concrete used in Arizona highway applications. Flexural stiffness, moment-curvature response, and reinforcement detailing were investigated to establish equivalency in serviceability and ultimate performance.

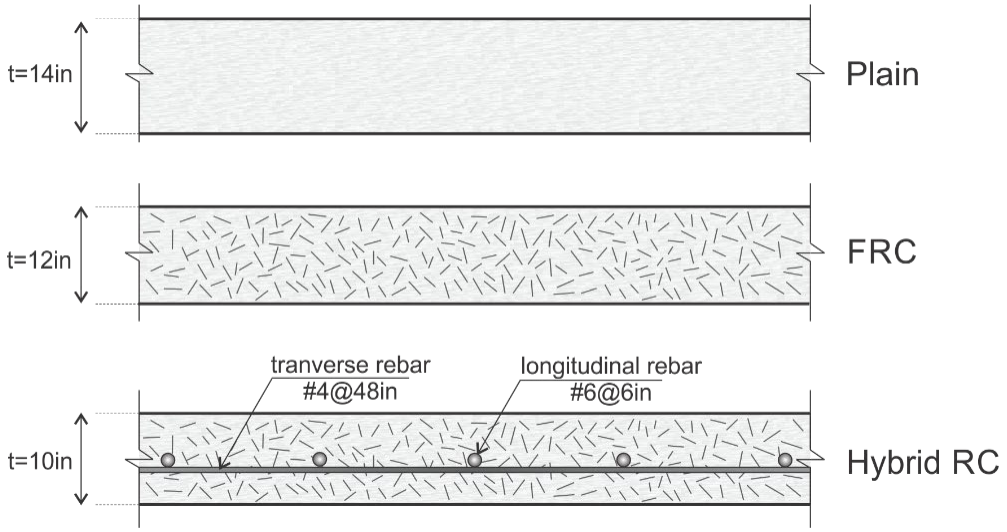

Figure 16. Cross-Section Comparisons of Plain Concrete vs. FRC vs. Hybrid RC.

The Effect of Residual Strength

The equivalent system analysis highlights that moment capacity and flexural stiffness can be preserved or enhanced through reinforcement strategies even as slab thickness is reduced (refer to Figures 57 and 58). In terms of moment capacity, the plain concrete section reaches 30 kip-ft before abrupt failure, while the FRC section sustains 33 kip-ft with only 10 percent strength reduction at large curvatures. The hybrid RC section develops 30kip·ft but demonstrates continuous hardening, with moment capacity increasing by 5–10 percent.

In the case of flexural stiffness, plain concrete pavement (t=14 inches) exhibits brittle loss of stiffness with a post-cracking reduction of more than 90 percent in secant stiffness, the FRC section (t=12 inches) retains approximately 15–33 percent of its initial stiffness at higher curvature levels. The hybrid RC section (t=10 inches) maintains about 30–60 percent of its peak stiffness through reinforcement engagement, providing greater ductility and energy absorption capacity.

These results show that:

- Slab thickness being reduced by 15 percent (14 inches → 12 inches) is feasible with FRC. This retained stiffness of FRC significantly enhances fatigue resistance by delaying crack growth and extending the number of load repetitions the slab can withstand.
- A greater reduction of 30 percent (14 inches → 10 inches) is feasible with hybrid RC. This higher retention not only compensates for reduced depth but also provides superior long-term fatigue performance compared to both plain and FRC systems.

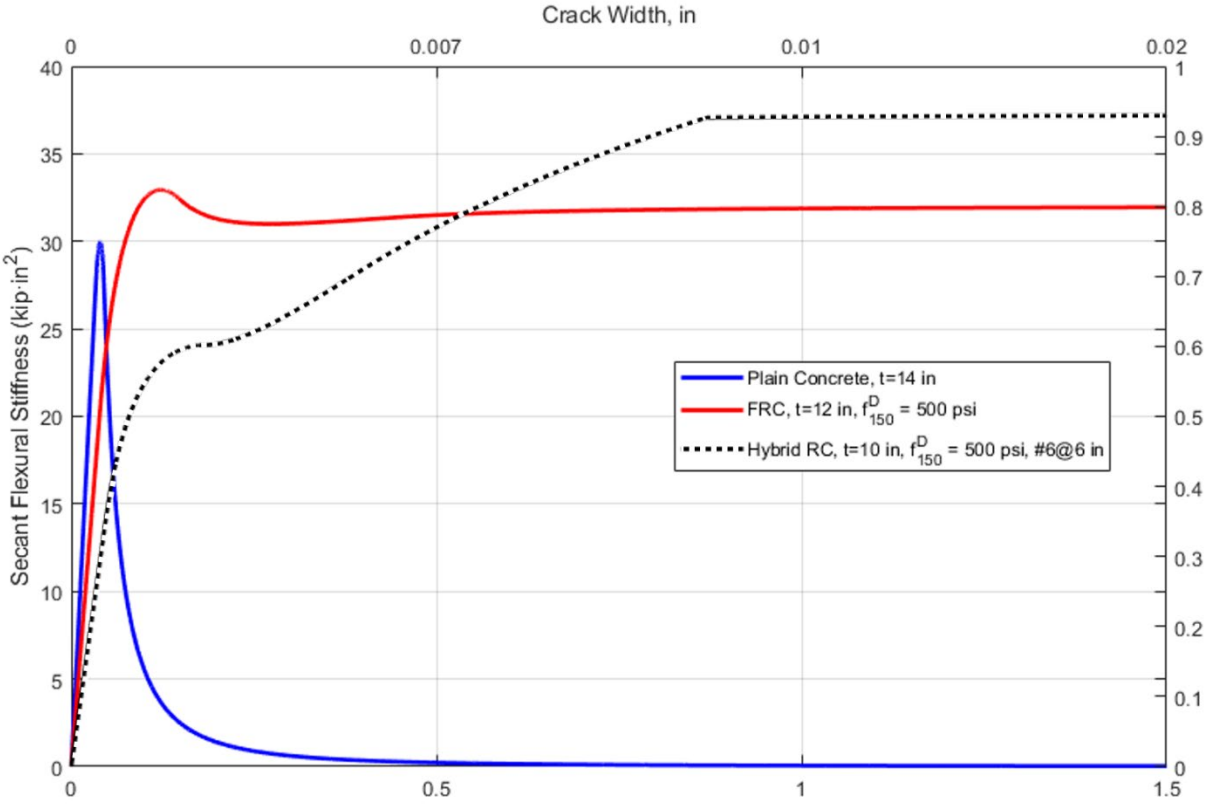

Figure 17. Moment and Curvature for JPCP.

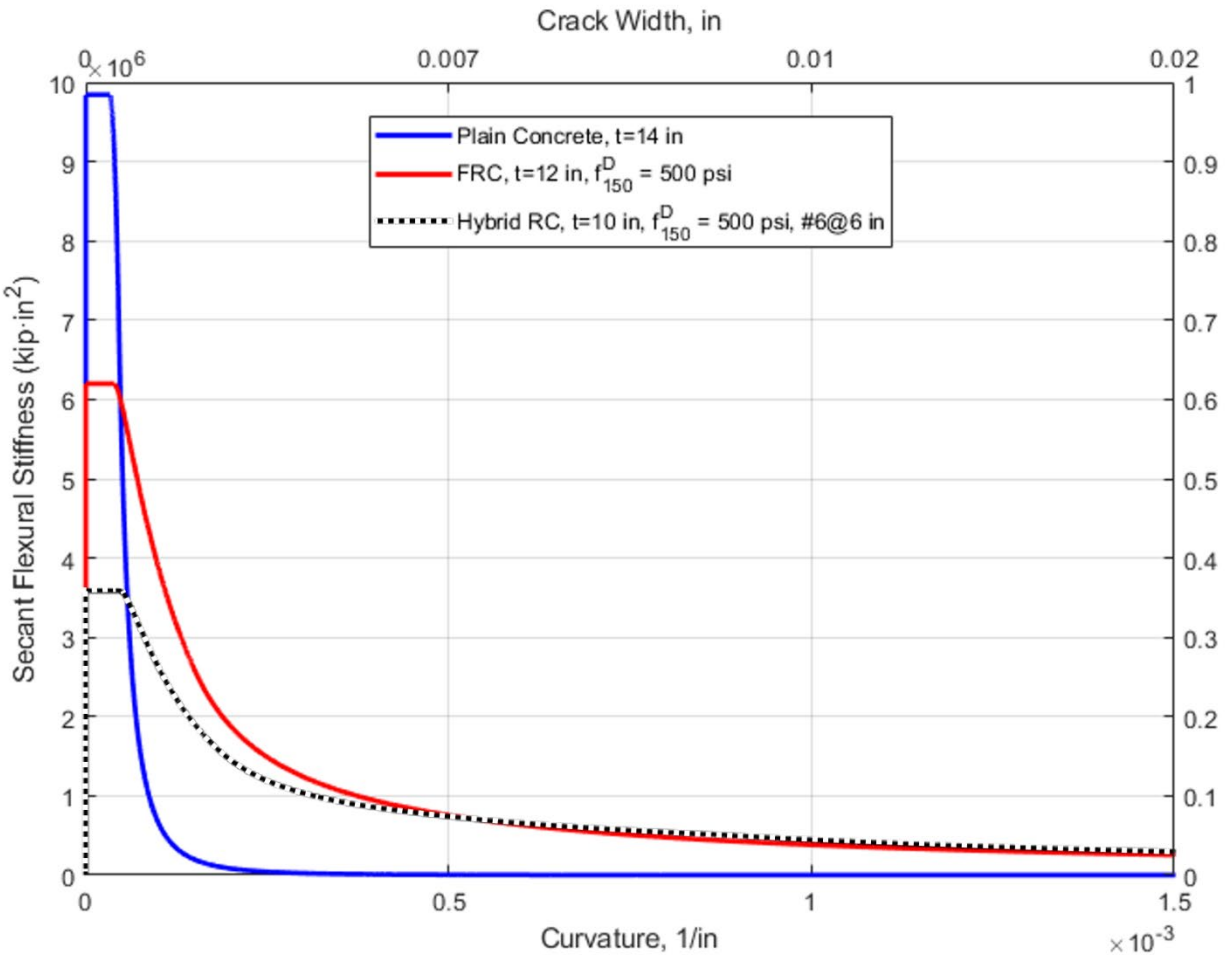

Figure 18. Secant Flexural Stiffness and Curvature for JPCP.

Reinforcing Steel Content in CRCP and the Role of Fibers

According to several studies (e.g., FHWA Tech Brief FHWA-HIF-019-098), CRCP typically requires a reinforcing steel content of about 0.5–0.8 percent of the cross-sectional area. However, this value can be significantly reduced when fibers are introduced to replace a major portion of the longitudinal reinforcement. The following references highlight the current state of practice and the potential for fiber reinforcement:

- **University of Illinois at Urbana–Champaign (FHWA-HIF-16-026)**

  Jeffery R. Roesler, Jacob E. Hiller, Alexander S. Brand, *"Continuously Reinforced Concrete Pavement Manual: Guidelines for Design, Construction, Maintenance, and Rehabilitation,"* FHWA-HIF-16-026, August 2016.

  - Reinforcing steel content = 0.7 percent of cross-sectional area at 3.5 inches (90 mm) cover (p. 28).
  - Field performance evaluations found that a longitudinal steel content between 0.7–0.85 percent effectively maintains tight crack widths over the service life of CRCP.

- **Texas A&M University (FHWA/AZ-18-705)**

  Anna C. Birely, Philip Park, Joshua A. McMahon, Xijun Shi, Younho Rew, *"Fiber Reinforced Concrete for Improved Performance of Transportation Infrastructure,"* ADOT-SPR-705, February 2018.

  - Summarizes research on the role of fibers in reducing traditional reinforcement demand and improving pavement performance.
  - Full-scale hybrid slab tests were conducted with longitudinal reinforcement ratios ranging from 0.16–0.86 percent, combined with steel fiber dosages of 65 lb/yd³.
  - The results confirm that a fiber dosage of approximately 0.5 percent by volume (65 lb/yd³) enables a reduction in reinforcement area, while still maintaining adequate capacity at both the serviceability and ultimate limit states.

- **FHWA Tech Brief (FHWA-HIF-019-098) (2019)**
  - Summarizes CRCP design and construction practices across the United States, confirming that fiber reinforcement can reduce the required amount of conventional longitudinal steel while maintaining performance

- **University of Texas at Austin (FHWA/TX-07/0-4392-2)**

  Kevin Folliard, David Sutfin, Ryan Turner, David P. Whitney, *"Fiber in Continuously Reinforced Concrete Pavements."*

  - Tests were conducted on CRCP slabs with a thickness of ten inches and longitudinal steel content of 0.5 percent (#6 at 8.25-inch spacing), both without and without fibers. The fiber-reinforced cases included synthetic fibers at 4–6 lb/yd³ and steel fibers at 25–40 lb/yd³.
  - The field data demonstrate the beneficial effects of fibers on crack control and durability in concrete pavements. Steel fibers at dosages of 25–40 lb/yd³ substantially reduced average crack spacing (from 7.5 ft in the control to 3.2–4.4 ft) and decreased crack widths by approximately 20–30 percent.
  - There is no spalling observed in the fiber system.
  - Synthetic fibers also reduced crack widths to levels comparable with steel fibers but introduced challenges in finishability. These findings highlight the trade-off between workability and crack performance in mix design.

Table 3. Summary of Reinforcements' Constructability.

Section	Fiber Type	Fiber Dosage (lb/yd³)	Ease of Placement	Finishability	Avg Crack Spacing (ft, 235 d)	Avg Crack Width (inches, 235 d)	Spalling (235 d)	Slump (inches)	f_{MOR}, psi
Control	—	0	Good	Good	7.5	0.018	Yes	4.0	675
SF1-25	Steel	25	Satisfactory	Satisfactory	4.4	0.016	No	2.6	605
SF1-40	Steel	40	Satisfactory	Satisfactory	3.2	0.014	No	3.1	560
SnF1-4	Synthetic	4	Satisfactory	Poor	3.4	0.015	No	2.8	665
SnF1-6	Synthetic	6	Poor	Poor	4.5	0.014	No	3.3	595

Equivalent System Analysis of CRCP With and Without Fibers

Two representative CRCP systems were analyzed to evaluate the potential for slab thickness reduction and rebar optimization. The baseline reference was drawn from FHWA/TX-07/0-4392-2 field studies, where performance was established for conventional CRCP design. For ADOT applications, where high shrinkage potential and thermal gradients are the dominant distress mechanisms, the improved residual performance of fiber-reinforced mixes suggests adopting higher dosages than typically used. A dosage of 9–12 lb/yd³ (5.2-7.12 kg/m³) of polypropylene fibers or 45-75 lb/yd³ (27–45 kg/m3) of steel fibers is recommended, which is expected to have f^{D}_{150} > 500 psi.

The comparison included:

- Control CRCP Section: Slab thickness t=10 in, longitudinal reinforcement #6 at 8.25 inches.
- (ρ = 0.53 percent), no fibers.
- Equivalent Fiber-Reinforced Section: Slab thickness reduced to t=8 in, longitudinal reinforcement reduced to #4 @ 12 inches (ρ = 0.20 percent), with added fiber reinforcement (f^{D}_{150} = 500 psi).

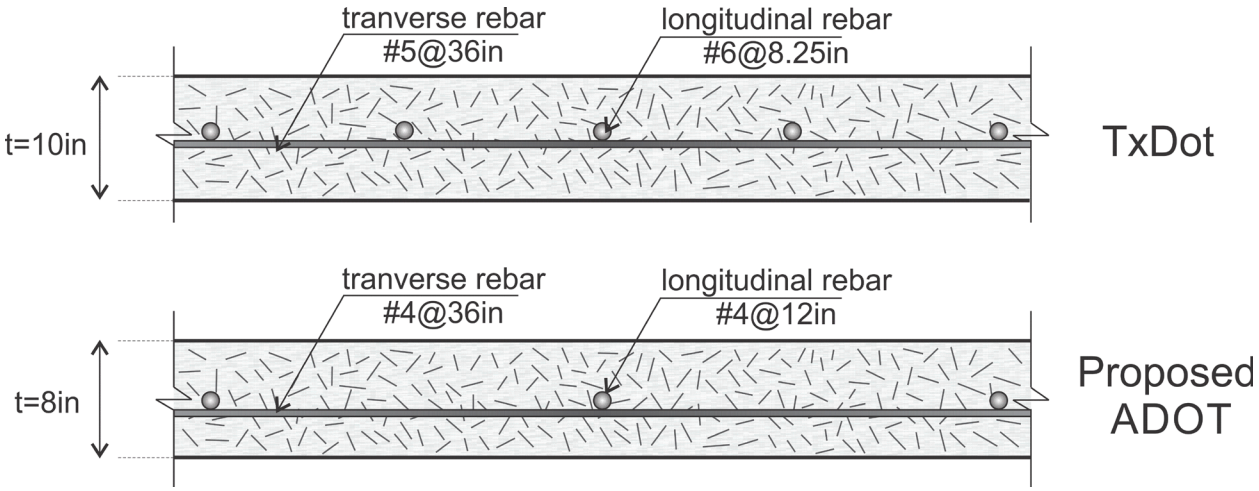

Figure 19. Cross-Section Comparison of TxDOT's Hybrid RC vs. Proposed Method for ADOT's Use.

The Effect of Fibers on System Equivalency

As shown in Figures 60 and 61, introducing fibers while reducing both slab thickness and reinforcement content preserved system-level performance:

- The equivalent 8-inch fiber-reinforced section demonstrated similar post-cracking stiffness retention compared to the 10-inch control section.
- Crack widths were effectively controlled despite the reduction in rebar ratio (0.53 percent → 0.20 percent), improving long-term durability.

These findings confirm that CRCP thickness can be reduced by up to 20 percent (10 inches → 8 inches) while substantially lowering rebar demand, if fibers are incorporated to sustain residual strength and crack control.

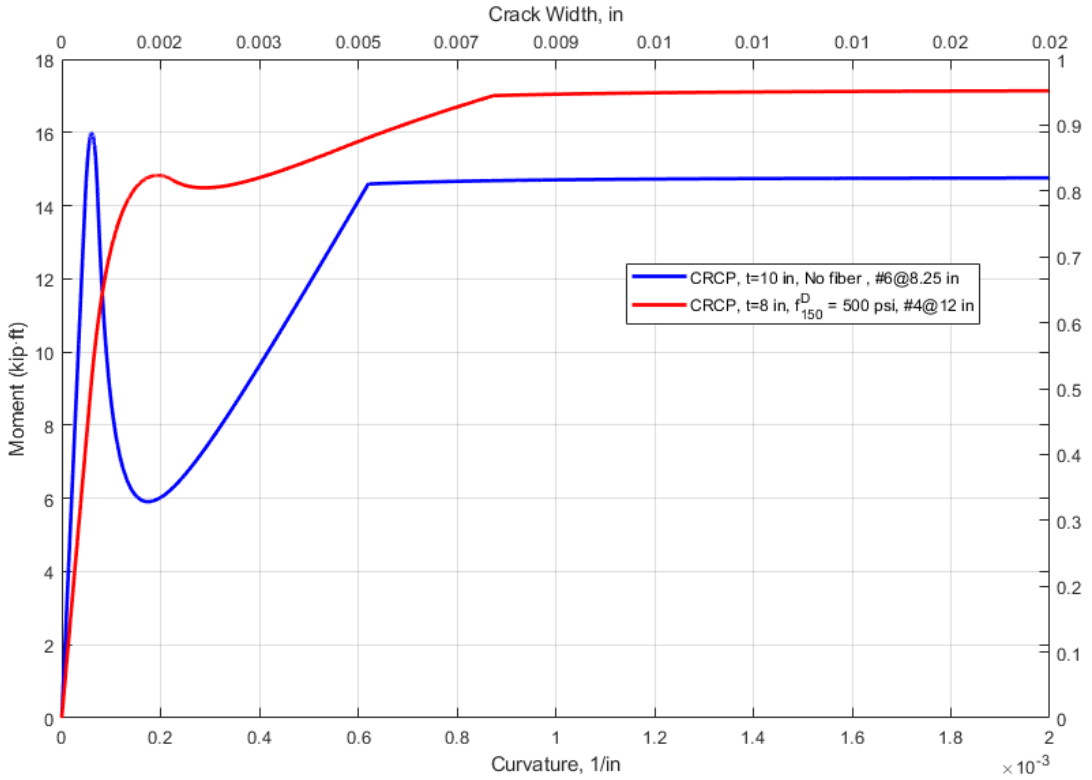

Figure 20. Moment and Curvature for CRCP.

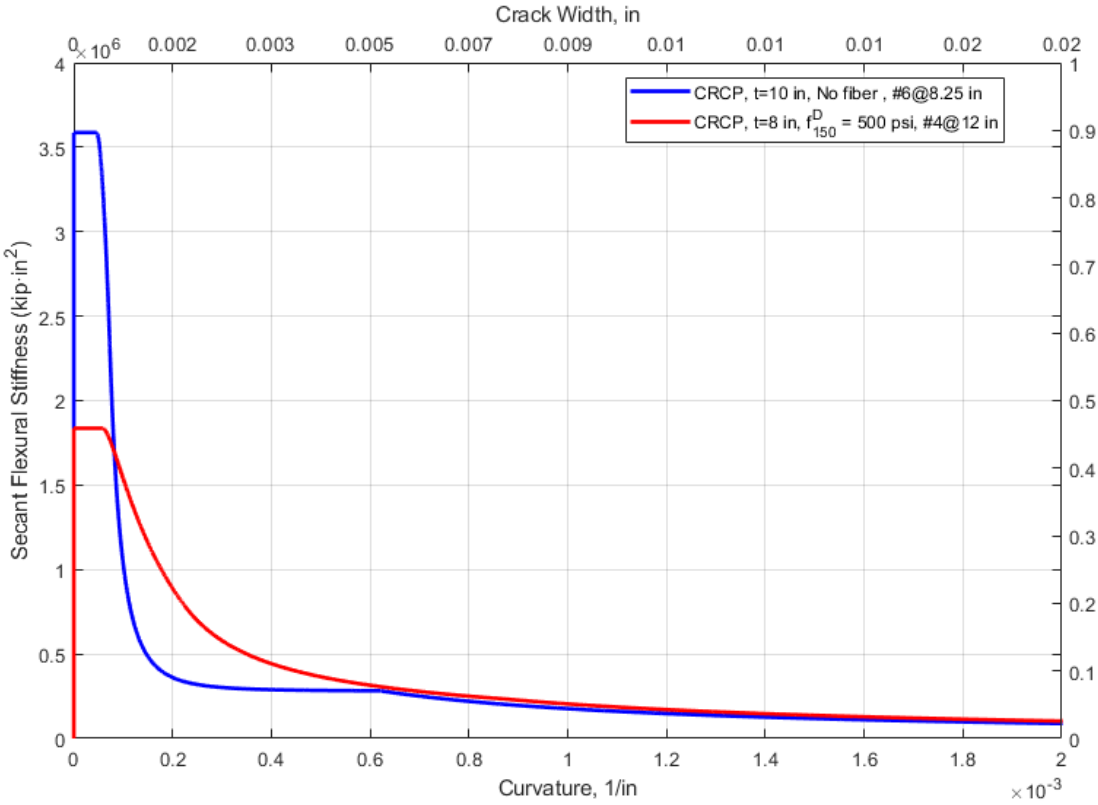

Figure 21. Secant Flexural Stiffness and Curvature for CRCP.

Field Checklist: FRC Pavement (ADOT)

Materials

☐ Cement Type II/V or IL approved

☐ SCMs 25–40% (fly ash, slag)

☐ Aggregates clean, ≤ 3% passing #200

☐ Synthetic fibers 9–12 lb/yd³ (or steel 40–75 lb/yd³)

☐ HRWR admixture present and available

Mix Design

☐ w/cm ≤ 0.45 but not less than 0.40

☐ Cementitious ≤ 560 lb/yd³

☐ $f'c$ ≥ max at 4,000 psi at 28days

☐ Residual strength f^{D}_{150} ≥ minimum required (ASTM C1609 and ACI 544-12R)

Placement & Compaction

☐ Slipform paver operational

☐ Slump 0–3 inches

☐ Fibers pre-blended, no balling

☐ Fogging/windbreaks in place

Jointing

☐ Saw-cut plan approved

☐ Saw cuts within 2–8 hours

☐ LTE ≥ 80% verified by FWD

Curing & Protection

☐ 14-day wet cure blankets/poly in place OR

☐ Compound at 1.25× + ≥ 7 days wet cure

☐ Surface protected from traffic

Conclusion

Concrete pavements provide durable infrastructure but remain prone to premature distresses that conventional ME design cannot fully address. FRC offers improved crack control, toughness, and fatigue resistance, yet its integration into pavement design is limited by knowledge gaps in long-term field performance, lab–field correlations, and ADOT-specific guidelines.

This report demonstrates that while classical models provide foundational insight, they oversimplify real behavior by neglecting post-cracking performance. In this study, first-principles mechanics were used as the starting point to better describe distress development and load response, rather than relying solely empirical models. Building on this foundation, design recommendations were formulated that explicitly incorporate the residual tensile capacity of FRC. This enables pavements to be evaluated beyond the point of first cracking, providing a more reliable basis for service life prediction and improved guidance for ADOT specifications. Design recommendations were formulated around post-cracking performance of FRC, which extends serviceability beyond the first-crack limit.

Three application cases were identified for ADOT: (1) plain FRC, replacing conventional reinforcement in situations where constructability is critical; (2) hybrid (RC + fibers), combining reinforcement and fibers to optimize ductility and load capacity; and (3) RCC with fibers, enabling rapid construction with enhanced crack resistance. Together, these approaches demonstrate a pathway for integrating FRC into ADOT specifications, improving long-term performance, reducing maintenance, and enabling more resilient pavement systems.

APPENDIX A: Pavement Distress as Associated with Joints



Blowup: Occurs during hot weather when transverse joints or cracks fail to accommodate slab expansion, often due to incompressible materials blocking joint movement. This leads to compressive stress that causes slab uplift or shattering.



Corner Break: A crack that intersects both joints within half the slab length from the corner. Unlike a corner spall, which is angled and partial-depth, a corner break extends through the full slab thickness. It is typically caused by repeated loading, loss of support, and curling stresses.



Corner Spalling: Deterioration or breaking away of concrete along joints or cracks. A corner spall differs from a corner break in that the spall usually angles downward to intersect the joint, while a break extends vertically through the slab. Spalling can be caused by factors like corrosion of reinforcement, excessive stresses, or D-cracking.



Faulting/Settlement: A difference in elevation across a joint or crack. Mean joint faulting is a predicted distress in AASHTOWare Pavement ME Design for JPCP and is a main distress in Bonded Concrete Overlay of Asphalt (BCOA). Faulting is typically measured across joints. Settlement can contribute to faulting.



Joint Spalling: The deterioration of concrete along the slab edges within approximately two feet (0.6 m) of a joint. It typically occurs at an angle and does not penetrate the full depth of the slab. This distress is caused by high stresses at the joint due to the intrusion of incompressible materials or repeated traffic loads.



LTD Cracking: Longitudinal, transverse, and diagonal (LTD) cracks that split the slab into parts are usually caused by repeated traffic loads, curling, and shrinkage. Small cracks are often due to warping or friction and are not serious. Larger cracks are active and considered major structural problems.



Punchouts: Localized areas of distress in CRCP. Punchouts are predicted by the AASHTOWare Pavement ME Design procedure [10] for CRCP and are related to factors like repeated traffic loading (fatigue), crack load-transfer efficiency, foundation support, and slab temperature. Loss of subbase support can be a fundamental cause, leading to short crack spacing and ultimately punchout failure.



Blowup: A localized buckling or shattering of the pavement, often occurring at transverse joints which crack due to excessive compressive stress.



Shattered Slab: Intersecting cracks split the slab into four or more pieces, usually due to heavy loads or poor support. When this damage is severe, it is called a shattered slab. If all the cracks are within a corner area, it is considered a severe corner break. This mode of cracking can be delayed by the use of fibers in making sure that the plastic hinges that are forming are delayed, or the moment capacity after the cracking is maintained so that the mechanisms of plastic collapse are not functional. The role of fibers will be extending the service life between the first cracking until such states of large-scale deformation.



Shrinkage Cracking: Shrinkage cracks are small, thin cracks less than a meter long that form as concrete sets and cures. They usually stay near the surface and do not go through the entire slab. Fibers have played a significant role on reducing the thermal and shrinkage cracking from opening to a point that the structural integrity is compromised.

APPENDIX B: Field Data of Distress Mechanism in Concrete Pavements

Stress Developed by Shrinkage and Creep

Drying produces a uniform shrinkage and creep strain in a restrained member of length, *L*.

- Without restraint, the member would shorten by $-\varepsilon_{sh}$.
- With restraint, a fictitious tensile load, $+\sigma_{sh}$ is introduced to prevent shortening. In the case of pavement. This restraint is often provided by friction between the slab and the subbase.
- Under this load, creep would cause an elongation, $+\varepsilon_{cr}$.
- To maintain the fixed length, an opposing stress develops, which reduces the net shrinkage stress through stress relaxation, $-\sigma_{cr}$. The total restraint stress left in the pavement is $\pm\sigma_{re}$.

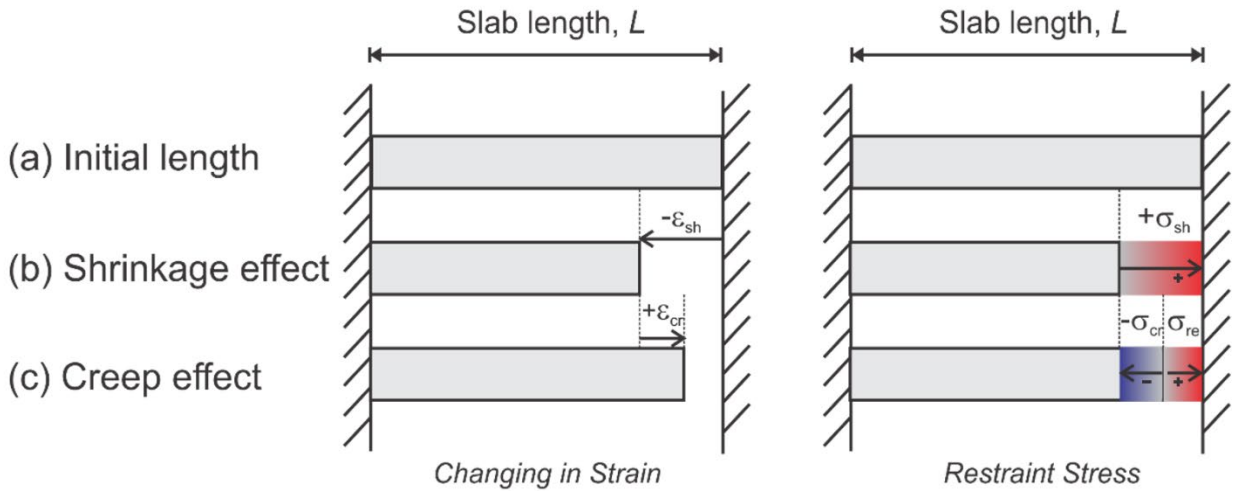

Figure 22. Restrained Shrinkage-Induced Stresses in Concrete.

Evaluation of Plastic Shrinkage

In the mechanism of slab-on-grade, the free-body diagram can be illustrated after the imposed free-shrinkage strain to the model, where z = distance measured from the outside surface inward the specimen; h_s and h_i = humidity (fraction) at the outside and inside surface; and erf(z) = error function. A cubic function is used to relate the free-shrinkage strain to the humidity profile [27].

$$\varepsilon_{sh}(z) = \varepsilon_{sh}(t)\left[1 - h(z)^3\right]$$

Equation 3

The free-shrinkage strain is defined as a function of time and distance z. For simplification to a one-dimensional case, the free-shrinkage strain is assumed to be uniformly distributed across the section.

A finite difference method developed by earlier works [43,47,48] was used to model tension stiffening in RC after cracking. The model simulates how multiple cracks form and open due to shrinkage. Figures 23 through 28 outline the schematic of stress development from shrinkage.

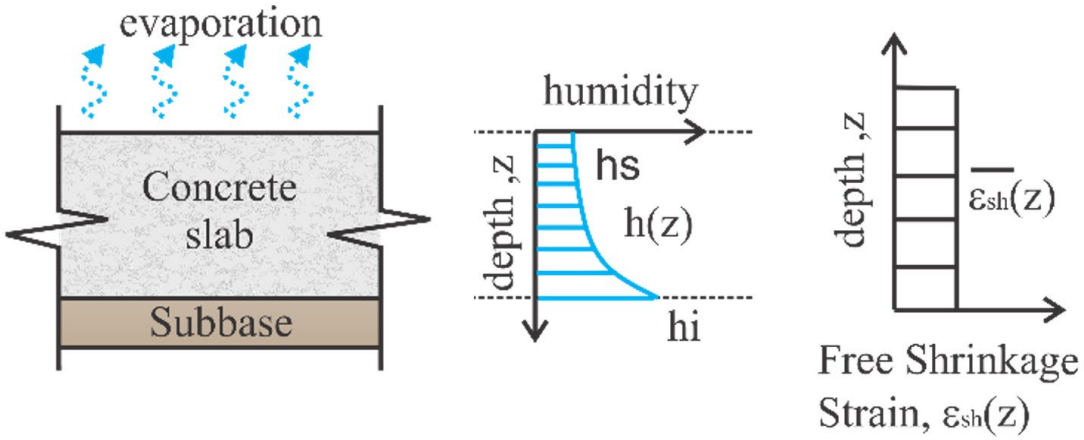

Figure 23. Humidity Profile Throughout the Thickness of the Concrete Slab Simulated by Fick's Law of Diffusion and Idealized Average Free-Shrinkage Strain Applied to the Tension-stiffening Model.

Deformation Terms in the Slab and Force Generated in Slab

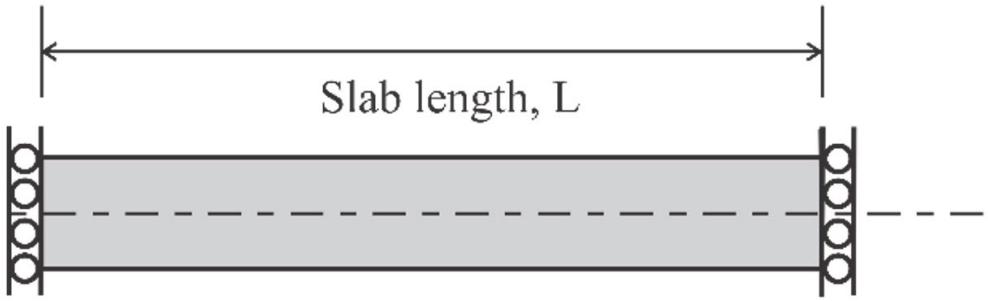

Figure 24. Initial Condition.

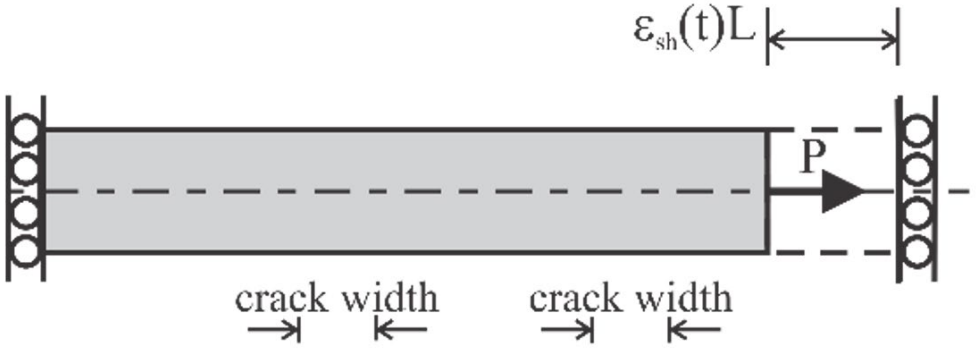

Figure 25. Shrinkage Effect.

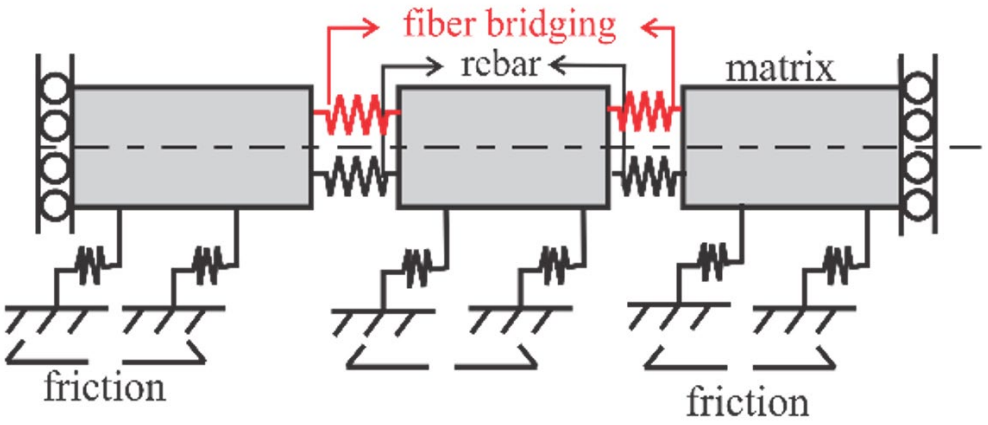

Figure 26. Cracking Sequence.

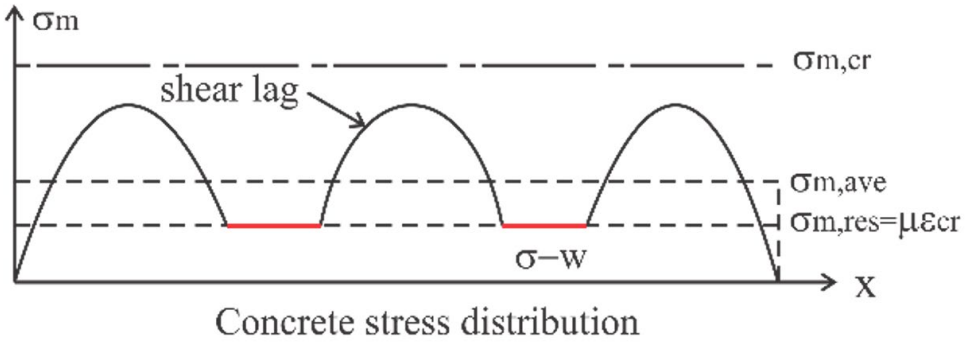

Figure 27. Conceptual Stress Distribution in Concrete.

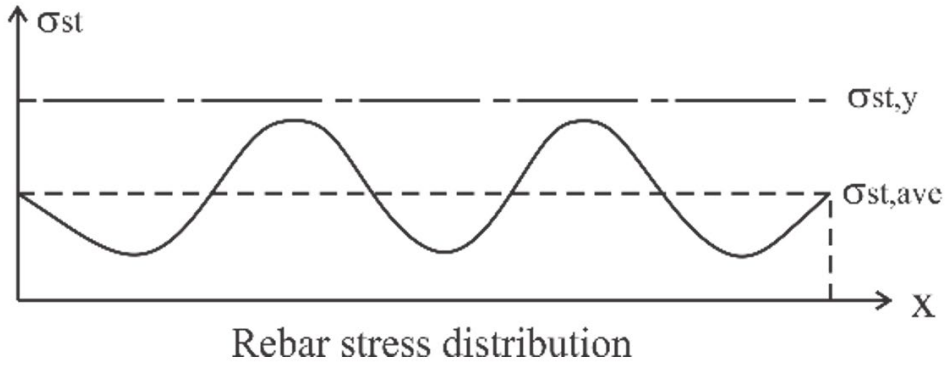

Figure 28. Conceptual Stress Distribution in Rebar.

1. **Initial condition (**Figure 24**):** The slab is restrained at both ends, with rollers allowing vertical movement.
2. **Shrinkage effect (**Figure 25**):** Free shrinkage changes the slab length by $\varepsilon_{sh}(t)$. A fictitious tensile load P is applied to satisfy deformation compatibility.
3. **Cracking sequence (**Figure 26**):** Tensile stress builds until it reaches the matrix cracking strength, $\sigma_{m,cr}$, causing a crack to form. The slab is then represented as two uncracked segments with a crack-opening zone. Additional cracks develop when the tensile stress in the uncracked segments again reaches $\sigma_{m,cr}$.

After the matrix cracks, both the rebar and fiber share the tensile load, transferring it back to the surrounding matrix through bond and bridging actions (refer to Figure 27 and Figure 28).

Characterization of Thermal Loading

The thermal loading regime for characteristic summer conditions is defined by two primary thermodynamic boundary conditions: ambient air temperature and incident solar irradiation flux. These environmental forcing functions are mathematically represented as periodic sinusoidal time-dependent functions that accurately capture the diurnal thermal cycling behavior. The thermal loading functions were derived from three years of continuous field monitoring conducted on a real highway slab with actual geometry from the D1 highway in the Czech Republic [49] (refer to Figure 29 and Figure 30).

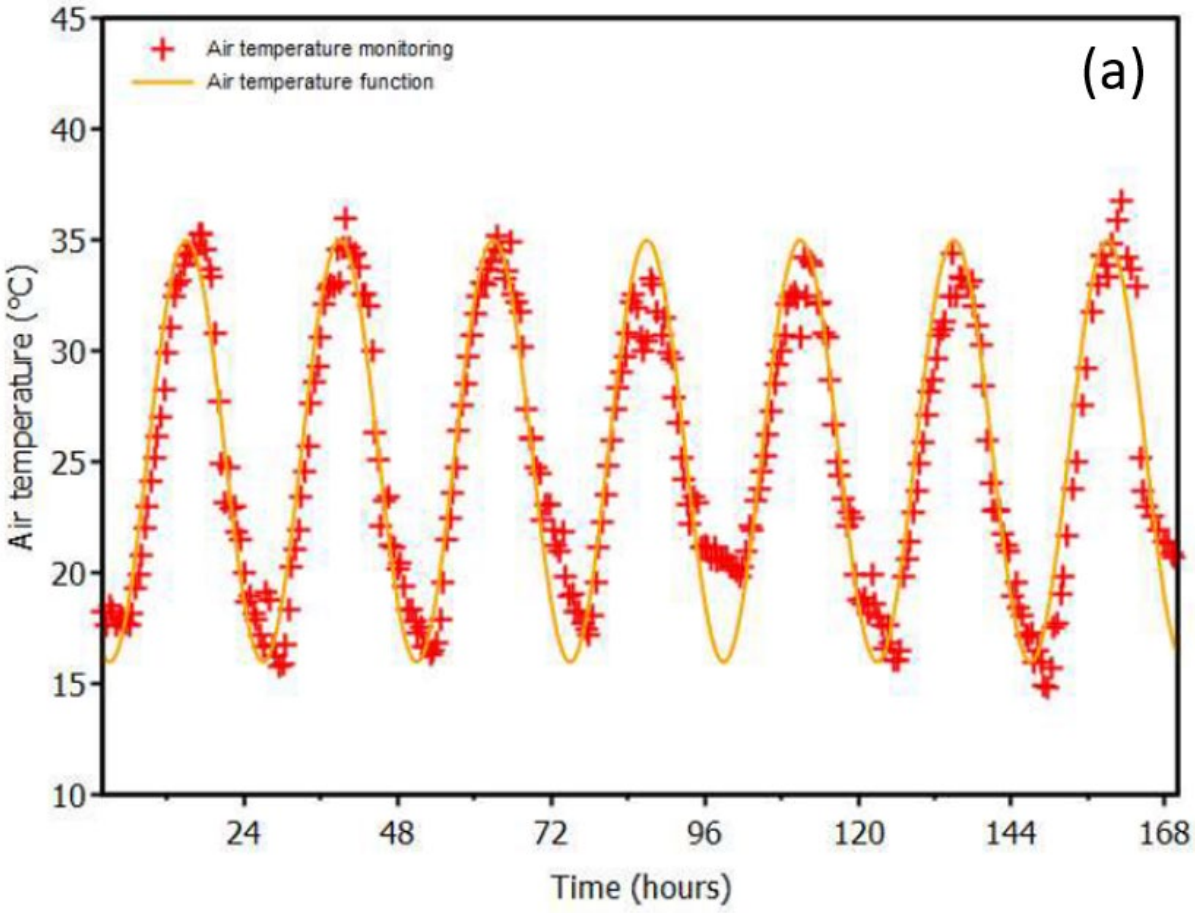

Figure 29. Finite Element Analysis of Concrete Pavement Subjected to Thermal Loading from Ambient Air Temperature [49].

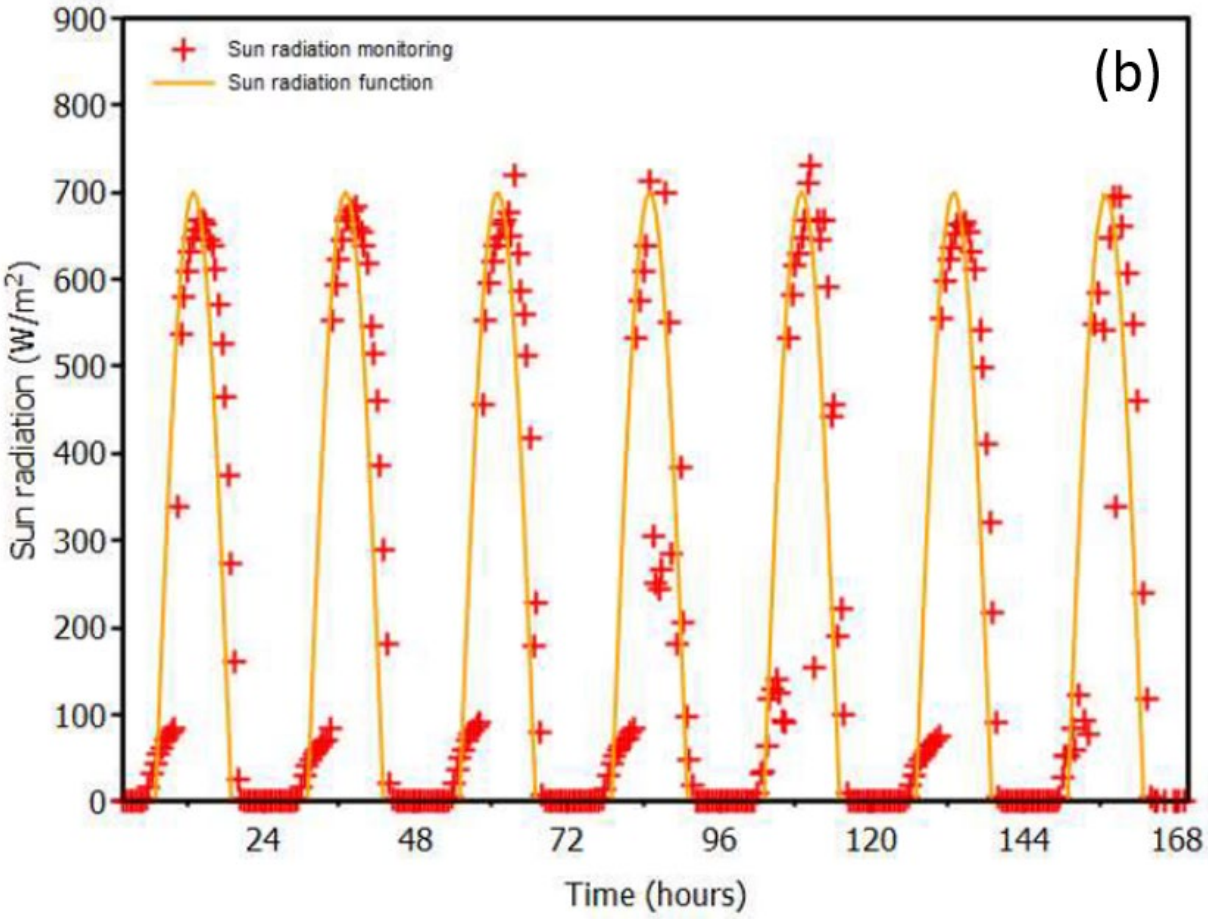

Figure 30. Finite Element Analysis of Concrete Pavement Subjected to Thermal Loading from Solar Radiation [49].

The relationship between air temperature and concrete pavement behavior can be used to develop heat transfer models for pavement analysis. Figure 31 shows a basic diagram of factors affecting heat flux through a pavement structure and the underlying soil. The heat flux at the upper boundary is influenced by solar radiation, convection, long-wave radiation, and surface emissivity [50]. Figure 32 shows the temperature variation at different depths within the slab. Repeated diurnal thermal cycles subject the pavement to alternating compression and tension stresses, creating a form of low-cycle thermal fatigue. The slab experiences maximum compression during peak heating (midday) and tensile stress during cooling periods (nighttime and early morning). Since concrete pavements are constructed with joints and supported on a deformable foundation, they are never in a truly stress-free state. The cumulative effect of these thermal stress cycles, typically exceeding 10,000–15,000 cycles annually, can initiate microscopic damage in the concrete matrix. Over the service life of the pavement (20–40 years), this thermal fatigue can manifest as fine surface warping cracks perpendicular to the pavement edges or contribute to the propagation of larger structural cracks when superimposed with mechanical loading from traffic.

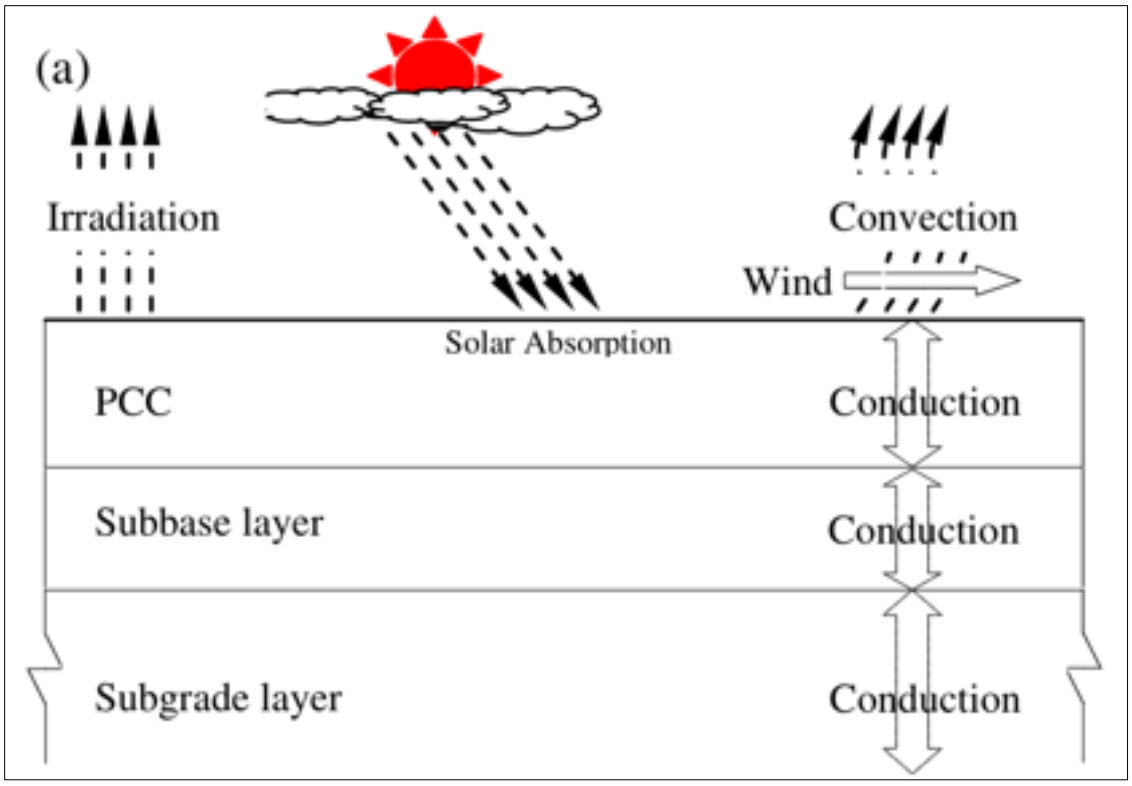

Figure 31. Factors Affecting Heat Transfer in Pavement Structures.

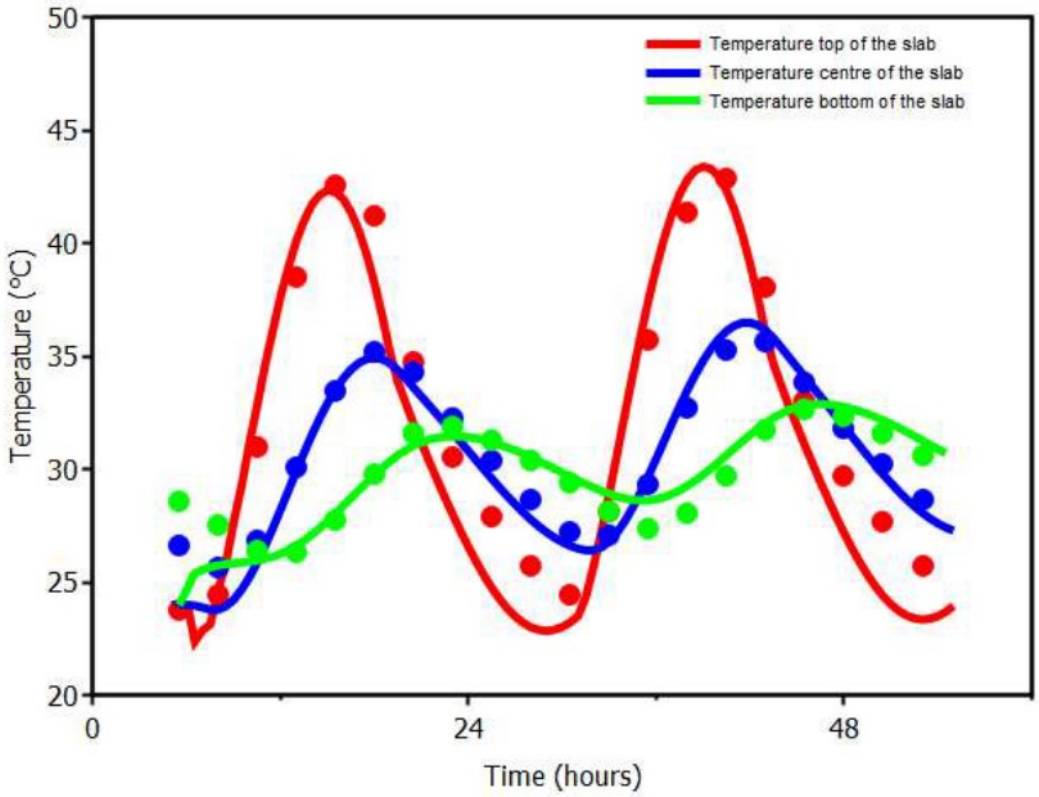

Figure 32. Temperature Calibration of the Thermal Model Against Experimental Data for the Characteristic Summer Cycle at Three Height Levels (Top, Center, Bottom) on the Slab [49,50].

Characterization of Traffic Loading

Park et al. [51] monitored strain variations in CRCP following construction. Due to environmental and temperature changes, the strain exhibited dynamic responses in the concrete at the bottom surface over 24-hour periods. After approximately 120 days of monitoring, a significant increase in strain was observed (Figure 34). At this point, the strain gauge began measuring displacements corresponding to the opening and closing behavior of the crack rather than the actual strains of the concrete slab.

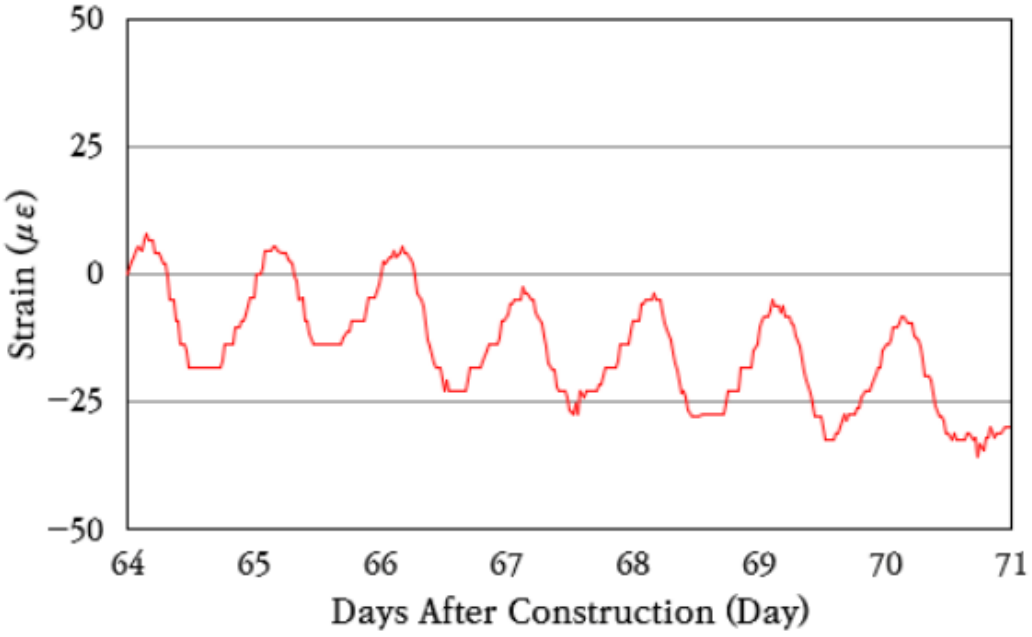

Figure 33. Concrete Strain Variation.

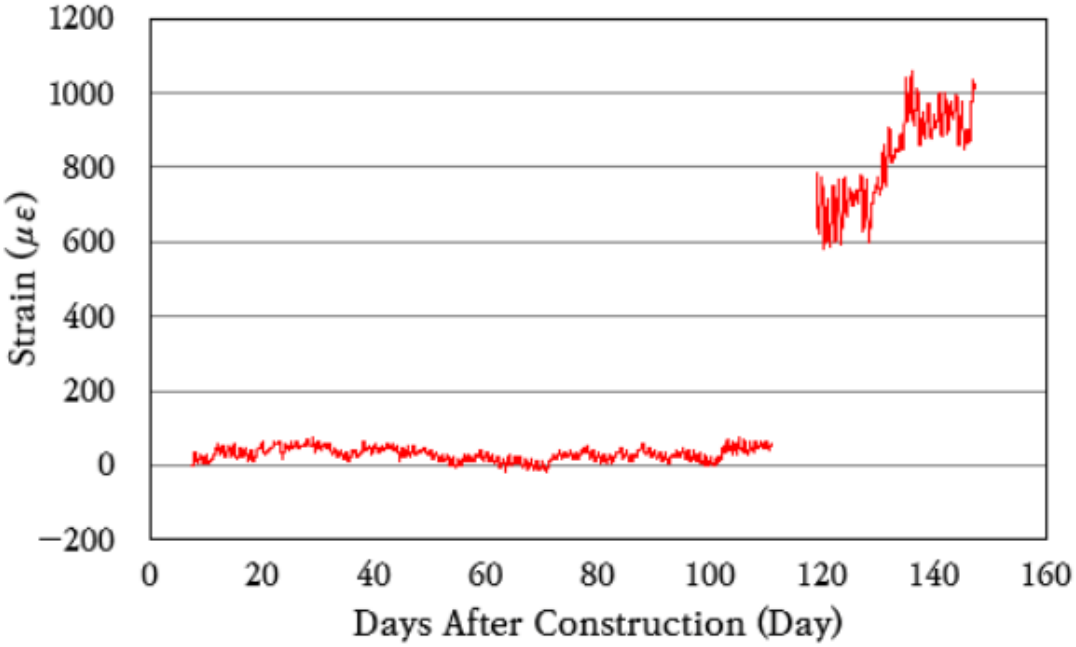

Figure 34. Concrete Strain Variation After Total Curing Period [51].

Darestani et al. [52] investigated the dynamic response of concrete pavements under vehicular loads and demonstrated that maximum strain varies continuously as truck velocity changes while the vehicle moves over the slab. Their findings revealed that the maximum tensile strength typically occurs at transverse joints. The study presented global maximum (GM) stress influence lines for different speeds when a tandem axle dual tire (TADT) load was applied to JPCP. Results showed that speed significantly affects tensile stress values in JPCP, with a speed of 110 km/h increasing the maximum tensile stress by approximately 12 percent compared to static conditions.

The deflection profile demonstrates that all nodes of the slab experience both compression and tension, indicating that design considerations must account for both tensile and compressive resistance in both the top and bottom portions of the slab.

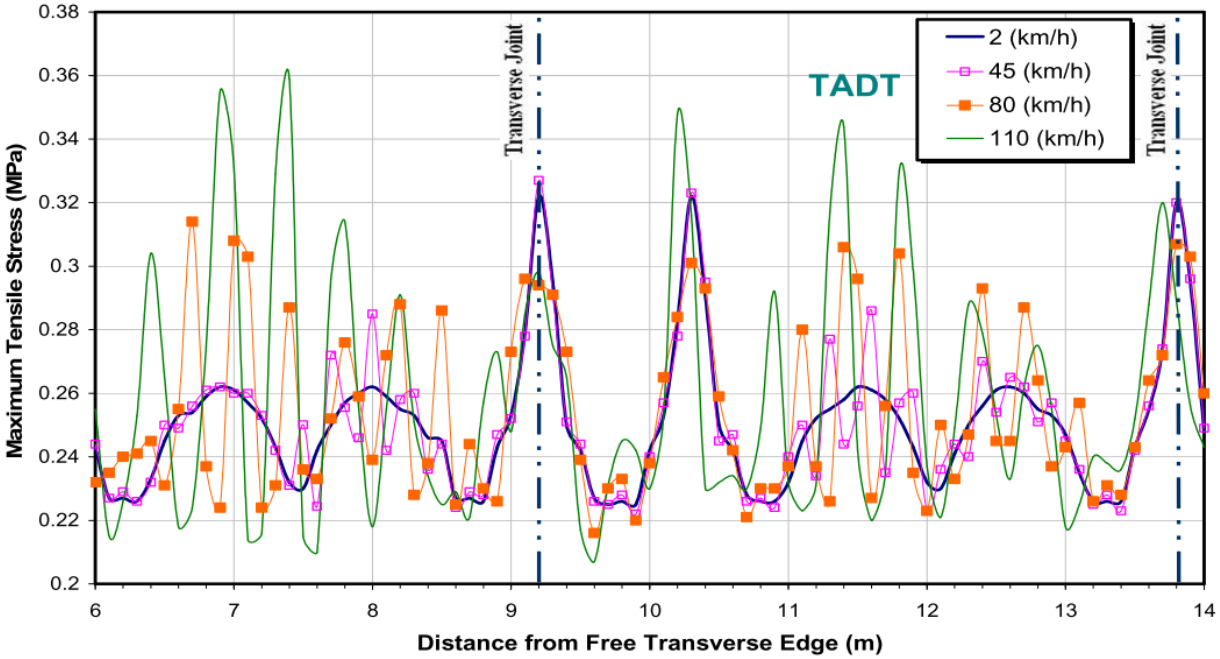

Figure 35. Tensile Stress Influence Line in JPCP [52].

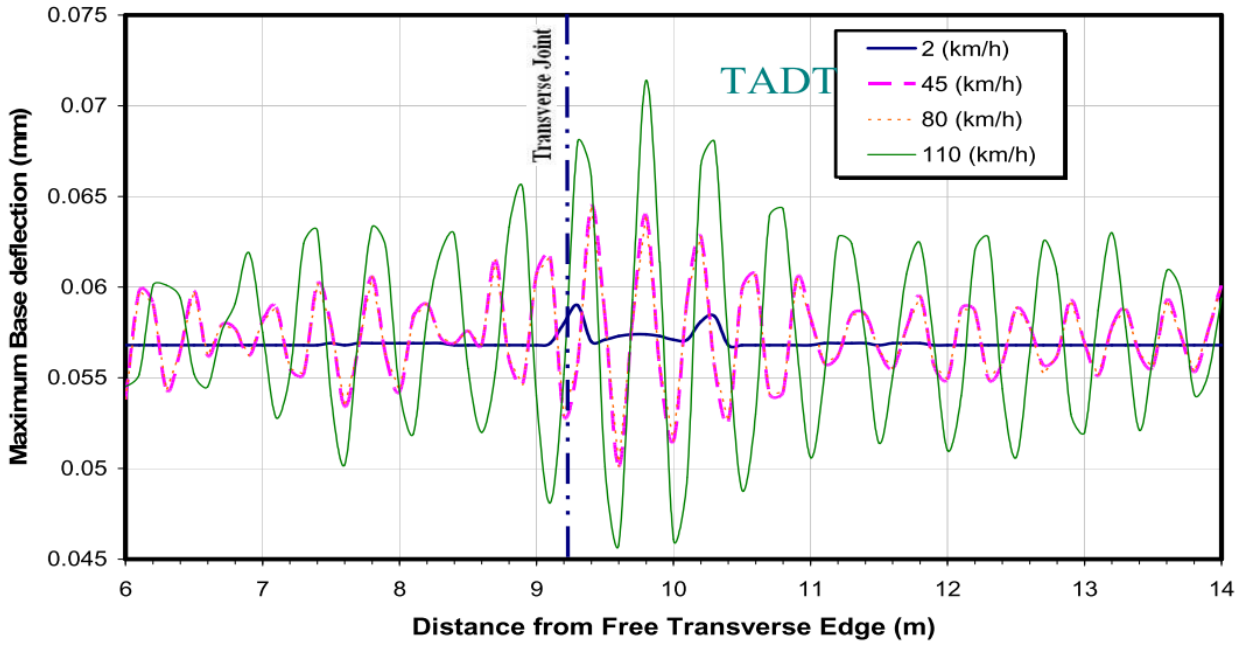

Figure 36. Base Deflection Influence Line in JRCP Due to TADT [52].

Limitations of Current Design Approaches on Dynamic Load

As cracks propagate within the pavement structure, the geometry and stiffness characteristics of individual slabs change substantially, effectively creating two distinct structural systems: the uncracked and cracked states. This transition necessitates careful consideration of load and stress redistribution mechanisms, as the structural behavior fundamentally shifts from the original design assumptions. The redistribution of stresses around crack tips and the altered load paths significantly impact on the overall pavement response. Relying solely on the 1993 AASHTO empirical methodology presents significant challenges when incorporating FRC pavement design, primarily because the dynamic loading effects occur randomly and continuously change based on multiple variables, including truck weight, speed, axle configuration, and subgrade conditions. Understanding the load and unload cycles in the interaction mechanisms between concrete-fiber and concrete-rebar interfaces is crucial for accurately accounting for fatigue response in pavement design. The fiber bridging effect across cracks, the bond-slip behavior of conventional reinforcement, and the synergistic effects of hybrid reinforcement systems all contribute to the complex stress-strain relationship under repeated loading. These mechanisms directly influence crack width control, energy dissipation capacity, and the overall fatigue resistance of the pavement system.

APPENDIX C: The Performance of PP and Steel Fiber Reinforcement

*Disclaimer

The fiber dosage data presented here were obtained from different companies and correspond to fibers with varying strengths, shapes, and concrete mix designs. Therefore, there is no direct correspondence between the reported dosages. The intent of this report is to show the general trends in residual tensile strength as observed in Arizona State University laboratory testing. **These results are not intended for direct use in structural design.** Practicing engineers must conduct appropriate testing (refer to Appendix J) and evaluation for the specific fiber type and dosage prior to implementation in actual structures.

- General Characteristics of Polypropylene (PP) and Steel Fiber
  - Polypropylene (PP) Fibers
    - At lower dosages (7–9 lb/yd³), the first-peak strengths were modest, in the range of 495–557 psi. The residual strength ratios (Re_3) remained around 0.4–0.5, indicating limited post-cracking load-carrying capacity (refer to Figure 37 and Table 4). Toughness values were also relatively low, reflecting rapid loss of stiffness beyond first cracking.
    - At higher dosage (12 lb/yd³), peak strength increased to approximately 605–662 psi, accompanied by improved residual strength values. The toughness at L/150 exceeded 600 lb-in, demonstrating enhanced energy absorption. The equivalent flexural strength reached 520 psi.
  - Steel Fibers
    - Steel fibers of 50–65 lb/yd³ exhibited substantially higher performance compared to PP fibers. First-peak and peak strengths were in the range of 710–780 psi, exceeding PP by approximately 20–30 percent (refer to Figures 37 through 40 and Table 5). Residual capacities were also superior, with residual loads and equivalent flexural strength (f_{e3}) reaching 575–700 psi. The residual strength ratio (Re_3) remained consistently high, between 0.7 and 0.9, indicating stable post-cracking load resistance. Toughness values at L/150 exceeded 800–900 lb-in, nearly double those of PP fibers at similar dosages, confirming the superior energy absorption capability of steel fibers.
- Summary
  - Steel fibers provide significantly greater crack bridging, residual capacity, and toughness compared to PP fibers. The higher stiffness and bond efficiency of steel fibers enable them to sustain post-cracking stresses more effectively, resulting in residual strength ratios (Re_3) consistently above 0.7 and toughness values nearly twice those of PP at comparable dosages. This makes steel fibers particularly suitable for structural applications where long-term load redistribution, fatigue resistance, and energy absorption are critical for pavement.

In contrast, increasing the dosage of PP fibers improves residual strength and toughness primarily through enhanced fiber bridging and crack distribution. However, the improvement in peak strength remains modest because of the relatively low modulus and tensile capacity of PP fibers, which limits their contribution to first-crack resistance. Consequently, PP fibers are more effective as a secondary reinforcement in hybrid section for shrinkage crack control and serviceability enhancement.

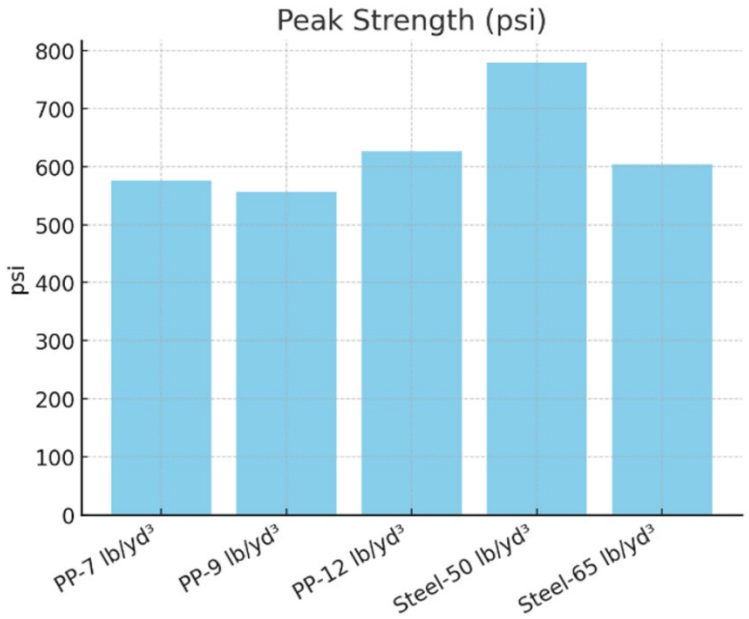

Figure 37. Comparison of Peak Flexural Strength Between Polypropylene (PP) and Steel FRC Tested Under ASTM C1609.

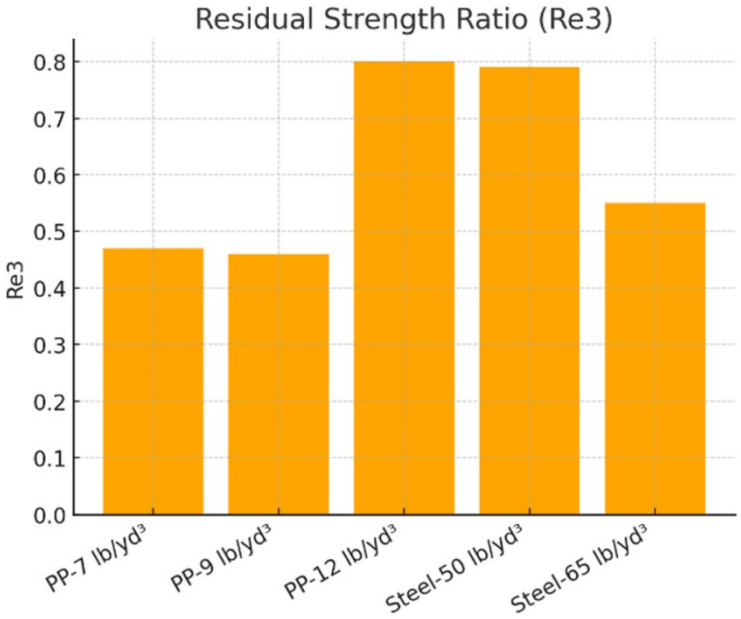

Figure 38. Comparison of Residual Strength Ratio (Re3) Between Polypropylene (PP) and Steel FRC Tested Under ASTM C1609.

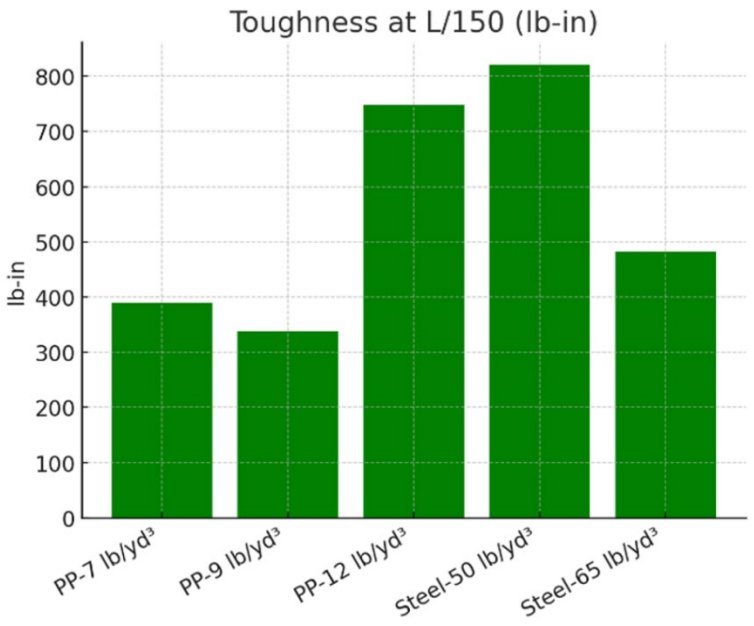

Figure 39. Comparison of Toughness at L/150 Between Polypropylene (PP) and Steel FRC Tested Under ASTM C1609.

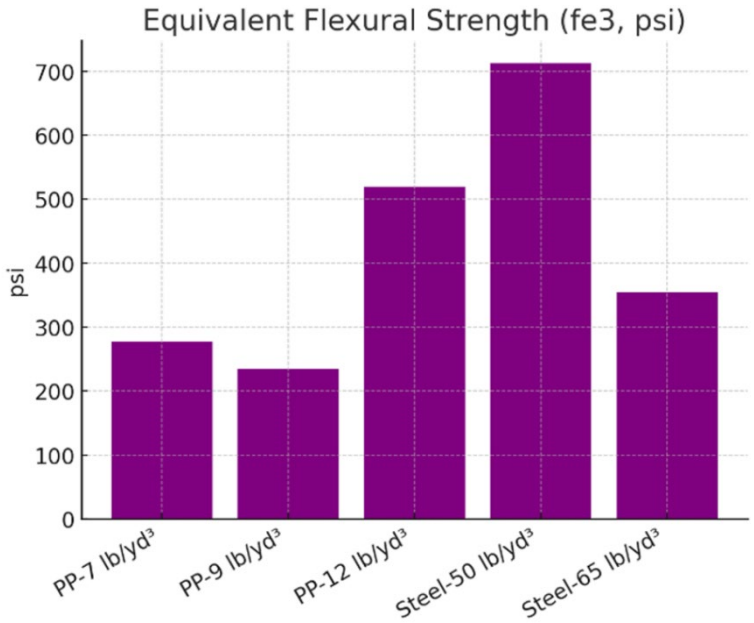

Figure 40. Comparison of Equivalent Flexural Strength (F_{e3}) Between Polypropylene (PP) and Steel FRC Tested Under ASTM C1609.

Summary of Flexural Test Results for Polypropylene (PP) and Steel FRC in Accordance with ASTM C1609

Table 4. Characteristics of Polypropylene Fiber.

Specimen ID	Dosage, V_f	First peak; Load (lbs), P_1	First peak; Strength (psi), f_1	First peak; Deflection (in), δ_1	Peak Load (lbs), P_P	Peak strength (psi), f_P	Peak; Deflection (in), δ_P	Residual load at L/600 (lbs), P^D_{600}	Residual strength at L/600 (psi), f^D_{600}	Toughness at L/600 (lb-in), T^D_{600}	Residual load at L/150 (lbs), P^D_{150}	Residual strength at L/150 (psi), f^D_{150}	Toughness at L/150 (lb-in), T^D_{150}	Equivalent Flexural Strength ratio, $R_{e,3}$	Equivalent Flexure Strength at L/150 (psi), f_{e3}
Fiber A1	7 lbs/yd^3	7032.07	586.01	0.003	7032.07	585.01	0.072	2999.00	249.90	90.40	3370.00	280.90	398.10	0.47	276.60
Fiber A2	7 lbs/yd^3	5948.98	495.75	0.003	6581.63	549.47	0.087	3982.00	331.80	118.30	4344.00	362.00	510.00	0.65	320.50
Fiber A3	7 lbs/yd^3	7451.90	620.99	0.003	7451.90	620.99	0.069	3006.00	250.50	84.40	3100.00	258.30	386.70	0.43	267.30
Fiber A4	7 lbs/yd^3	7172.01	597.67	0.003	7172.01	597.67	0.071	3095.00	258.00	96.90	2991.00	249.20	388.80	0.45	268.60
Mean	—	6690.81	557.57	0.078	6690.81	557.57	0.078	2541.00	211.70	87.10	2815.00	234.60	339.30	0.42	234.60
Std Dev.	—	525.19	43.77	0.011	525.19	43.77	0.011	709.00	59.10	20.70	916.00	76.30	99.40	0.11	68.70
Fiber B1	9 lbs/yd^3	7042.80	586.90	0.003	7042.80	586.90	0.082	2155.00	179.60	73.80	2478.00	206.50	290.80	0.35	202.60
Fiber B2	9 lbs/yd^3	5947.47	495.62	0.002	5947.47	495.62	0.062	1762.00	146.90	65.70	1785.00	148.80	227.70	0.32	158.50
Fiber B3	9 lbs/yd^3	6693.58	557.80	0.003	6693.58	557.80	0.086	3317.00	276.40	99.40	3949.00	329.10	450.90	0.56	312.90
Fiber B4	9 lbs/yd^3	7079.41	589.95	0.003	7079.41	589.95	0.083	2930.00	244.10	109.30	3048.00	254.00	388.00	0.46	269.50
Mean	—	6901.24	575.10	0.072	7059.40	588.28	0.075	3271.00	272.60	97.50	3451.00	287.60	420.90	0.50	283.30
Std Dev.	—	658.40	54.87	0.003	363.20	29.86	0.009	476.00	39.70	14.80	616.00	51.30	59.60	0.10	25.20
Fiber C1	12 lbs/yd^3	7941.69	661.81	0.001	7941.69	661.81	0.001	4193.15	349.43	112.74	5400.41	450.03	565.50	0.59	392.71
Fiber C2	12 lbs/yd^3	7381.92	615.16	0.002	7451.90	620.99	0.002	5643.82	470.32	131.43	5971.72	497.64	721.03	0.81	500.71
Fiber C3	12 lbs/yd^3	7265.31	605.44	0.001	7265.31	605.44	0.001	4901.48	408.46	129.50	4926.18	410.52	629.29	0.72	437.01
Fiber C4	12 lbs/yd^3	7265.31	605.44	0.001	7335.28	611.27	0.001	5776.31	481.36	146.68	6752.79	562.73	748.47	0.86	519.77

Specimen ID	Dosage, V_f	First peak; Load (lbs), P_1	First peak; Strength (psi), f_1	First peak; Deflection (in), δ_1	Peak Load (lbs), P_P	Peak strength (psi), f_P	Peak; Deflection (in), δ_P	Residual load at L/600 (lbs), P^D_{600}	Residual strength at L/600 (psi), f^D_{600}	Toughness at L/600 (lb-in), T^D_{600}	Residual load at L/150 (lbs), P^D_{150}	Residual strength at L/150 (psi), f^D_{150}	Toughness at L/150 (lb-in), T^D_{150}	Equivalent Flexural Strength ratio, $R_{e,3}$	Equivalent Flexure Strength at L/150 (psi), f_{e3}
Mean	—	7463.56	621.96	0.001	7498.54	624.88	0.001	5128.69	427.39	130.09	5762.77	480.23	666.07	0.75	462.55
Std Dev.	—	323.46	26.96	0.001	305.29	25.44	0.001	732.95	61.08	13.89	786.34	65.53	84.22	0.12	58.48
Fiber D1	14 lbs/yd^3	8514.58	709.55	0.0012	8534.02	711.17	0.001	6070.15	505.85	151.78	8107.52	675.63	828.31	0.81	575.22
Fiber D2	14 lbs/yd^3	7097.67	591.47	0.0298	8645.77	720.48	0.103	5465.93	455.49	47.86	8387.25	698.94	558.37	0.66	387.75
Fiber D3	14 lbs/yd^3	7150.15	595.85	0.0229	7176.38	598.03	0.023	4595.72	382.98	85.48	7688.16	640.68	673.26	0.78	467.54
Fiber D4	14 lbs/yd^3	7303.21	608.60	0.0275	9693.88	807.82	0.097	5955.40	496.28	79.83	9269.69	772.47	688.86	0.79	478.37
Mean	—	7516.40	626.37	0.020	8512.51	709.38	0.056	5521.80	460.15	91.24	8363.15	696.93	687.20	0.76	477.22
Std Dev.	—	671.14	55.93	0.013	1032.65	86.05	0.052	670.68	55.89	43.63	669.17	55.76	110.62	0.07	76.82

Table 5. Characteristics of Steel Fiber.

Specimen ID	Dosage, V_f	First peak; Load (lbs), P_1	First peak; Strength (psi), f_1	First peak; Deflection (in), δ_1	Peak Load (lbs), P_P	Peak strength (psi), f_P	Peak; Deflection (in), δ_P	Residual load at L/600 (lbs), P^D_{600}	Residual strength at L/600 (psi), f^D_{600}	Toughness at L/600 (lb-in), T^D_{600}	Residual load at L/150 (lbs), P^D_{150}	Residual strength at L/150 (psi), f^D_{150}	Toughness at L/150 (lb-in), T^D_{150}	Equivalent Flexural Strength ratio, $R_{e,3}$	Equivalent Flexure Strength at L/150 (psi), f_{e3}
Fiber E1	50 lbs/yd^3	9635.57	802.96	0.001	9664.72	805.39	0.001	7940.46	661.70	218.53	6998.13	583.18	888.74	0.77	617.18
Fiber E2	50 lbs/yd^3	8173.47	681.12	0.001	8199.71	683.31	0.001	5798.82	483.23	168.02	5005.91	417.16	660.28	0.67	458.53
Fiber E3	50 lbs/yd^3	9489.80	790.82	0.001	9518.95	793.25	0.001	9074.01	756.17	257.25	7808.66	650.72	1018.06	0.89	706.99
Fiber E4	50 lbs/yd^3	10093.29	841.11	0.001	10198.25	849.85	0.001	6274.27	522.86	189.85	5514.11	459.51	716.87	0.59	497.83
Mean	—	9348.03	779.00	0.001	9395.41	782.95	0.001	7271.89	605.99	208.41	6331.70	527.64	820.99	0.73	570.13
Std Dev.	—	824.17	68.68	0.000	848.93	70.74	0.000	1512.15	126.01	38.57	1297.65	108.14	163.40	0.13	113.47
FiberF1	56 lbs/yd^3	7241.98	603.50	0.129	7265.31	605.44	0.13	4270.09	355.84	135.36	3714.62	309.55	482.04	0.55	334.75
Mean	—	—	—	—	—	—	—	—	—	—	—	—	—	—	—
Std Dev.	—	—	—	—	—	—	—	—	—	—	—	—	—	—	—

APPENDIX D: Review of Several DOT Specifications for FRC Applications

Applications of FRC-Based Design in Pavements by Several States

Various DOTs and FHWA funded projects have looked at adopting fibers in rigid pavements. An overview of their approach and findings are necessary to draw some conclusive learnings that can be translated to design in some fundamental sense. Their summary is as follows:

TxDOT/FHWA Study: Fiber in CRCP (FHWA/TX-07/0-4392-2) [53]

Purpose: This two-year research project, conducted in cooperation with the TxDOT and the FHWA, investigated the use of fiber reinforcement to address pavement distresses, particularly spalling, in CRCP containing siliceous river gravel. The goal was to determine whether fibers could reduce crack width, increase toughness, and mitigate plastic shrinkage.

Dosage Determination: The study focused on low-dosage fibers due to economic feasibility, aiming for the greatest improvement in spalling performance at the lowest cost. Both steel and synthetic fibers with varying geometries were evaluated. Specific dosages included steel fibers (SF1 at 25 and 40 lb/yd^3) and synthetic fibers (SnF1 at 4 and 6 lb/yd^3, SnF2 at 1.5 lb/yd^3).

Pavement Design Properties: Field trials involved a 10-inch thick, 10-foot wide CRCP section on a frontage road, with standard Grade 60 steel reinforcement (No. 6 longitudinal bars at 8.25-inch spacing, No. 5 transverse bars at 36-inch spacing) which was not altered due to fiber addition, as fibers were for durability enhancement. A second field study used a slipform paver, with adjustments to the mix (replacing coarse aggregate with fine aggregate, increasing water and air entraining agent) to maintain workability for stiffer mixes required by slipform paving.

Conclusions and Unclear Aspects: Within the two-year timeframe, fiber reinforcement appeared to prevent or limit spalling in field test sections compared to control sections. Lab tests showed fibers significantly improved flexural toughness but had minimal impact on other hardened properties like compressive or flexural strength before cracking. Steel fibers generally provided greater toughness and residual strength than synthetics. While fibers were found to be constructible, finishing issues like fibers protruding from the surface were observed, particularly with some synthetic and steel fibers. The long-term efficacy of fibers in reducing spalling remains unclear due to the short study duration, with future monitoring strongly recommended. Permeability tests for steel fiber sections were flawed due to the fibers' conductivity.

Illinois DOT/FHWA Study: Design and Concrete Material Requirements for UTW (FHWA-ICT-08-016) [54]

Purpose: This research aimed to provide the IDOT with an enhanced design method and guidelines for UTW, focusing on material selection and construction. The core objective was to utilize structural fibers to reduce the required slab thickness, limit crack widths, expand slab sizes, and extend the service life of fractured slabs in UTW projects.

Dosage Determination: The study proposed a Residual Strength Ratio (R_{150}), calculated from ASTM C1609-07, to characterize FRC performance, with a recommended minimum of 20 percent for all UTW mixtures. The exact fiber type and dosage are not prescribed; instead, the R_{150} performance value must be met through testing.

Pavement Design Properties: UTW projects involved concrete overlays on existing hot mix asphalt (HMA) pavements. Structural fibers are highly recommended for concrete thicknesses of four inches or less, and considered for four to six inches. The minimum UTW thickness is three inches, and the minimum existing HMA thickness is 2.5 inches. Early UTW projects (e.g., UIUC parking lots) used 3 lb/yd³ of straight synthetic fibers in 3.5-inch thick slabs with 4-foot joint spacing. The design procedure is based on fatigue cracking at the corner loading position.

Conclusions and Unclear Aspects: Structural fibers are recommended to allow for reduced concrete slab thickness or increased joint spacing. Fibers enhance slab capacity, reduce crack propagation, and maintain continuity across cracks. The study found that synthetic FRC generally showed more repeatable performance than steel FRC. High cement content in concrete was linked to early-age distress and de-bonding. While fibers can help maintain a small crack width to preserve aggregate interlock, they also make it more difficult for initial saw-cut cracks to propagate early.

VDOT/FHWA Study: High-Performance FRC in a Bridge Deck (FHWA/VTRC 06-R11)

Purpose: This research by the Virginia Transportation Research Council, in cooperation with Virginia DOT and FHWA, aimed to compare high-performance FRC with conventional concrete in a bridge deck. The primary expectation was for FRC to increase toughness, provide residual strength, and minimize cracking (plastic shrinkage, drying shrinkage, settlement, loading, and environmental factors), especially negative moment cracks over piers.

Dosage Determination: A specific FRC mix with 8.75 lb/yd³ of polypropylene-polyethylene blend synthetic fibers was used. The FRC was specified to achieve a flexural strength of 600 psi and a residual strength of 400 psi.

Pavement Design Properties: The study focused on a 26-foot wide section of a continuous steel plate girder bridge deck (Route 11 over Maury River, Virginia), where FRC was placed over one of four piers. The deck concrete was designed for a minimum 28-day compressive strength of 4,000 psi and a maximum permeability of 2500 coulombs.

Conclusions and Unclear Aspects: Over a five-year monitoring period, the FRC sections exhibited fewer and narrower cracks compared to the control sections, despite higher shrinkage in FRC specimens. The permeability of FRC was comparable to conventional concrete. The report highlighted that workability lost due to fibers should be recovered using high-range water-reducing admixtures (HRWRA), not additional water, to avoid compromising durability. The study concluded that fibers could control cracking and minimize reinforcement corrosion, extending service life and reducing maintenance. Continued evaluation of fibers in continuous decks, especially over steel beams, was recommended.

Iowa DOT/IHRB Study: Field Performance of FRC Overlays (IHRB Project TR-816) [55]

Purpose: This field investigation in Iowa evaluated the performance of FRC overlays, specifically their impact on pavement smoothness, load-transfer efficiency (LTE), curling/warping, and the potential to extend joint spacing.

Dosage Determination: The FRC overlay projects in Iowa generally used a fiber dosage rate of 4 lb/yd³ (about 0.3 percent by volume), selected to achieve a residual strength of 150 psi. A specific joint-free test section utilized a higher macrofiber content of 7.5 lb/yd³ (about 0.5 percent by volume), with an increased cementitious content to maintain workability.

Pavement Design Properties: The study focused on thin concrete overlays, typically four to six inches thick, mainly concrete-on-asphalt (COA) overlays (both bonded and unbonded) and some concrete on concrete (COC) unbonded overlays. A notable design was a 636-foot section of 6-inch thick FRC overlay designed without transverse joints in Worth County, Iowa.

Conclusions and Unclear Aspects: The study found that fiber reinforcement did not appear to have a significant impact on load transfer, smoothness, or curling and warping at the investigated sites. However, fibers were confirmed to provide residual strength, enhancing fatigue life, and contribute to long-term durability by keeping cracks and joints tight. Fibers were determined to potentially allow for extending design life or reducing overlay thickness. The study highlighted the critical importance of the bond between concrete and asphalt, even in designs not explicitly intended to be bonded. The poor performance of dominant joints in the joint-free sections underscored the challenges of entirely eliminating transverse joints.

ADOT/FHWA Study: Steel FRC for Transportation Infrastructure (FHWA/AZ-18-705) [56]

Purpose: This study, sponsored by the ADOT, investigated the application of Steel FRC (SFRC) in pavements and bridge decks to reduce traditional steel reinforcement and enhance service-level performance. The goal was to control cracking, improve tensile strength, and increase post-cracking ductility.

Dosage Determination: Two main fiber volume philosophies were explored: 2.0 percent by volume for maximum strength and ductility gains, and 0.5 percent by volume to meet service and strength limit states while using traditional steel reinforcement. These were based on prior findings.

Pavement Design Properties: The report reviewed applications for slab-on-grade pavements and bridge decks. The pavement case study referenced Folliard et al. (2006) for a Houston CRCP (10 inches thick, steel-reinforced with 0.2–0.3 percent steel fibers by volume). For bridge decks, the study investigated structural components, including a full-scale SFRC bridge deck specimen that was 7.5 inches deep with #4 rebar at 9-inch spacing, and 0.5 percent fibers by volume.

Conclusions and Unclear Aspects: Increased fiber volume generally decreased concrete workability. SFRC showed substantial increases in tensile strength and ductility, but minimal effect on compressive strength. For slab-on-grade, the analysis indicated that average crack width and punchout decreased with increasing steel fiber content, with improvements becoming gradual after 0.5 percent fiber content. The study recommended 0.5 percent hooked steel fibers for slab-on-grade. For bridge decks, SFRC increased moment capacity and could be used in combination with reduced steel and/or slab depth to meet service limit states. SFRC also nearly doubled the shear capacity of plain RC slabs. The Mechanistic-Empirical Pavement Design Guide (MEPDG) predictions for crack width slightly overestimated the fiber reinforcing effect in the Houston case.

MoDOT/FHWA Study: FRC for Bridge Deck Overlays (CMR 23-003) [57]

Purpose: This project, prepared for the Missouri Department of Transportation (MoDOT), aimed to identify best practices for FRC overlay mixtures for bridge decks by reviewing existing research and conducting a laboratory program. The goal was to establish performance criteria and evaluate protocols for FRC products.

Dosage Determination: Twelve fiber types (synthetic and steel) were tested at three dosage levels (low, medium, high) based on manufacturer recommendations. To achieve a 20-percent residual strength (a performance criterion): synthetic fibers required 3.5–8 lb/yd^3 (0.25–0.53 percent by volume), while steel fibers required 11–64 lb/yd^3 (0.08–0.48 percent by volume). Generally, a lower volume of steel fibers was needed compared to synthetic fibers to achieve the same residual strength, especially for deformed steel fibers.

Pavement Design Properties: The study focused on FRC overlays for bridge decks, evaluating fibers in a representative concrete mixture compliant with MoDOT specifications.

Conclusions and Unclear Aspects: FRC can be incorporated into concrete mixtures to achieve workable mixes with minimal changes to underlying concrete mixture proportions. A good correlation between flexural toughness and fiber dosage was observed. Higher fiber dosages significantly improved resistance to restrained shrinkage cracking. While fibers led to improved crack resistance, they generally caused a slight decrease in compressive strength (up to 25 percent in some cases) and varied effects on the MOE. The high variability in strength and MOE results indicated that a generalized relationship between these properties and fiber characteristics could not be established. The study emphasized that FRC can offer similar strength and durability to traditional concrete with improved crack resistance, making it ideal for preventing reflection cracks in overlays.

Nationwide State DOTs' Specifications for the Use of Macrofibers in Bridge Decks and Overlays for Bridge Decks [57]

- **CA:** ≥ 1 lb/yd³ micro, ≥ 3 lb/yd³ macro-polymer fibers.
- **CO:** Macro/hybrid polyolefin ≥ 4 lb/yd³ or the Approved Product List's minimum; may reduce if ASTM C1609 fres ≥150 psi; meets ASTM C1116/D7508;
- **DE:** Type III; L 0.5–1.5 in; 1.5 lb/yd³ (or 0.5 lb/yd³ nylon).
- **FL:** Polymeric/steel/basalt; ARS ≥215 psi (ASTM C1399) from five beams.
- **GA:** Virgin polyolefin macros: L ≥ 1.5 in, AR 45–150, ARS ≥150 psi (C1399), ≥3 lb/yd³.
- **ID:** Type III; ≥1.5 lb/yd³ (silica-fume overlays).
- **IL:** Recommend 3 lb/yd³ synthetic; no mesh-type macro; L_max macro 1.75 in, L_min micro 0.75 in; mono or bundled mono L 1.0–2.5 in, AR ≤ 150; R150,3 ≥20% (IL Mod C1609); max. 5.0 lb/yd³ unless field proves workability/no clumping.
- **LA** (patching): Steel A820 Type I/II; L 1–1.5 in; AR 40–60; 85–90 lb/yd³.
- **MI:** Virgin PP collated 2 lb/yd³ (silica-fume overlays), L 0.75 in, Type III.
- **MN:** Type III; ≥4 lb/yd³; RDT,150 ≥25% (C1609); CRR ≥85% (C1579).
- **MS:** 100% virgin PP, L 0.75 in, Type III; dosage to achieve R150,3 =20% (C1609); bridge decks use 1.25× approved rate.
- **MO:** Stainless steel fibers, L ~2 in, A820, ≥2000 fibers/lb, AR 40–60, no hooks/90° bends; 1-in Helix allowed.
- **NH:** Synthetic from the Qualified Product List (QPL); 7 lb/yd³ unless approved otherwise.
- **NM:** Steel A820 or synthetic C1116 if specified.
- **NY:** Synthetic fibrillated, C1116 Type III; acceptance via Approved List + cert.
- **NC:** Macro-synthetic virgin polyolefin, ASTM D7508; L ≥ 1.5 in, AR 45–150; f_t ≥40 ksi, E ≥400 ksi (ASTM D3822); dosage per manufacturer to meet ARS ≥ that of replaced steel and ≥5 lb/yd³; air 4.5% ±1.5%; *f'c* ≥4000 psi @28 d; ASTM C995 flow 7–25 sec.
- **OK:** PP (100% PP, collated/fibrillated/graded), Type III; Steel A820 Type II, AR 30–60, L 1⅛–2 in.
- **OR:** Synthetic from QPL (Sec 02045) at QPL rate; no packaged fiber clumps; furnish synthetic polyolefin macro fibers.
- **PA:** PP Type III 4.13; perf ref C1018 Level 1 + Residual Strength; mono/bundled mono L 1.0–2.5 in, AR ≤ 150; $R_{150,3}$ ≥20% (IL Mod C1609); ≤ 5.0 lb/yd³ unless workability proven.
- **UT:** Macro-synthetic 4 lb/yd³; $R_{e,3}$ ≥25% (C1609).
- **VA:** Steel and synthetic from the Approved Products list

IDOT: Performance and Design of CRCP (FHWA-ICT-24-009) [58]

Purpose: This report focused on updating and recalibrating IDOT CRCP design procedure to a ME method and developing designs for unbonded CRCP overlays. The study involved reviewing CRCP performance data, including punchouts, crack spacing, and crack widths.

Scope and Relevance to Fibers: This report primarily focuses on traditional CRCP design with steel reinforcement and its performance. While it mentions design features like "active crack control," it does not delve into the use or effects of fiber reinforcement in CRCP designs. Therefore, specific details on fiber dosage or cross-section properties related to fiber use are not within this report's scope.

Conclusions and Unclear Aspects: The study updated CRCP design framework based on field performance data, noting factors like concrete CTE correlating with spalling (lower CTE means less spalling) in Texas. It also highlighted that stabilized bases and tied concrete shoulders led to minimal distress, while asphalt shoulders and heavy truck traffic resulted in punchouts. The report's conclusions are pertinent to traditional CRCP design rather than FRC applications.

Indiana DOT Specification for Synthetic Fibers (sample specification sheet)

Synthetic Fibers for Use in PCC

General: Synthetic, non-metallic, fibers are used for concrete three-dimensional reinforcement to promote post-cracking control and improve the long-term performance of PCC. Synthetic fibers shall be introduced into PCC mixtures at a dosage subject to required properties in Table 6, a dosage no less than 4 lb/yd3, at the batching plant or a ready-mix truck

Acceptance: Synthetic fibers for use in PCC shall be selected from the Department’s list of approved materials. A list of approved synthetic fibers will be maintained by the Department. Synthetic fibers may be added to the approved list by completing the requirements in ITM 806, Procedure F.

Requirements: Synthetic fibers shall be Type III in accordance with ASTM C 1116 and ASTM D 7508 with the following exceptions:

- Aspect Ratio – Length/Equivalent Diameter, min: 70, max. 100
- Tensile Breaking Strength, min.: 70,000 psi
- Modulus of Elasticity, min.: 800,000 psi
- Length: 1.5–2.25 in

Acceptance Testing of Hardened FRC: Testing in accordance with ASTM C 1609 and ASTM C 1579 shall be performed by a recognized laboratory regularly inspected by the Cement and Concrete Reference Laboratory for PCC materials and for specifications listed in this section.

Table 6. Required Hardened FRC Properties.

Physical Test	Specification	Requirement
Equivalent Flexural Strength Ratio (RT150)*	ASTM C1609	Minimum of 25%
Crack Reduction Ratio (CRR)	ASTM C 1579	Minimum reduction >85%

* The specimens shall be tested when the concrete flexural strength at first crack (f1) is a minimum of 600 psi.
For 6 x 6 x 20 in FRC beam the maximum required net deflection value of 1/150 of the 18 in span length is 0.12 in.

APPENDIX E: Conventional Concrete Pavement Design Approaches

Sensitivity Analysis of ADOT Specifications for Rigid Concrete Pavements

The 1993 AASHTO Rigid Pavement Design Equation (Equation 4) is as follows:

$$\log_{10}(W_{18}) = Z_R \cdot S_o + 7.35 \cdot \log_{10}(D+1) - 0.06 + \frac{\log_{10}\left(\frac{\Delta PSI}{4.5-1.5}\right)}{1+\frac{1.624\times10^7}{(D+1)^{8.46}}} + (4.22 - 0.32 \cdot p_t) \cdot \log_{10}\left(\frac{S_c' \cdot C_d \cdot (D^{0.75} - 1.132)}{215.63 \cdot J \cdot \left(D^{0.75} - \frac{18.42}{(E_c/k)^{0.25}}\right)}\right)$$

Equation 4

Where

W_{18}	Design ESALs (18-kip Equivalent Single Axle Loads)
D	Slab thickness (inches)
Z_R	Standard normal deviate for reliability (typically −1.645 for 95%)
S_o	Overall standard deviation (usually 0.35–0.45)
ΔPSI	Loss in serviceability index (typically 4.5 − 2.5 = 2.0)
p_t	Terminal serviceability index (typically 2.5 for highways)
Sc’	MOR of concrete (psi)
C_d	Drainage coefficient (0.80–1.0 based on drainage quality)
J	Load-transfer coefficient (1.0 to 3.2 depending on joint condition)
E_c	Elastic modulus of concrete (psi)
K	Modulus of subgrade reaction (psi/in)

The effect of each parameter are further studied below based on some assumed values unless otherwise varied for the parametric study:

- Traffic Loading
  - Data-year average annual daily traffic: e.g., 20,000 veh/day
  - Annual growth rate (r): e.g., 0.03 (3 %)
  - Years to opening (n): e.g., 3 years
  - Vehicle-class distribution (VCD1…VCD13): percentages for FHWA classes 1–13
  - Truck-load factors (TLF1…TLF13): rigid pavement ESAL equivalencies (Table A-6)
  - Design life (Y): 20 years
  - Directional distribution (DD): 0.50
  - Lane distribution (DL): e.g., 0.90

$$AADT_{build} = AADT_{data}(1+r)^n$$ (a) **Equation 5**

$$G = \frac{(1+r)^Y - 1}{r}$$ (b)

$$N_c = AADT_{build,c} \times G \times 365$$ (c)

$$W_{18} = \left(\sum_{c=1}^{13} N_c \, TLF_c\right) \times DD \times DL$$ (d)

$$W_{18} = 1.11 \times 10^8$$ (e)

- Reliability & Performance
  - Standard normal deviate (Z_R): –1.645 (95 % reliability)
  - Combined standard error (S_o): 0.25
  - Initial serviceability (P_o): 4.2
  - Terminal serviceability (P*t*): 1.5
- Concrete & Drainage
  - Compressive strength (f_c): 5 000 psi
  - Elastic modulus (E_c): 57000*($f_c^{0.5}$) psi
  - Drainage coefficient (C_D): 1.17 (“good” drainage)
  - Load-transfer coefficient (J): 2.8 (plain joint with dowels)
  - Modulus of rupture (Sc’): 670 psi
- Subgrade Support
  - Resilient modulus (M_R): 15000 psi
  - Initial k-value (k_0): M_R/19.4 pci
  - Loss of support (LS): 0 (none)
  - Corrected k-value (k_{corr}): via ADOT Fig 2-6

Parametric Study of AASHTO (1993) Design Equation

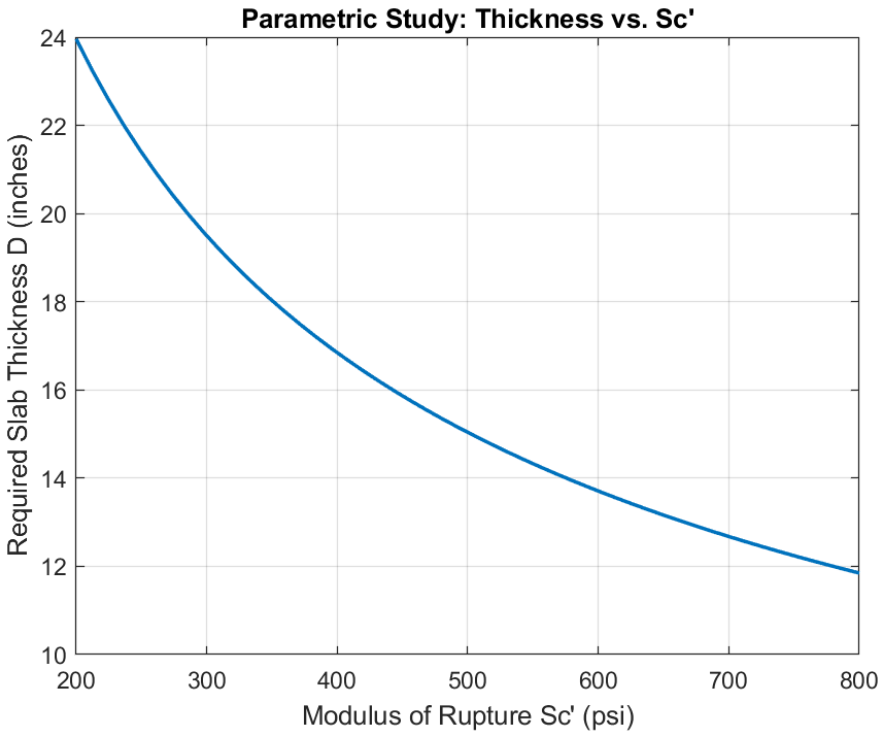

Studies the effect of concrete modulus of rupture Sc' varying from 200 psi to 800 psi on required slab thickness.

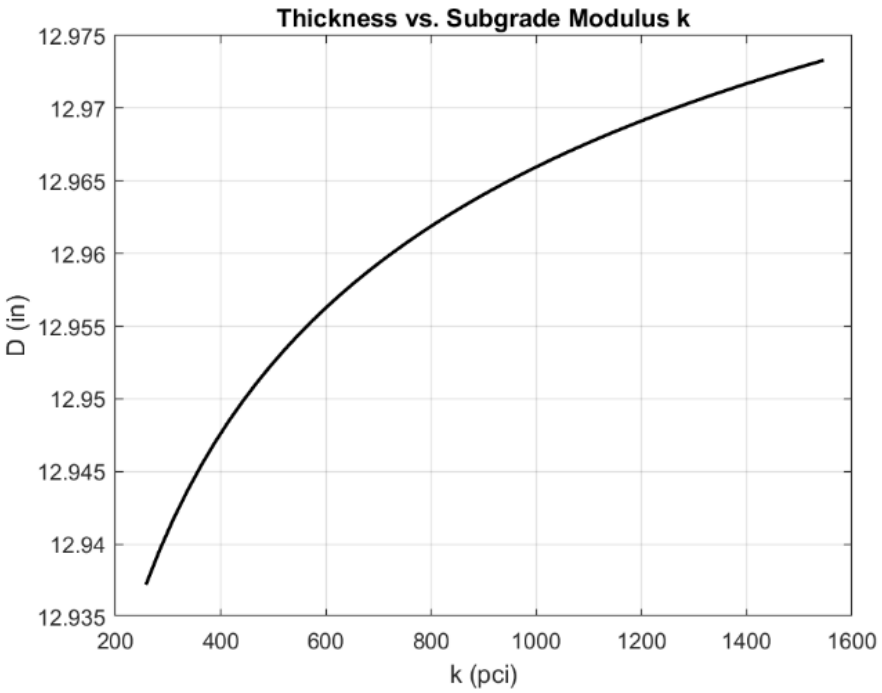

Studies the effect of subgrade resilient modulus MR varying from 5000 psi to 30000 psi (i.e. k from ~250 pci to ~1550 pci) on required slab thickness.

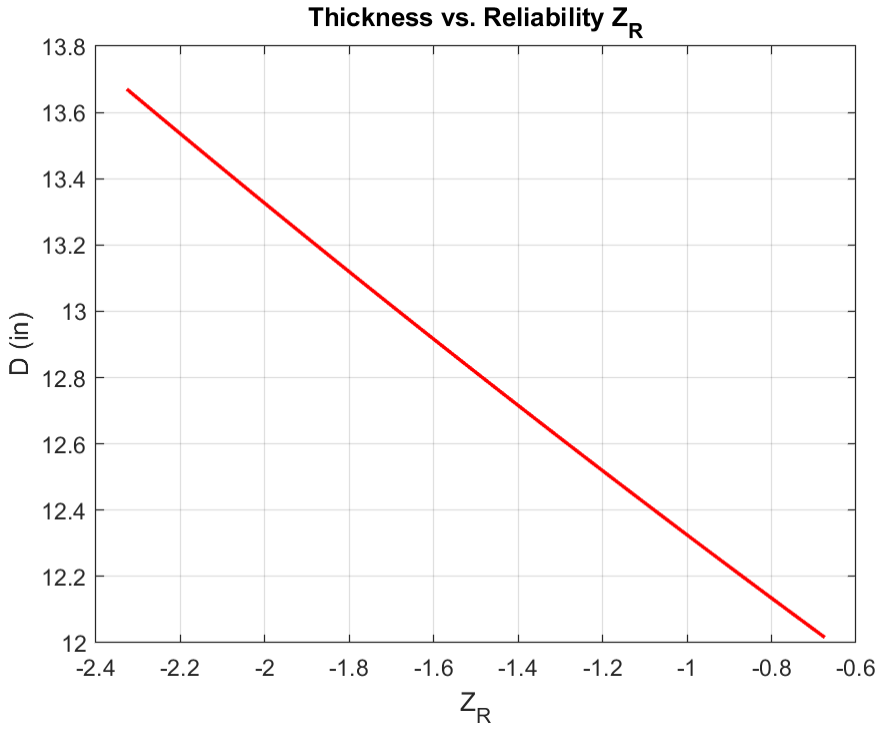

Studies the effect of reliability deviate ZR varying from –2.327 (99 % reliability) to –0.674 (75 % reliability) on required slab thickness.

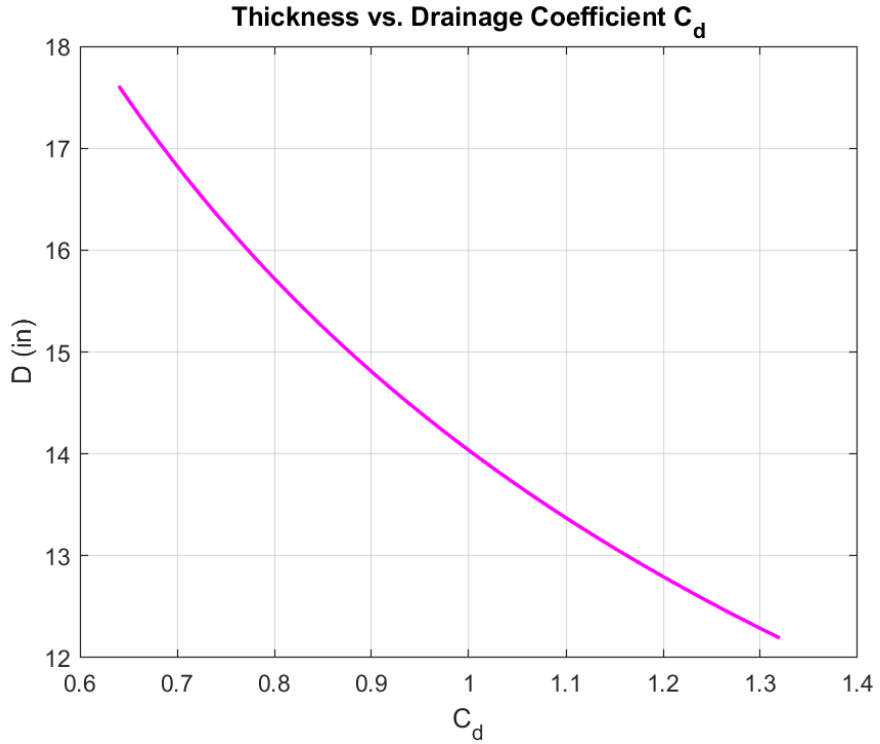

Studies the effect of drainage coefficient C_D varying from 0.64 (“very poor”) to 1.32 (“excellent”) on required slab thickness.

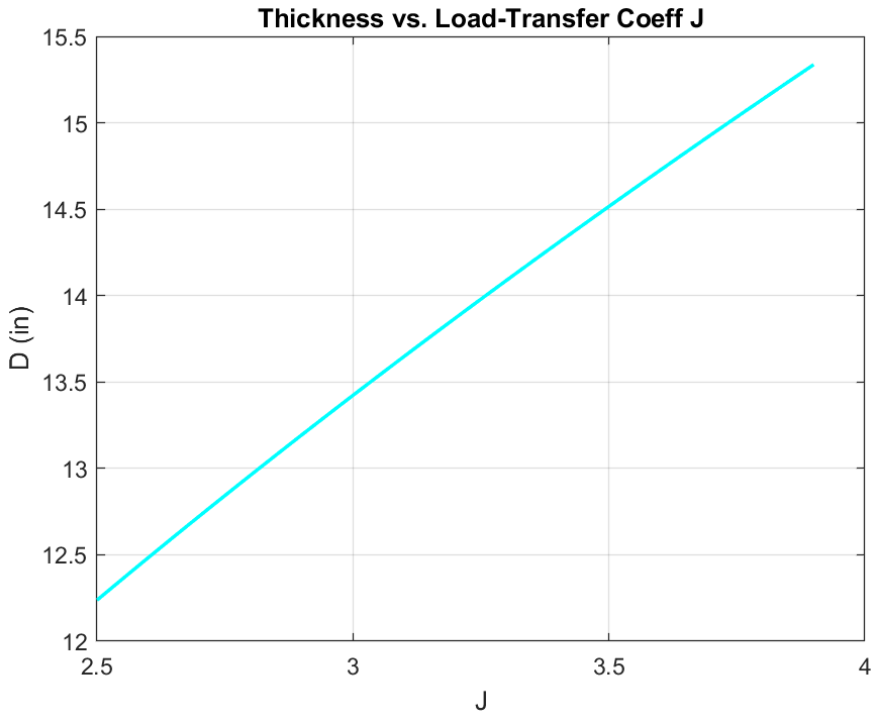

Studies the effect of load-transfer coefficient J varying from 2.5 to 3.9 on required slab thickness.

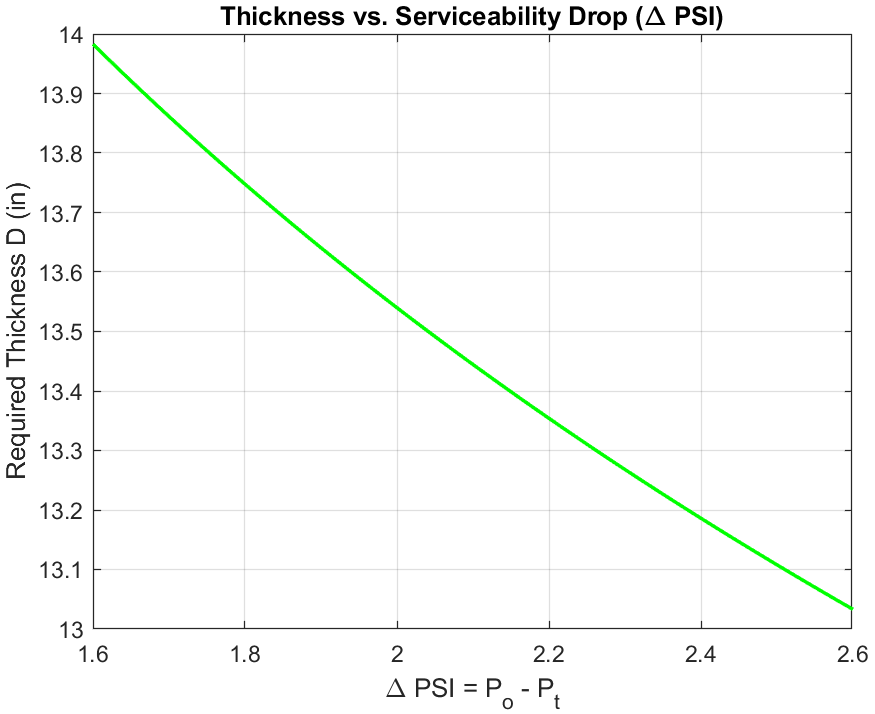

Studies the effect of allowable serviceability drop ΔPSI=Po−Pt varying from 1.6 to 2.6 on required slab thickness.

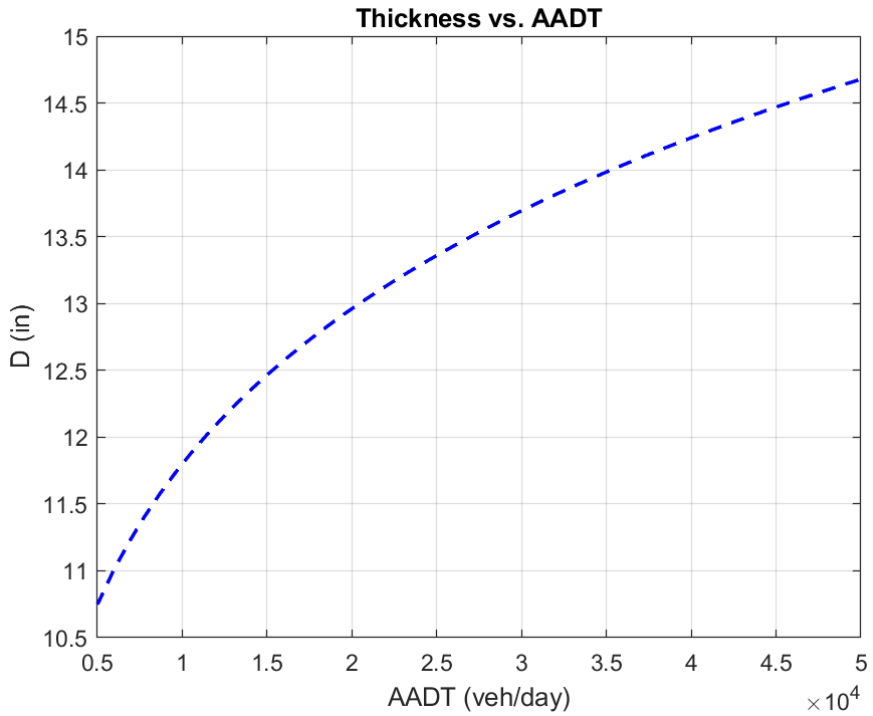

Studies the effect of data-year AADT varying from 5000 vehicles per day to 50,000 vehicles per day on required slab thickness.

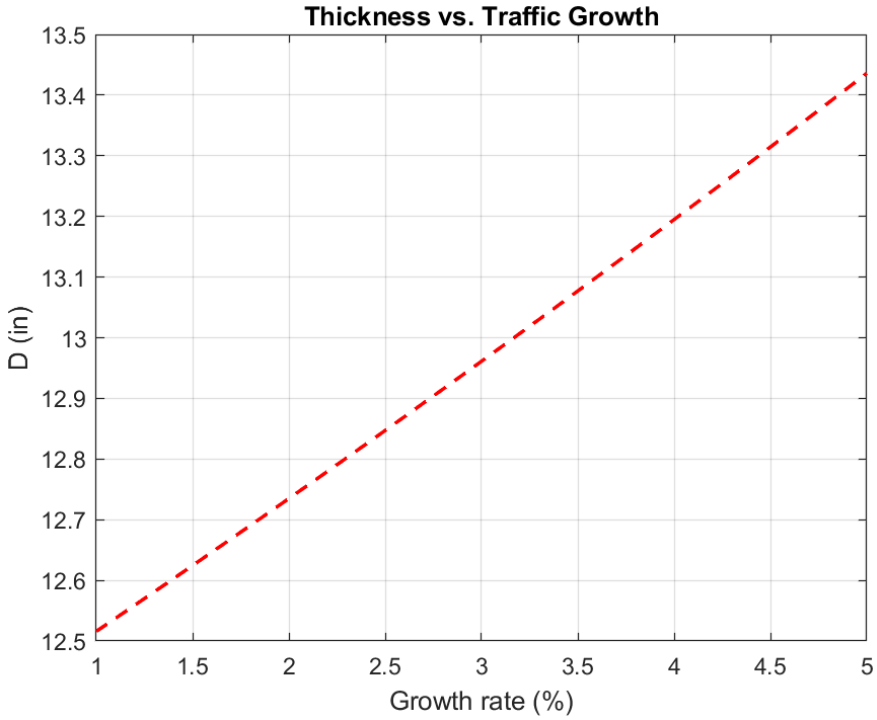

Studies the effect of annual growth rate (r) varying from one percent to five percent on required slab thickness.

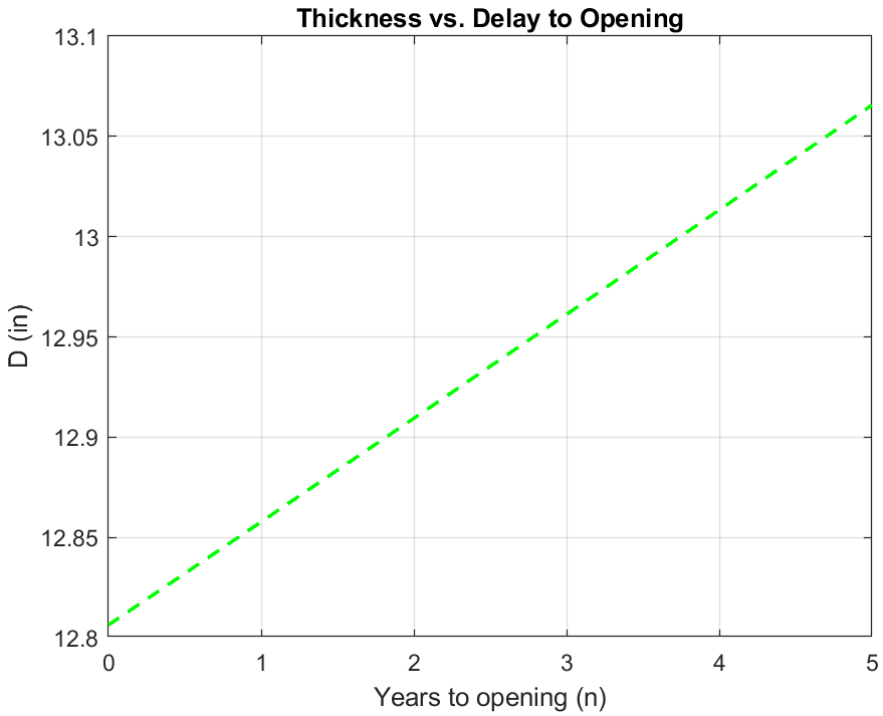

Studies the effect of years to opening (n) varying from 0 to 5 years on required slab thickness.

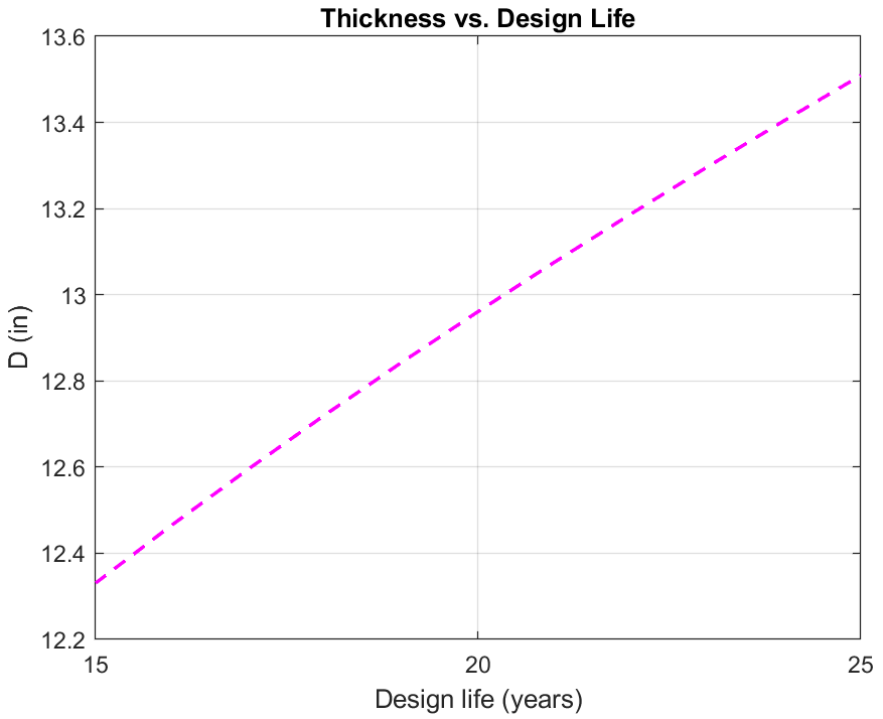

Studies the effect of design life Y varying from 15 to 25 years on required slab thickness.

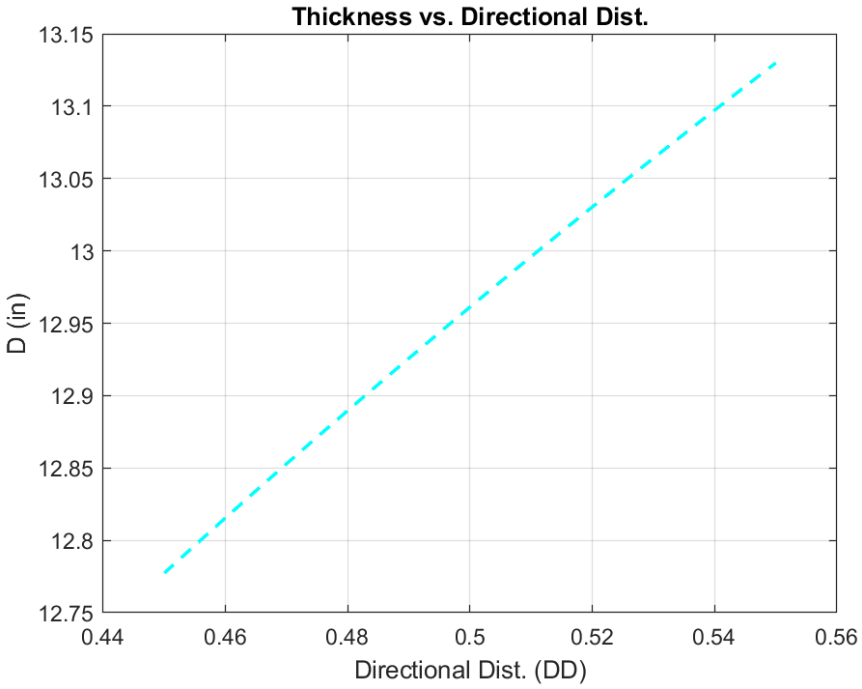

Studies the effect of directional distribution factor (DD) varying from 0.45 to 0.55 on required slab thickness.

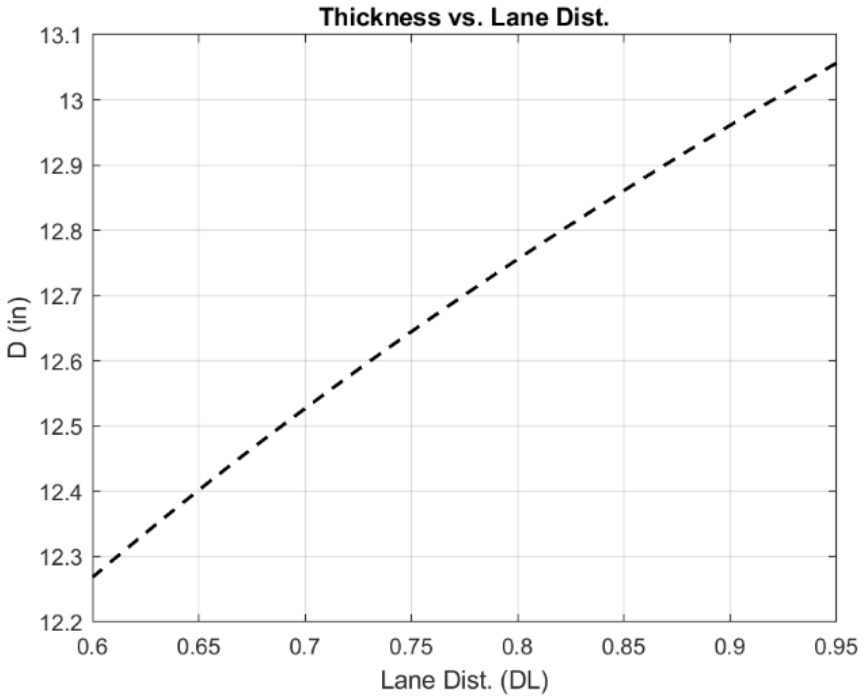

Studies the effect of lane distribution factor (DL) varying from 0.60 to 0.95 on required slab thickness.

A comprehensive parametric study helps identify which inputs most strongly influence slab thickness. By understanding sensitivity of the design parameters one can better optimize pavement sections for long-term durability. Out of the 12 key parameters studies, the MOR and the drainage coefficient C_D are found to be most sensitive in selecting the slab thickness.

Westergaard Approach

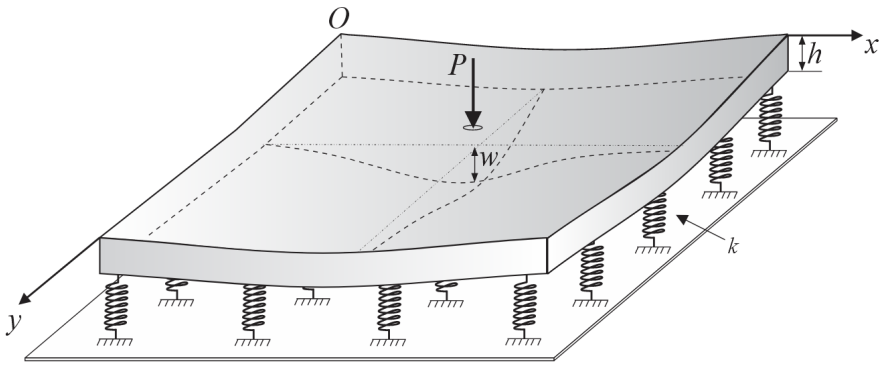

Figure 41. Plate on Elastic Foundation.

For a slab on elastic foundation, the governing plate bending equation is:

$$\frac{\partial^4 w}{\partial x^4} + 2\frac{\partial^4 w}{\partial x^2 y^2} + \frac{\partial^4 w}{\partial y^4} = \frac{p - kw}{D}$$

Equation 6

Where

$$D = \frac{Eh^3}{12(1-\nu^2)}$$

w	Deflection
q	Applied load per unit area
k	Modulus of subgrade reaction
h	thickness of slab
E	Elastic modulus of slab

To solve this equation and characterize the spatial extent of load influence, he introduced the radius of relative stiffness ℓ. The relative stiffness ℓ, defines the characteristic length over which stresses and deflections decay from the point of loading.

$$D = \frac{Eh^3}{12(1-\nu^2)}$$

Equation 7

With this, Westergaard derived closed-form analytical solutions for deflection and stress under different loading positions specifically interior, edge, and corner loading. Westergaard derived equations to estimate the maximum tensile stresses in the slab. These stresses depend on factors such as slab thickness, MOE, Poisson's ratio, and the modulus of subgrade reaction. His work provides a theoretical framework that remains essential for understanding how wheel loads induce stresses in rigid pavements.

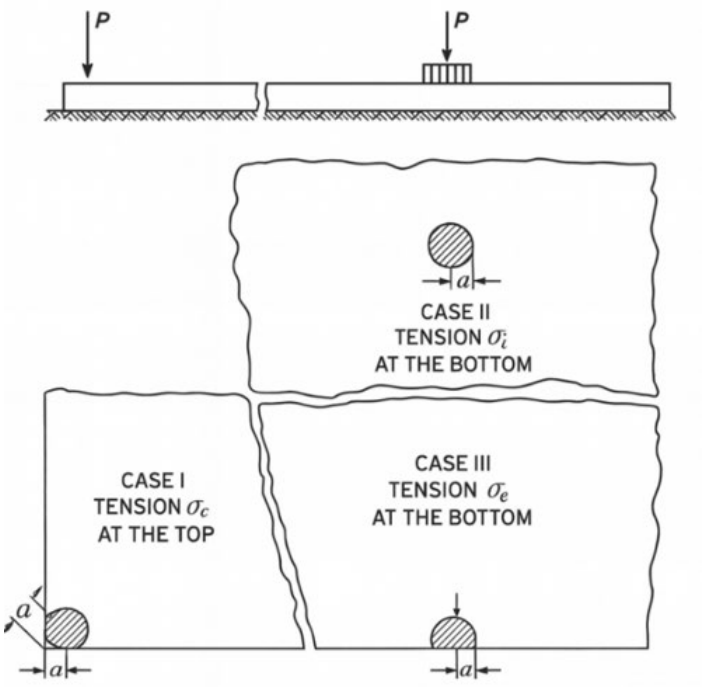

Figure 42. Westergaard's Case: Internal, Edge and Corner Loading [37].

The assumptions underlying the calculation are that the concrete slab behaves as an uncracked, continuous laminar plate. It is considered large enough that joint effects do not influence interior behavior. For edge and corner loading, adjacent slabs are assumed to have no structural connection. The subgrade is modeled using the modulus of subgrade reaction k, treating the support as a series of independent springs, though an equivalent foundation modulus Es may also be used.

The Westergaard analysis for various loading accounts for stress magnitudes of the slab under load where 'a' is the radius of loading circle.

Corner loading condition: $$\sigma_c = \frac{3P}{h^2}\left[1-\left(\frac{a_1}{l}\right)^{0.6}\right]$$ (a) **Equation 8**

Equation 8

Internal loading condition: $$\sigma_i = \left(\frac{3P(1+\nu)}{2\pi h^2}\right)\left[\ln\left(\frac{\ell}{a}\right)+0.6159\right]$$ (b)

Edge loading condition: $$\sigma_e = \frac{3P(1+\nu)}{\pi h^2}\left[\ln\left(\frac{1.84l}{a}\right)+0.25\right]$$ (c)

Meyerhof Approach (TR34 and ACI 360)

Meyerhof approach assumes failure as a mechanism of rotating triangular segments forming along yield lines caused by tensile bending cracks [59]. The critical failure moment Mo is calculated based on equilibrium between applied loads and the moment capacity along these yield lines.

Key assumptions:

- Cracks form due to tensile bending stresses.
- Slab breaks into rigid triangular plates rotating about yield lines.
- Failure is modeled by equating applied load moment with limiting moment capacity.

The Meyerhof resisting moment expressions assume that M_o is the sum of the negative and positive resisting moments. A positive moment creates sagging; a negative moment creates hogging.

$$M_o = M_n + M_p \qquad \textbf{Equation 9}$$

Where

P = applied load

a = radius of contact area

l = the radius of relative stiffness

M_o = limiting moment of resistance of the slab per unit length

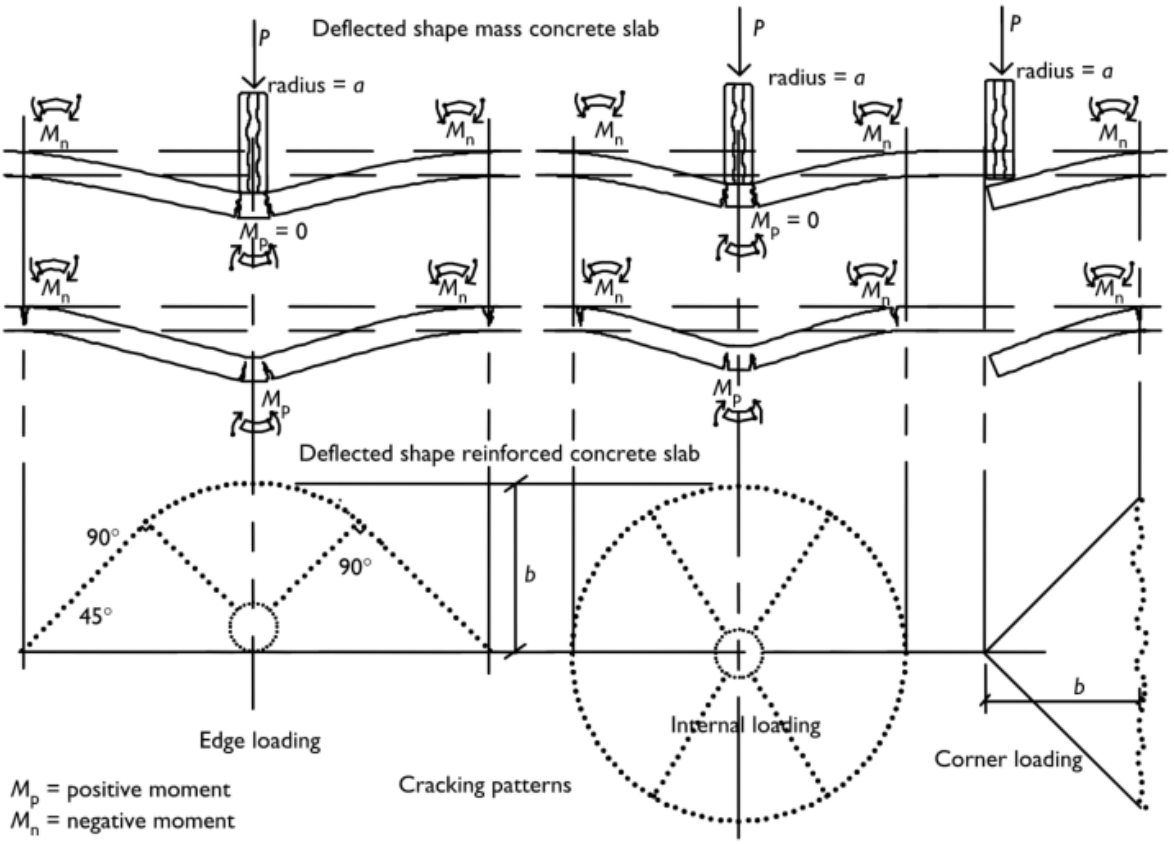

Figure 43. Slab on Foundation Cases with M_p and M_n [59].

Internal Loading Condition

General Conservative Expression: $$M_o = \frac{P}{6}\cdot\left(\frac{\ell}{\ell+2a}\right)$$ (a) **Equation 10**

Large Slabs: $$M_o = \frac{P}{4\pi}$$ (b)

Small Slabs: $$M_o = \frac{P}{2\pi}$$ (c)

Edge Loading Condition

General Conservative Expression: $$M_o = \frac{P}{3.5}\cdot\left(\frac{\ell}{\ell+3a}\right)$$ (a) **Equation 11**

Large Slabs: $$M_o = \frac{P}{2+\pi}$$ (b)

Small Slabs: $$M_o = \frac{P}{2+0.5\pi}$$ (c)

Corner Loading Condition

General Conservative Expression: $$M_o = \frac{P}{2}\cdot\left(\frac{\ell}{\ell+4a}\right)$$ (a) **Equation 12**

Small and Large Slabs: $$M_o = \frac{P}{2}$$ (b)

Limiting Moment

Design Cases I: Unreinforced (Limiting Tensile Capacity of an Uncracked Section)

The positive moment, M_p, is not considered to contribute toward resisting failure and is therefore ignored. For this case, $M_o = M_n = M_c$ (a) **Equation 13**

Limiting moment of resistance per unit length: $$M_c = \frac{f_t h^2}{6}$$ (b)

Design Cases II: Reinforced Condition

The RC load case is more complex. The net resultant longitudinal and transverse reinforcement is used to estimate the moment of resistance. It can then be suggested that the following moments of resistance might occur.

Limiting Moment Type 1: Internal and Edge Load Cases

$M_o = M_n + M_p$ (a) **Equation 14**

$M_n = M_c$ (b)

$M_p = M_s$ (c)

Limiting Moment Type 2: Corner Cases

$M_o = M_n$ (a) **Equation 15**

$M_n = M_c$ (b)

$M_p = M_s$ (c)

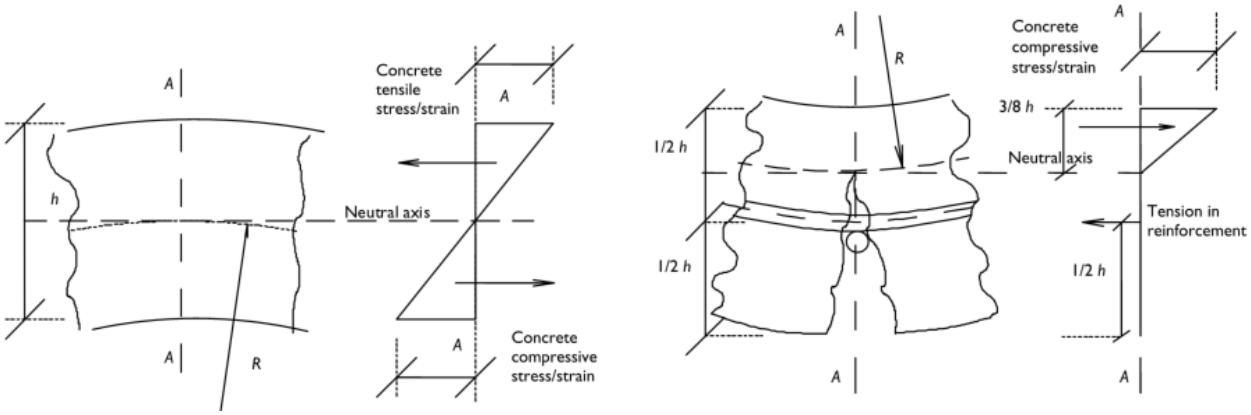

Figure 44. Difference Between M_c (left) and M_s (right) [59].

The net moment of longitudinal and transverse reinforcement where:

$M_s = (M_t M_l)^{0.5}$ (a) **Equation 16**

$$M_s = a_s f_s \left(\frac{h}{8}\right)^2$$ (b)

M_s is the limiting moment of resistance for centrally RC slab per unit length and fs is steel tensile stress at failure.

Moment Capacity Calculation as Per British Standards TR34

FRC is tested using a 150 mm × 150 mm cross-section beam with a 500 mm span. A notch of 25 mm depth is saw-cut on the tension face. Central-point loading is applied, and either crack mouth opening displacement (CMOD) or midspan deflection is recorded at standardized values (CMOD = 0.5, 1.5, 2.5, 3.5 mm).

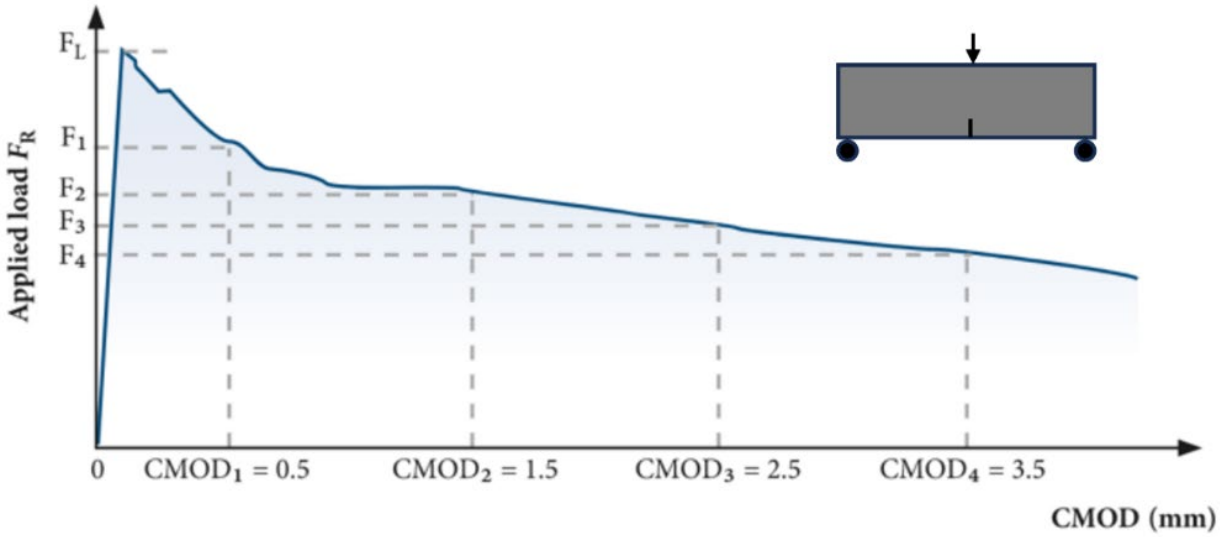

Figure 45. Typical Graph of Test Load Flexural Stress vs. CMOD.

The applied load at each CMOD is recorded as f_i and converted to residual flexural tensile strength $f_{R,i}$ using:

$$f_R = \frac{3F_R \ell}{2bh_{sp}^2}$$

Equation 17

Where

f_R	Load at each CMOD
l	500 mm (Span)
b	150 mm (Width)
h_{sp}	125 mm (Distance from top to notch tip)

The four values f_{R1}, f_{R2}, f_{R3}, and f_{R4} are averaged over 12 specimens.

Strain hardening is indicated if:

$f_{R1} \geq f_L$ and $f_{R4} \geq f_L$

Calculation of Residual Axial Tensile Strength (RILEM TC 162-TDF)

To estimate axial residual tensile strengths at crack depths, the following conversions are used:

$\sigma_{r1} = 0.45 f_{R1}$

$\sigma_{r4} = 0.37 f_{R4}$

Ultimate Moment Capacity Estimation

For fiber-only reinforced slabs, moment capacity is governed by the ultimate compressive strain ε_{cu}=0.0035, assuming simplified mechanics:

Assumptions:

- Fiber tensile strength and concrete compressive strength reach limits simultaneously. Strain compatibility is achieved, but equilibrium is not achieved, as the compressive force in the concrete will always exceed the tensile force in the fiber concrete.
- Neutral axis depth is proportional to the section depth.

Based on these assumptions, the ultimate moment capacity per unit width is calculated as follows:

Fiber Only:

Simplified:

$$M_u = \frac{h^2}{\gamma_m}\left(0.29\sigma_{r4} + 0.16\sigma_{r1}\right)$$ **Equation 18**

For Hybrid Sections: Fiber + Reinforcement

$$M_u = \frac{h^2}{\gamma_m}\left(0.29\sigma_{r4} + 0.16\sigma_{r1}\right) + \frac{A_s f_y (d - 0.048h)}{\gamma_s}$$ **Equation 19**

ACI 360 Concrete Slabs on Ground

The ACI method [60] adopts yield line theory for ground-supported slabs, accounting for plastic hinge formation at critical moments. These hinges enable full redistribution of moments, allowing the slab to reach its ultimate load-carrying capacity. The method is particularly suited for FRC slabs, where toughness is important. A residual strength index $R_{e,3}$ (per ASTM C1609) is used to enhance moment capacity.

Meyerhof (1962)[61] proposed formulas for three loading cases: central, edge, and corner. Each case expresses the ultimate load Po based on the location of the applied load and effective moment capacity Mo. The same above equation from Meyerhof is used:

For central and edge loads:

$$M_o = M_n + M_p = \left[1 + \frac{R_{e,3}}{100}\right] \cdot \frac{f_r \cdot b \cdot h^2}{6}$$ (a) **Equation 20**

For corner load:

$$M_o = M_n = \frac{f_r \cdot b \cdot h^2}{6}$$ (b)

For multiple loading case from TR34 [62]and ACI-360 [60] :

Dual wheels: $$M_o = \frac{P\ell}{2\pi\ell + 1.8x} \quad \text{(c)}$$

Dual tandem (quadruple) wheels: $$M_o = \frac{P\ell}{2\pi\ell + 1.8(x+y)} \quad \text{(d)}$$

Where

P_o	ultimate load capacity
M_o	total moment resistance of slab
M_n	negative moment (tension at top)
M_p	positive moment (tension at bottom)
f_r	modulus of rupture (MPa)
h	slab thickness (mm)
b	unit width (1 mm)
a	radius of load-contact area (mm)
L	radius of relative stiffness
$R_{e,3}$	residual strength index (JSCE SF4 or ASTM C1609)

ACPA, AASHTO Approaches for Incorporating FRC in Pavements

The guidelines proposed by ACPA and AASHTO [58,63–65] propose an effective strength method to account for the increased flexural capacity of FRC slabs by modifying the MOR. Since traditional MOR values from beam tests fail to capture the post-cracking toughness contributed by fibers, the authors introduce the equivalent flexural strength ratio, $R_{e,3}$, obtained from ASTM C1609 beam toughness tests. They justify increasing the conventional MOR to an effective MOR, denoted as MOR', using the following equation:

$$MOR' = MOR\left(1 + \frac{R_{e,3}}{100}\right)$$

Equation 21

This adjustment incorporates both the base strength from non-FRC concrete (MOR) and the post-cracking residual strength due to fibers (via $R_{e,3}$). The approach was validated through large-scale slab testing and showed that even low-volume fiber additions (producing $R_{e,3}$ between 20 and 50 percent) significantly increased both the flexural cracking and ultimate capacity of slabs. Thus, the proposed method allows for fiber benefits to be integrated into existing linear elastic pavement design frameworks without overhauling the design methodology.

Strength and Weaknesses of Design Approach:

The suggested modification of MOR by [4,66–69] for its use of the conventional method of thickness design of rigid pavements is based on some invalid assumptions. Adding residual strength to MOR cannot address or allow one to correctly design FRC in pavements as it overestimates contribution of FRC and suggests that the MOR is increased but that is not the case. Apparent Strength values measured at two different levels during the loading stage cannot be added to one another and used as design parameters. This is mathematically and logically inconsistent. FRCs contribution needs to be looked at simply from post-cracking stiffness and crack width retention which can influence the service life of the structure. For reference, the nominal flexural stress vs. deflection response in shown in Figure 46. The max. stress value, f_{cr}, is the MOR and the residual nominal stress at higher deflections is the elastic equivalent stress scaled to the elastic cracking stress value.

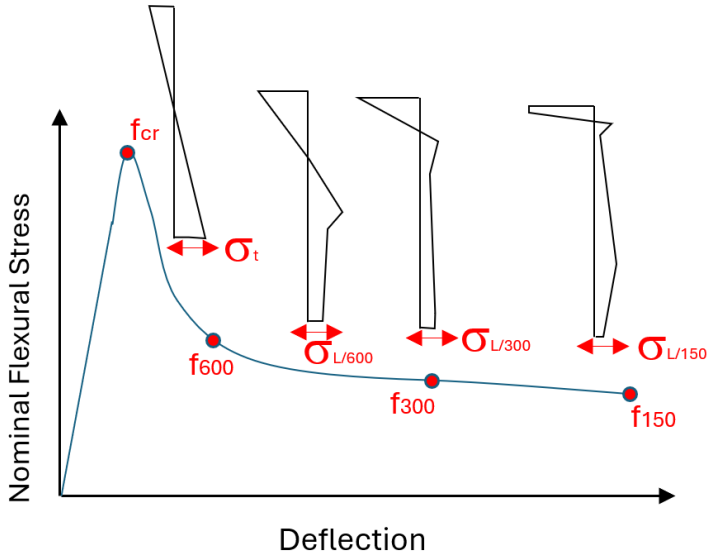

Figure 46. ASTM C1609 Test Response with Stress Distributions.

Here: $R_{e,3} = \frac{f_{150}}{f_{cr}} \times 100$ is the equivalent residual flexural stress ration to cracking stress.

Substituting this equation,

$$MOR' = f_{cr}\left(1 + \frac{f_{150}}{f_{cr}}\right) = f_{cr} + f_{150}$$ **Equation 22**

would result in very high estimation of fibers performance. In case of hardening will even make the case worse as f_{cr} is not equivalent to MOR and the definition of MOR based on the assumption of the Neutral axis at the centroid of the uncracked section. The approach is conceptually flawed because it conflates fundamentally different material behaviors: MOR represents the elastic limit or first-crack strength of plain concrete, while $R_{e,3}$ captures post-cracking apparent strength due to fiber bridging normalized with respect to the maximum stress. Simply scaling MOR with $R_{e,3}$ treats this post-cracking benefit as if it were a pre-cracking property, which is not physically accurate. This leads to an over-simplification of the

true nonlinear response of FRC, especially since elastic design methods are only valid up to the initial cracking point. Furthermore, this method assumes a linear relationship between $R_{e,3}$ and slab flexural capacity, even though large-scale test data suggest a more complex, fiber-type-dependent behavior. It provides no means of capturing serviceability concerns like deflection limits or crack width control, and is only applicable within a narrow range of fiber volume fractions ($R_{e,3}$ between 20–50 percent). Finally, this approach may mislead engineers into believing that FRC slabs behave elastically to higher loads without cracking, which undermines the need for more accurate nonlinear or limit-state analysis that fully acknowledges the transition from cracking to post-cracking behavior. Thus, while convenient, this method is technically flawed and should not be used by any organization.

Design Procedures Using Residual Strength and Moment Capacity of FRC

Simplified approach for plain FRC: Consider the same approach as of TR34 or ACI 360 but assume the negative moment (surface cracking) in cracked and use the ACI 544.4R equation for ultimate moment case:

For example:

$$M_n = M_p = M_{frc} = \left[\frac{6\mu\sqrt{f_c'}}{\xi\mu + 2\sqrt{f_c'}}\right] M_{cr} \qquad \textbf{Equation 23}$$

Where

ξ	15.8 in imperial units and 1.32 in International System (SI) units
μ	Normalized Residual tensile strength of FRC

This residual moment capacity calculation is based on elastic-perfectly plastic idealization of tension and compression models of FRC.

Full Nonlinear Sectional Analysis with Inverse Analysis:

Using the ASTM C1609 test data, the flexure response of FRC can be used by means of inverse analysis to get the tension model characterization of particular FRC mix. With a high order tension model solved in closed-form parametrically, the flexure response can be simulated thus justifying the tension model. This procedure has been validated in previous publication [70,71]and ACI committee such as ACI 544.8R reports [72]. Figure 47 shows the ASTM C1609 experimental test results and the model fit is solid curves in (a) the extracted tension model from the inverse-analysis procedure is shown in (b).

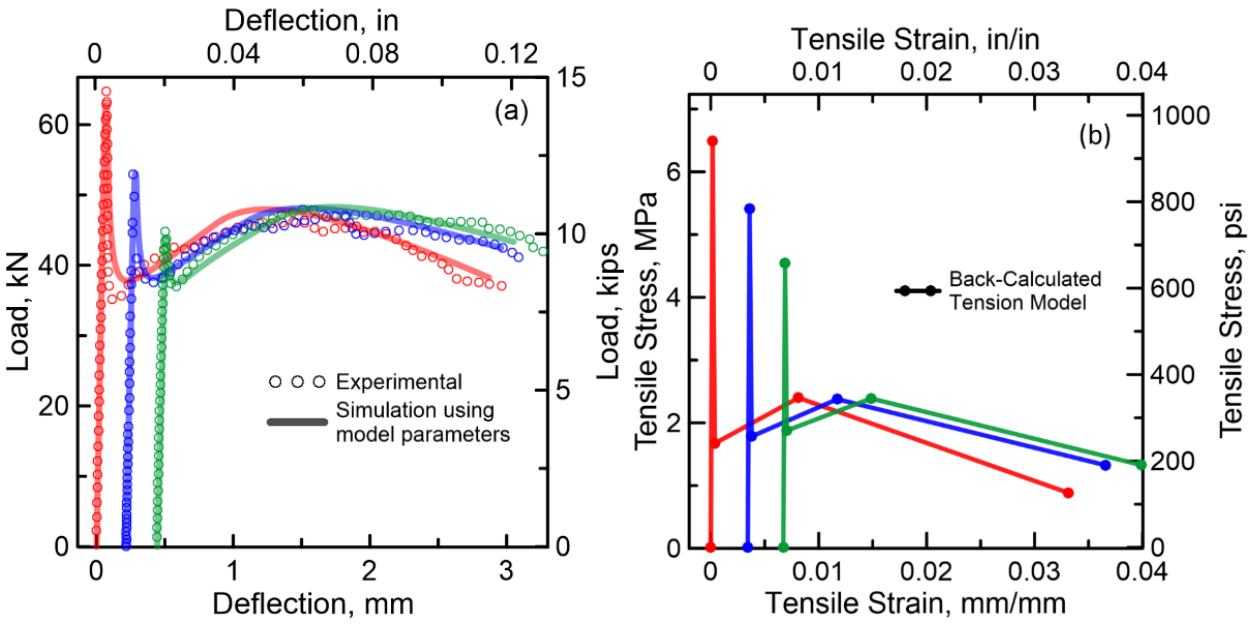

Figure 47. Quad-Linear Tension Model for High Dosage FRC (left) and the Simulated Responses (right) Using the Tension Model [70].

The tension model can then be used to derive sectional performance in terms of moment-curvature response as a preliminary design step. A freeware software has been developed for inverse analysis and design of FRC and hybrid sections. A step-by-step procedure has been laid out in the section below for design of a pavement section and its service-level performance can be evaluated. The method of inverse analysis and model details are given in detail in [70]. A similar procedure has been developed for the EN14651 which uses a notched beam test for the 3point bend flexural test.

Inverse Analysis and Design Examples for Fiber Concrete Slab Design (ACI 544.8R vs. TR34)

The following procedure uses the mean values from standard beam test like EN14651 (ASTM C1609 equivalent) test results of 85 lb./yd^3 (50 kg/m^3) dosage, 2.5-inch-long hooked steel fibers that uses inverse-analysis technique (based on ACI 544.8R) to extract tension model of the FRC to use it for flexure analysis and moment calculation of cross section per unit of width. Note that to draw comparison with the British standard for slab-on-grade design (TR34), the calculation are done in SI units.

Exact inverse analysis of mean value 85 lb./yd^3 (50 kg/m^3):

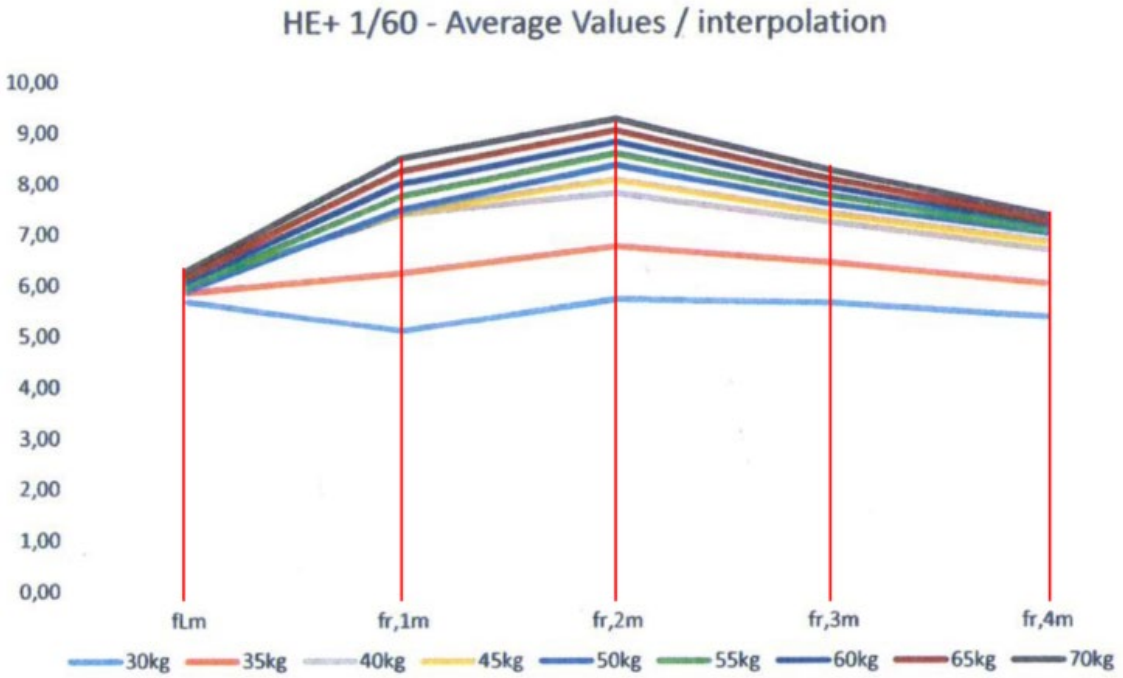

Figure 48. Available Data of EN14651 for FRC Characterization.

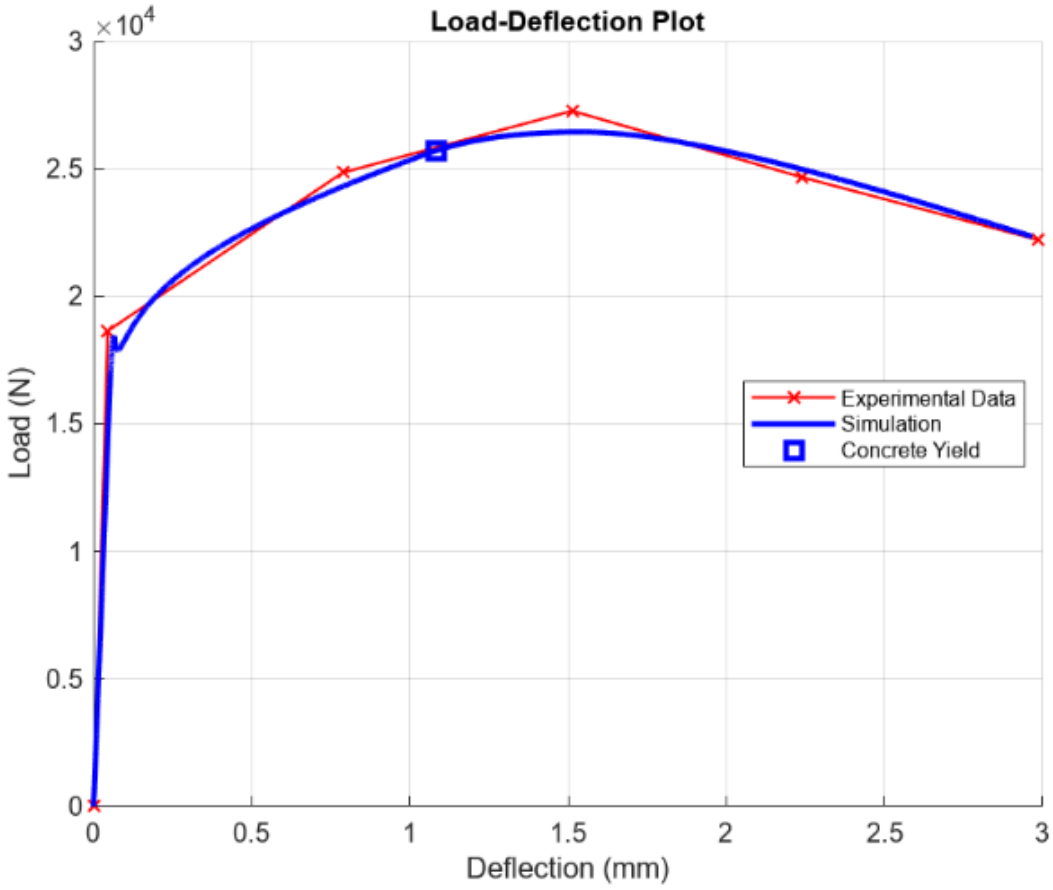

Figure 49. Load vs. Deflection with Inverse Analysis Fit of Simulation.

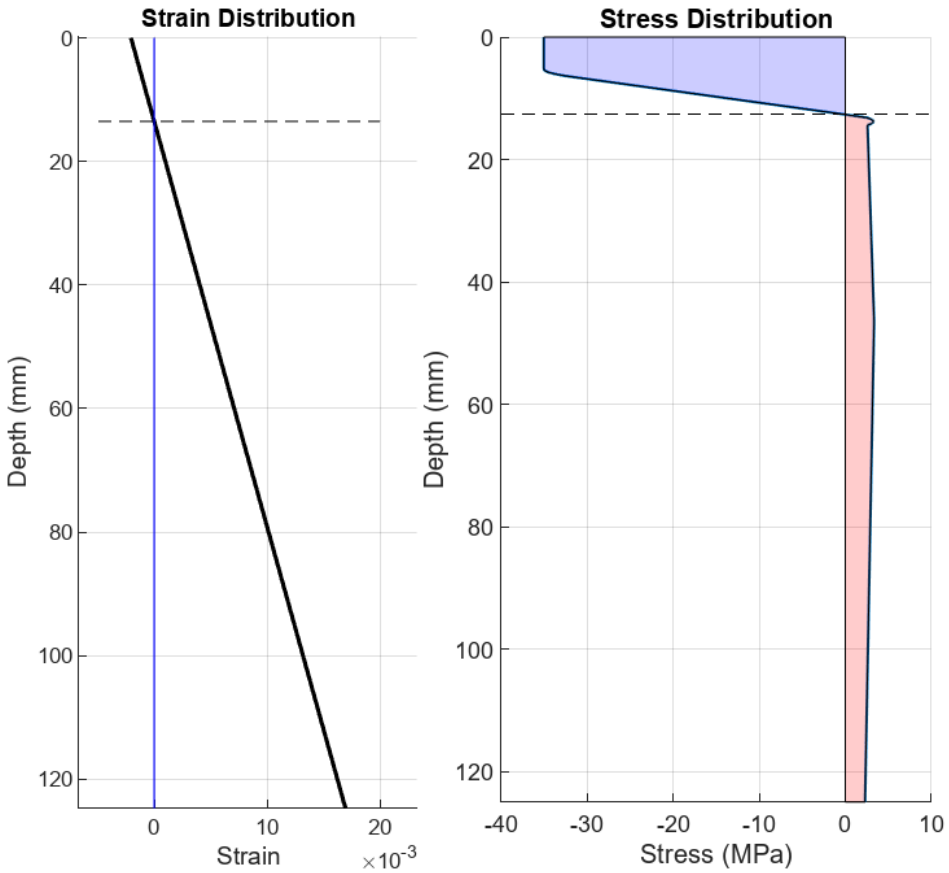

Figure 50. Stress Distribution Measured Using Inverse Analysis of the EN14651 Data at Strain Value of 0.017 at the Beam Bottom.

The exact material models are extracted from curve fitting of experimental data as:

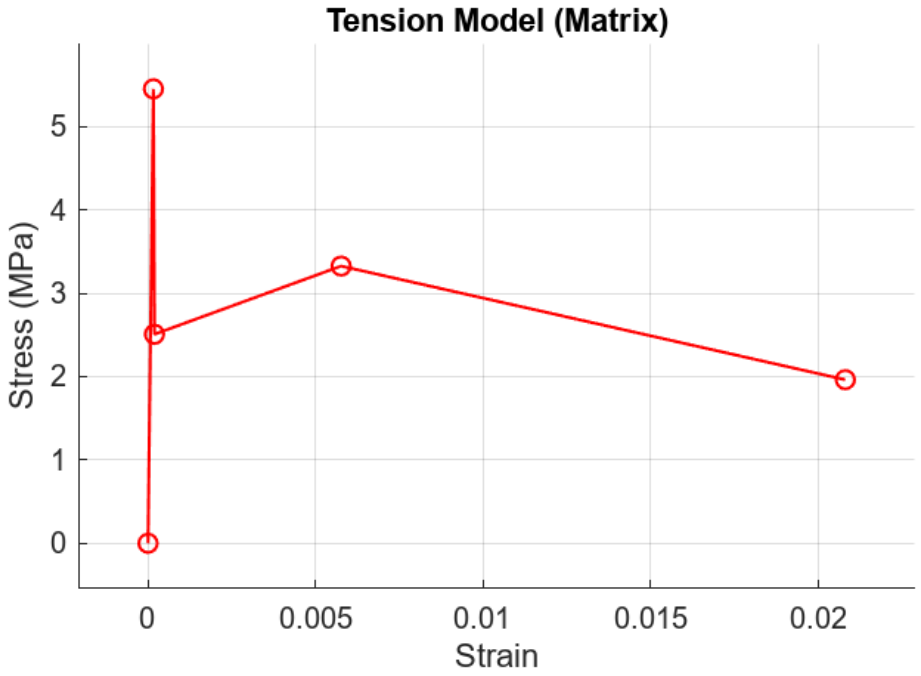

Figure 51. Extracted Tension Model from Inverse Analysis.

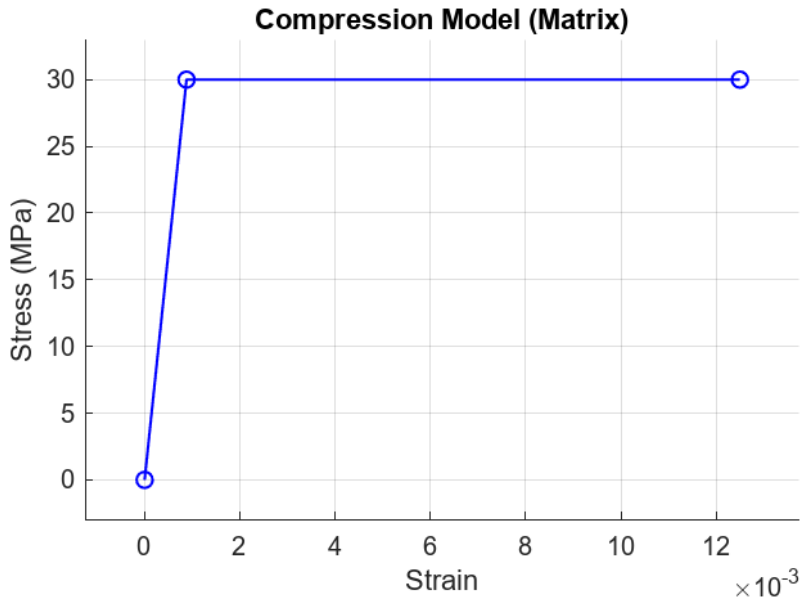

Figure 52. Extracted Compression Model from Inverse Analysis.

Extracted Tension Model Parameters

Model parameters:

- E (MPa) 34,077
- ε_{cr} 0.00016
- μ_1 0.46
- μ_2 0.6
- μ_3 0.33
- w 6.5

Tensile stress values:

- σ_{cr} 5.5 MPa
- σ_1 2.5 MPa
- σ_2 3.3 MPa
- σ_3 2.0 MPa

A unit length of one meter is designed with tension, the extracted tension model from the above approach. The cross section for the designed member is shown in Figure 53.

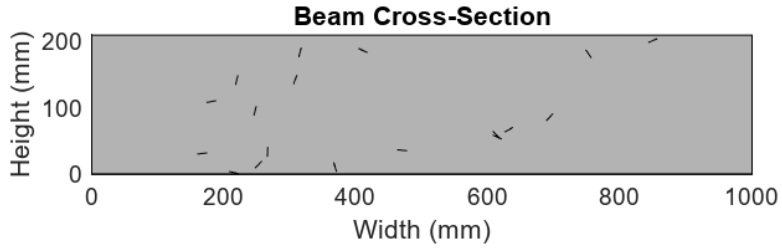

Figure 53. Cross Section of the Designed Slab Section of 210 mm (per unit length).

Moment capacity from TR34 (plain FRC):

Input data:

h = 210 mm

f_{R1} = 8 MPa (from EN14651)

f_{R4} = 7 MPa (from EN14651)

f_{ck} = 30 MPa

Calculations:

σ_{r1}=0.45*f_{R1} = 3.6 MPa

σ_{r4}=0.37*f_{R4} = 2.59 MPa

$$\gamma_m = 1.15 \text{ (FRC)} \qquad \text{(a)} \qquad \textbf{Equation 24}$$

$$M_u = \frac{h^2}{\gamma_m}\left(0.29\sigma_{r4} + 0.16\sigma_{r1}\right) = 51\ KN.m \qquad \text{(b)}$$

Moment capacity from ACI 544.8R approach with TR34 results (plain FRC):

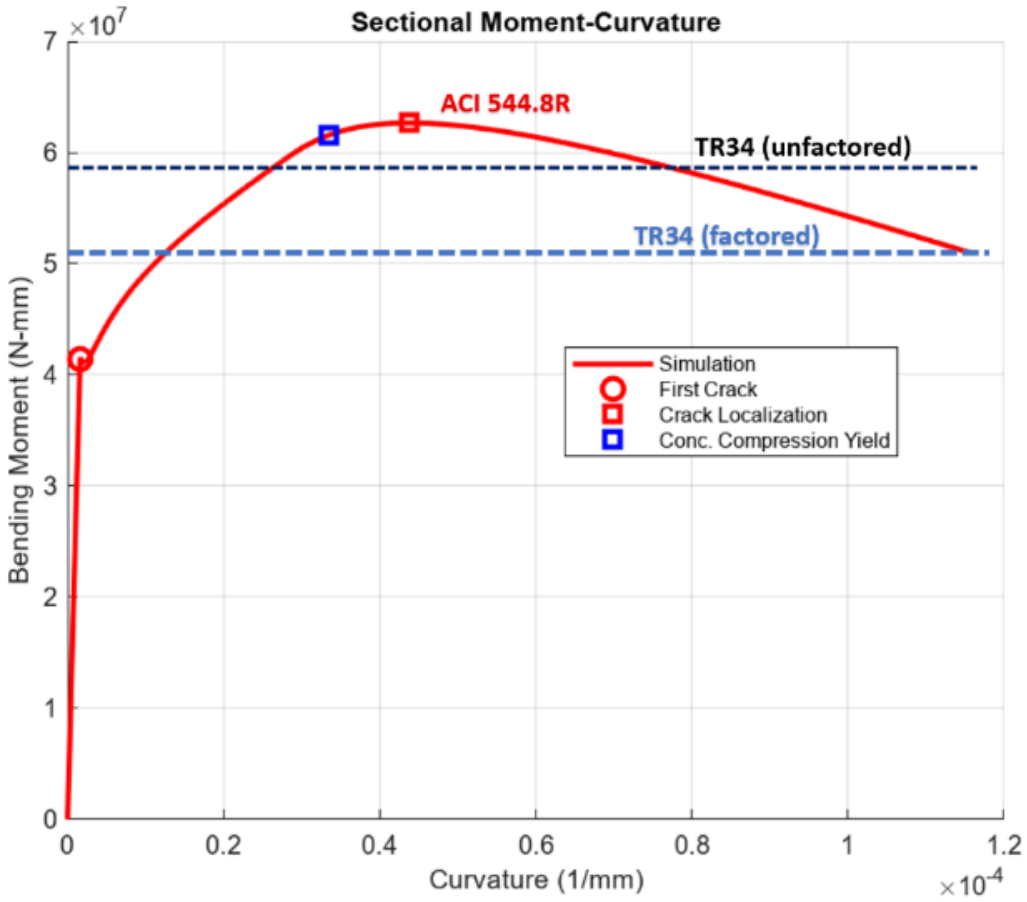

Figure 54. Full Moment-Curvature Relation from ACI 544.8R Approach.

Results show that the ACI approach shows full moment-curvature response including the hardening effect and the maximum moment capacity higher than the TR34 approach. This allows for better calibration of the tension model of FRC and more accurately simulates the moment capacity of the section. This method is available in a user-interface format or and excel sheet for design of plain FRC of reinforced FRC pavements. For example, an RC section:

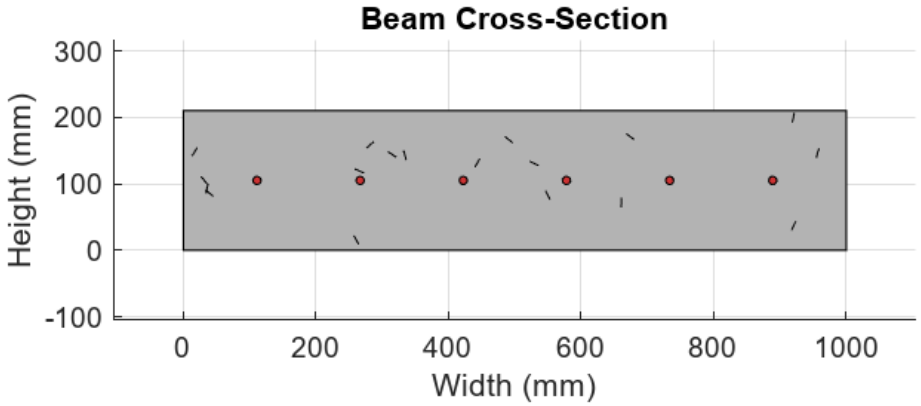

Figure 55. Beam Cross-Section of Hybrid Reinforcement.

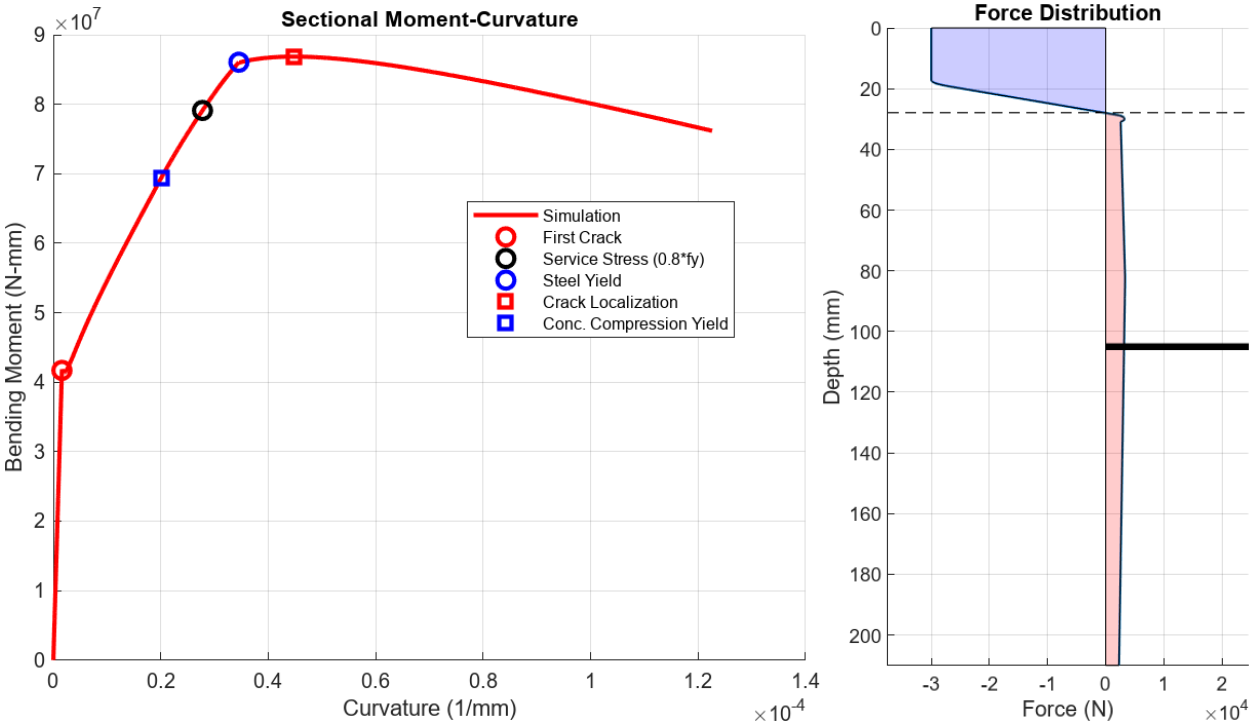

Figure 56. Hybrid Case Using ACI 544.8R Approach.

Software Link and User Guide

This software provides a closed-form analytical platform for simulating, designing, and characterizing the flexural behavior of FRC, UHPC, and hybrid reinforced concrete systems. It supports inverse analysis of standard beam tests (ASTM C1609, EN 14651), design of custom reinforcement layouts, and generation of output plots and reports for research and engineering applications. The software is available for download on this link: Software Download

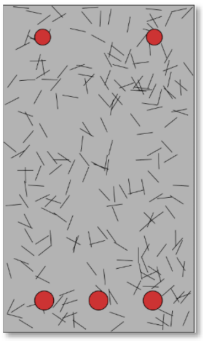

HRC DESIGNER

& INVERSE ANALYSIS

VERSION 3.4 (BETA)

User Guide

03/2025

Figure 57. Title Page of the "HRC Designer Software User Guide."

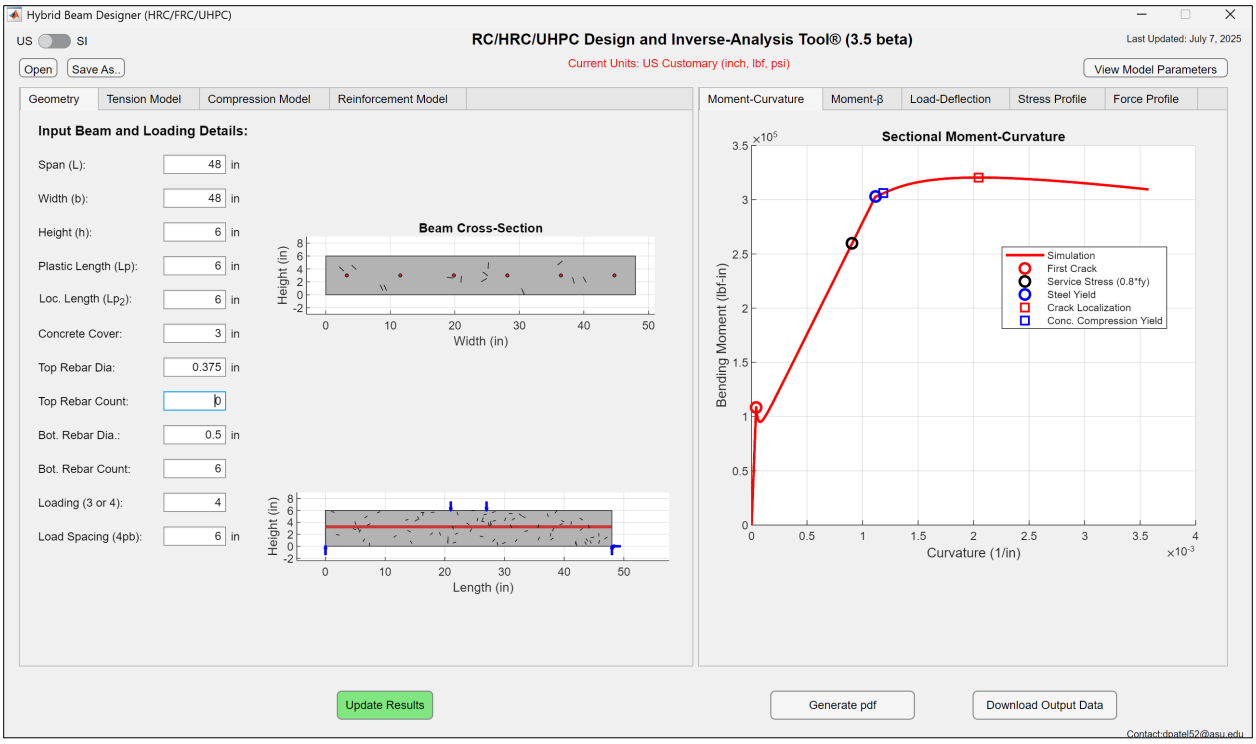

Figure 58. Hybrid Beam Designer.

[Link to landing page and download for HRC Designer Software.]

(https://www.researchgate.net/publication/389270631_An_Inverse_Analysis_and_Design_software_for_FRC_UHPC_TRC_HRC_Cement_Composites)

APPENDIX F: The Comparison of Full-Scale Testing Results on Conventional RC and Plain Fiber Reinforced Concrete Labs

In an earlier research project of a full-scale traditional RC slab and a plain FRC slab were compared by flexural testing using panels measuring 7 ft in width, 5 ft in depth, and 6 inches in thickness. The tests were conducted at the ASU laboratory. The span was fully supported at both ends, while an additional point support was placed along the edges to introduce an indeterminacy into the system, as shown in Figure 59.

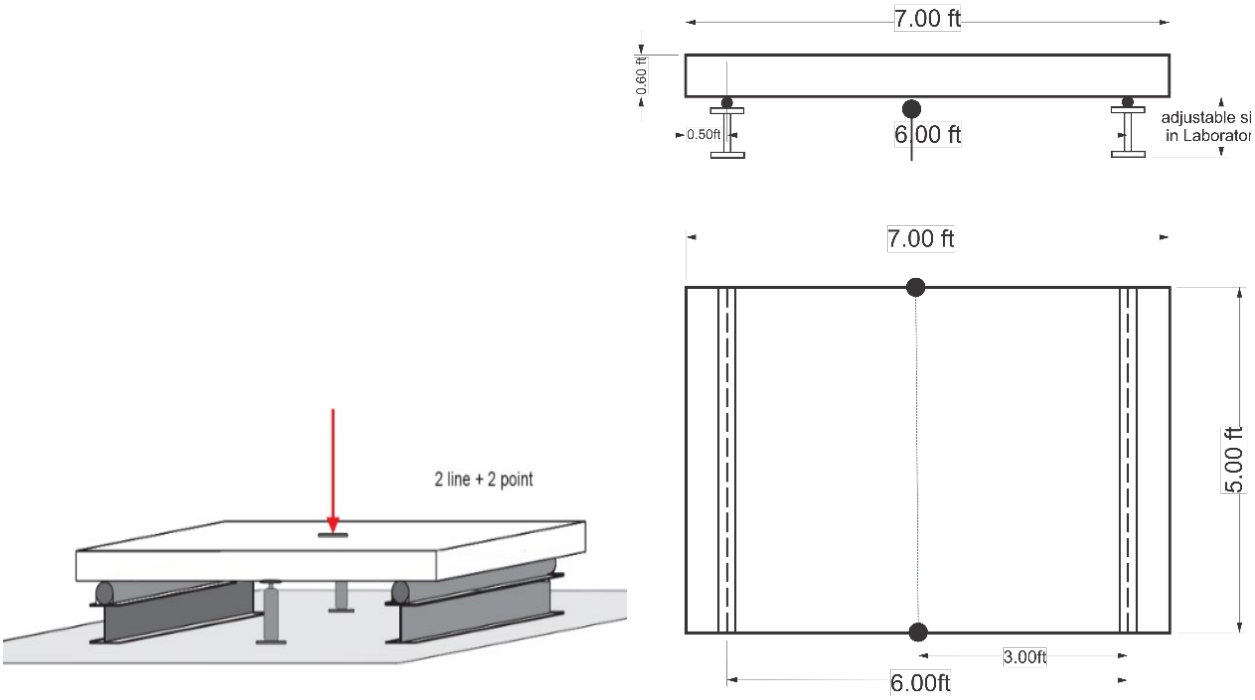

Figure 59. Testing Configuration.

Study on the ultimate load, P, and bottom failure diameter, d_1. The input section geometry is based on panel size 6x5 ft with #4@12" (ρ=0.33 percent) in both X-axis and Y-axis.

- Load pistol diameter, d = 6 in
- Slab thickness, h = 6 in
- Compressive strength
  - plain concrete f_c = 4268 psi
  - fiber-reinforced concrete = 4600 psi
- Residual tensile strength, f_t
  - plain concrete f_t = 0 psi (no residual tensile strength)
  - fiber-reinforced concrete = $\mu\sigma_{cr}$ = (0.2)(376) = 74 psi (following ACI 544 back-calculation approach [72])
- Rebar yield strength, f_y = 60 ksi

Load-Deflection Response of RC vs. Hybrid RC

The comparative performance of conventional RC and hybrid RC panels is summarized in Table 7. The hybrid RC panel exhibited a higher first-crack load of 18.8 kips, which is about 47 percent greater than the 12.8 kips observed in the conventional RC panel. This confirms that fiber significantly delays the initiation of cracking and enhances pre-cracking stiffness. At the serviceability limit state of 0.5 in, both systems carried similar loads, with hybrid RC sustaining 24.7 kips compared to 23.6 kips for RC. However, the significant contribution of fiber was observed between the first crack and deflection of 0.5 in, as shown in the shaded area in Figure 60. The advantages of hybrid RC became more pronounced in the post-cracking regime. The maximum load of hybrid RC reached 34.2 kips, about 10 percent higher than the 31.0 kips capacity of RC. Importantly, the hybrid RC panel maintained this maximum load up to its ultimate stage without noticeable strength reduction, while the RC panel reached its peak load at 31.0 and subsequently experienced punching shear failure at 30.4 kips at the ultimate deflection of 1.76 in. The Hybris RC panel experienced more than 12 percent of ultimate deflection at 1.98 in.

Overall, the results confirm that the inclusion of fibers in hybrid RC improves cracking resistance, stiffness at early stages, maximum load capacity, and deformation capacity. These combined effects are expected to translate into improved durability and longer service life in practical applications.

Table 7. The Load Performance of Conventional RC and Hybrid RC Panels.

Panel Name	First Crack load, kip	First Crack def, in	SLS[1] at 0.5 in load, kip	Max. load, kip	Max. def, in	Ultimate load, kip	Ultimate def, in
RC	12.8	0.05	23.61	30.95	39.17	30.37	1.76
Hybrid RC, V_f=9 lb/yd^3	18.8	0.09	24.70	34.15	50.28	34.15	1.98

1: SLS = serviceability limit state

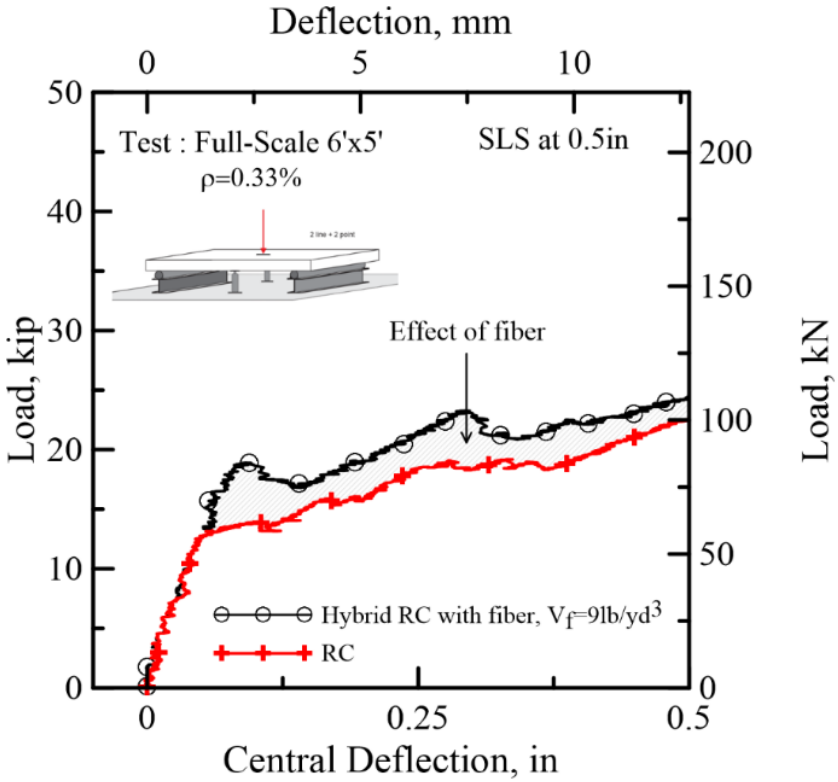

Figure 60. Load-Deflection Response RC and Hybrid RC Panels Effect of Fiber in SLS at 0.5 in.

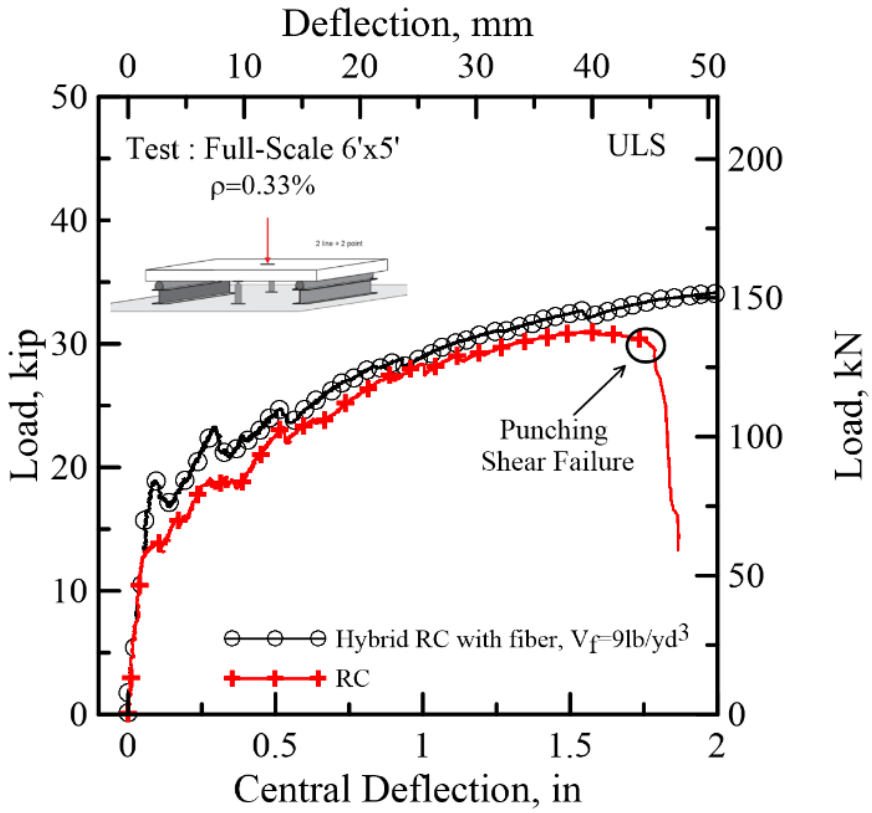

Figure 61. Effect of Fiber at Ultimate Limit State (ULS).

Crack Pattern at The End of The Test

Hybrid RC Panel

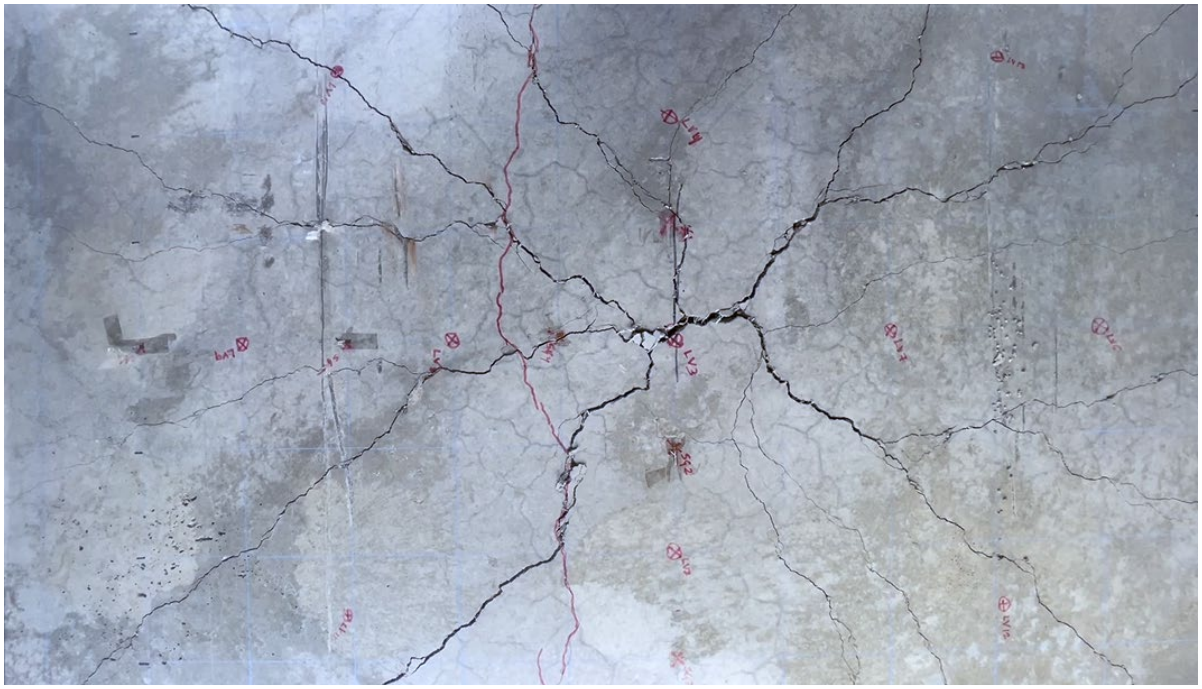

Figure 62. Bottom Crack.

Conventional RC Panel

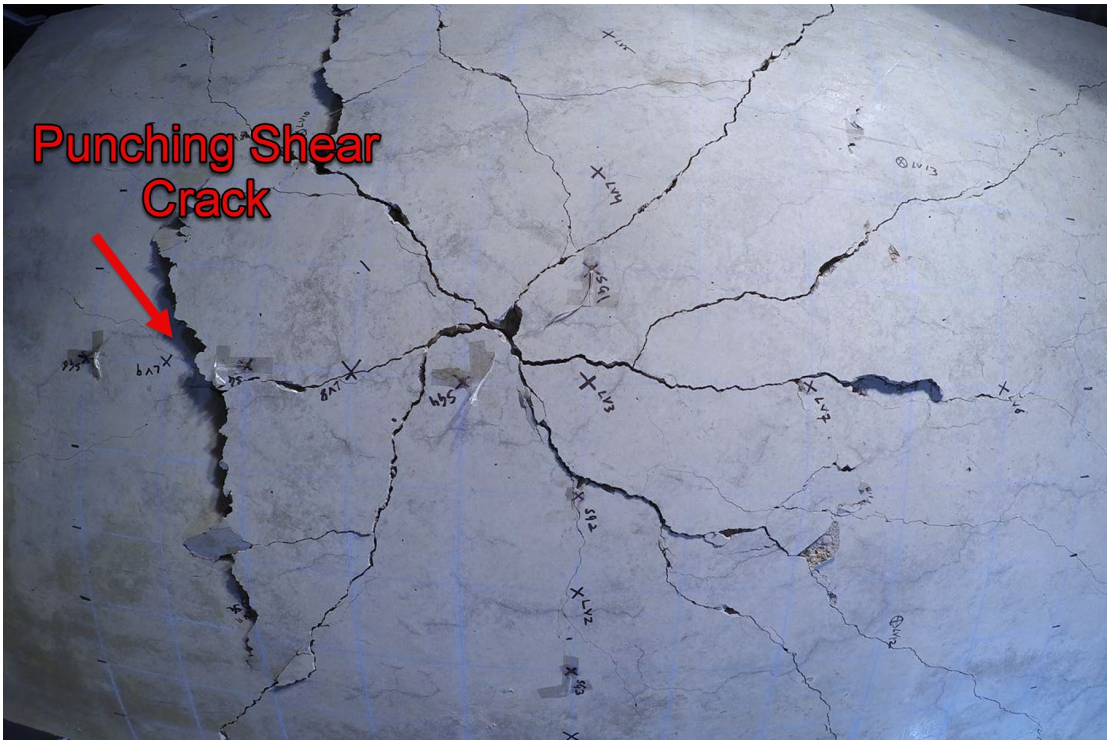

Figure 63. Bottom Crack.



Figure 64. Top Crack.

Evaluation of Average Moment (Mp+)

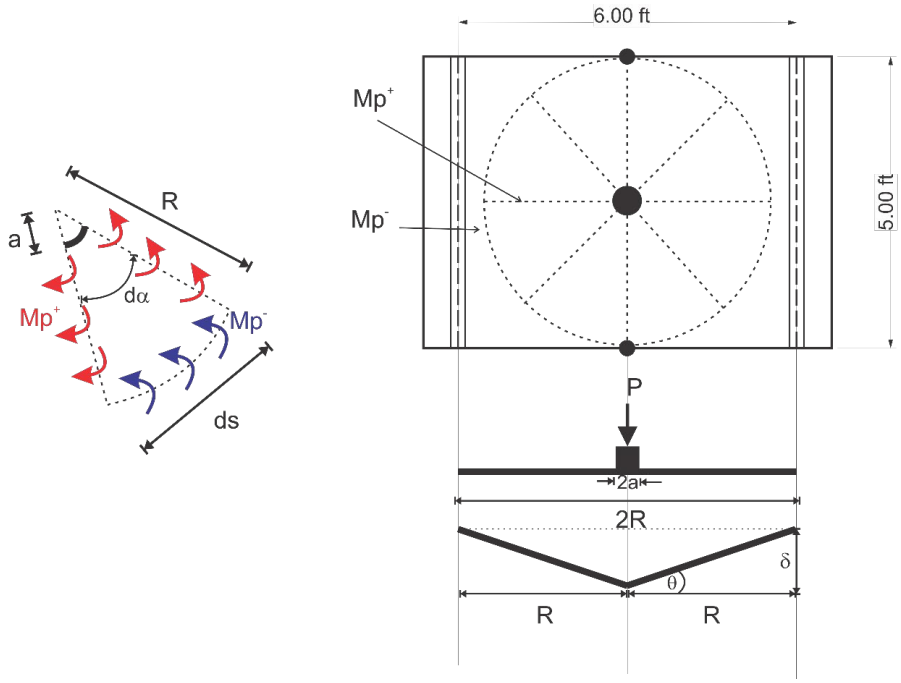

Figure 65. Schematic of a Slab Subjected to a Point Load Exhibiting Fan Pattern Cracking.

Figure 65 illustrates the schematic of the full-scale slab subjected to a point load. The load spans are six feet and five feet along the x- and y-axes, respectively. The red arrow indicates a positive moment (tension at the bottom), while the circumferential blue arrows represent a negative moment (compression at the bottom).

To predict the load-deflection response of the slab, the flexural response per unit length was fully calculated using the generalized model of hybrid fiber reinforcement presented in previous studies [44,45]. The balance between external work and internal work was then employed to establish the relationship between internal energy and external energy.

Where $$\int dW_E = \int dW_I$$ (a) Equation 25

External work = $$dW_E = \left[\left(\frac{P_{ult}}{2\pi}\right)\delta\right]d\alpha = \left[\left(\frac{P_{ult}}{2\pi}\right)(R-a)\theta\right]d\alpha$$ (b)

Internal work = $$dW_I = \left(M_P^+ + M_P^-\right)\delta d\alpha = \left(M_P^+ + M_P^-\right)(R-a)\theta d\alpha$$ (c)

Assuming $$\phi_r = M_P^- / M_P^+$$ (d)

Then, $$dW_I = \left(M_P^+ + \phi_r\right)\delta d\alpha = \left(M_P^+ + M_P^-\right)(R-a)\theta d\alpha$$ (e)

Substituting Eq (b) and (d) in energy Eq (a):

$$\int_0^{2\pi} M_P^+ (1+\phi_r) R\theta d\alpha = \int_0^{2\pi} \left[\frac{P_{ult}}{2\pi} (R+a)\theta \right] d\alpha \quad \text{(f)}$$

Therefore, the positive moment per unit length on the yield line is:

$$M_P^+ = \frac{P_{ult}\left(1-\frac{a}{R}\right)}{2\pi(1+\phi_r)} \quad \text{(g)}$$

For the case study fan pattern was assumed to have a diameter of five ft (R = 2.5 ft). The loading point had a diameter of six inches (a = 3 inches). Since the slab edges were simply supported and free to rotate, the negative moment was assumed to be zero, making the ratio of negative to positive moment equal to zero, ϕ_r=0.

$$M_P^+ (kip \cdot ft / ft) = \frac{P_{ult}\left(1-\frac{a}{R}\right)}{2\pi(1+\phi_r)} = \frac{P_{ult}\left(1-\frac{6}{(12)(5)}\right)}{2\pi(1+0)} = 0.143 P_{ult} \quad \text{(h)}$$

The nonlinear load-deflection relationship was calculated using the closed-form solution [44,45] to generate the moment–deflection response of a section with a width of 1 ft (12 in) and a span of 2R=5 ft, as presented in Figure 60 and Figure 61. Equation (g) was then adopted to simulate the load response. The material parameters used in the analysis were obtained through a back-calculation procedure from standard ASTM C1609 tests and are summarized in Table 8 through Table 10.

Table 8. Material Parameters of Conventional RC and Hybrid RC Panels.

Panel	ε_{cr} x 10^{-6}	E (psi)
RC	98*	3828996*
Hybrid RC, V_f=9lb/yd^3	98	3828996

*Assuming the first crack has the same value since there is no flexural testing on plain concrete.

Table 9. Tension Parameters of Conventional RC and Hybrid RC Panels.

σ_{cr}(psi)	τ	η	μ	μs_{cr}(psi)
376*	—	—	0.00	—
376	4.98	−0.224	0.20	74

*Assuming the first crack has the same value since there is no flexural testing on plain concrete.

Table 10. Compression Parameters of Conventional RC and Hybrid RC Panels.

γ	ω	λ_{cu}
1	—	40
1	12.00	40

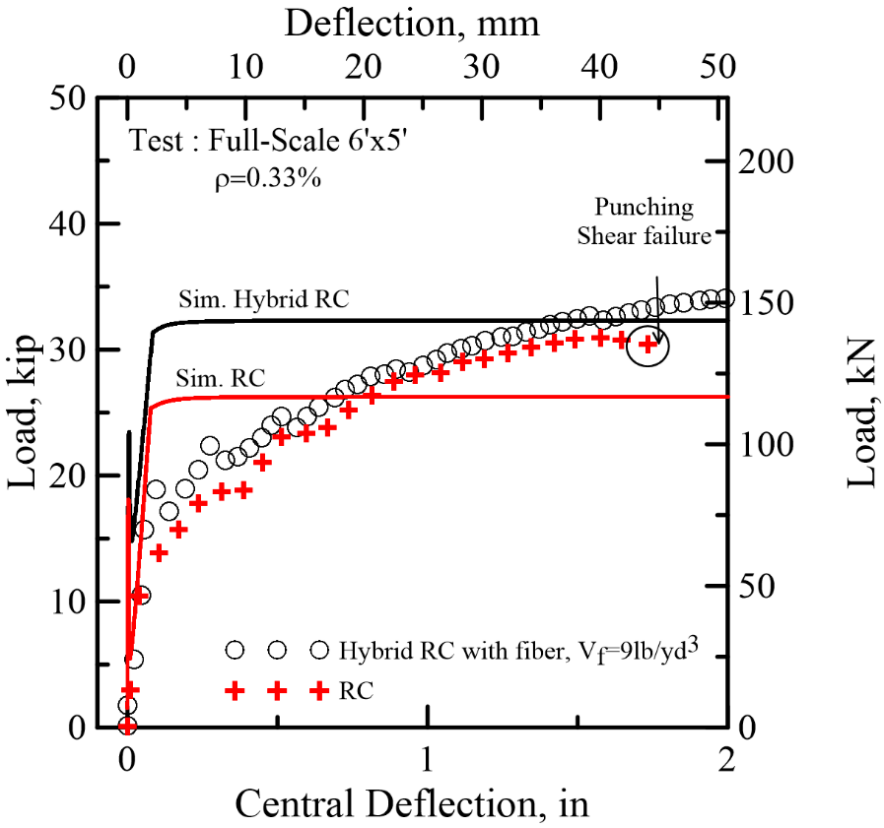

Figure 66. The Simulation of Load-Deflection Response.

Table 11. The Ultimate Load Capacities.

Panel Name	Experiment	Simulation
RC	30.37	25.97
Hybrid RC, V_f=9lb/yd^3	34.15	32.12

Table 11 compares the ultimate load capacities of a conventional RC panel and a hybrid RC panel from experiment and simulation. The experimental ultimate load for the RC panel was 30.37 kips, while the simulation predicted a slightly lower value of 25.97 kips. This represents an underestimation of about 14 percent. For the hybrid RC panel, the experimental ultimate load was 34.15 kips, whereas the simulation predicted 32.12 kips. In this case, the difference is smaller, approximately six percent, indicating a much closer agreement between simulation and experiment. The inclusion of fibers improved both the experimental load capacity and the accuracy of the simulation model. These results highlight the beneficial role of fibers in enhancing load-carrying capacity and suggest that the simulation framework is more reliable for hybrid RC than for plain RC.

APPENDIX G: Specifications for Addressing Temperature and Shrinkage Requirements of FRC for Slab

The most important resource for the specification development is the ACI 544-12R-23 spew that can be used in conjunction with sample specifications developed by other states listed in Appendix D.

This specification can be communicated directly with the concrete suppliers, and the only required test is ASTM C 1609, which is discussed in Appendix H.

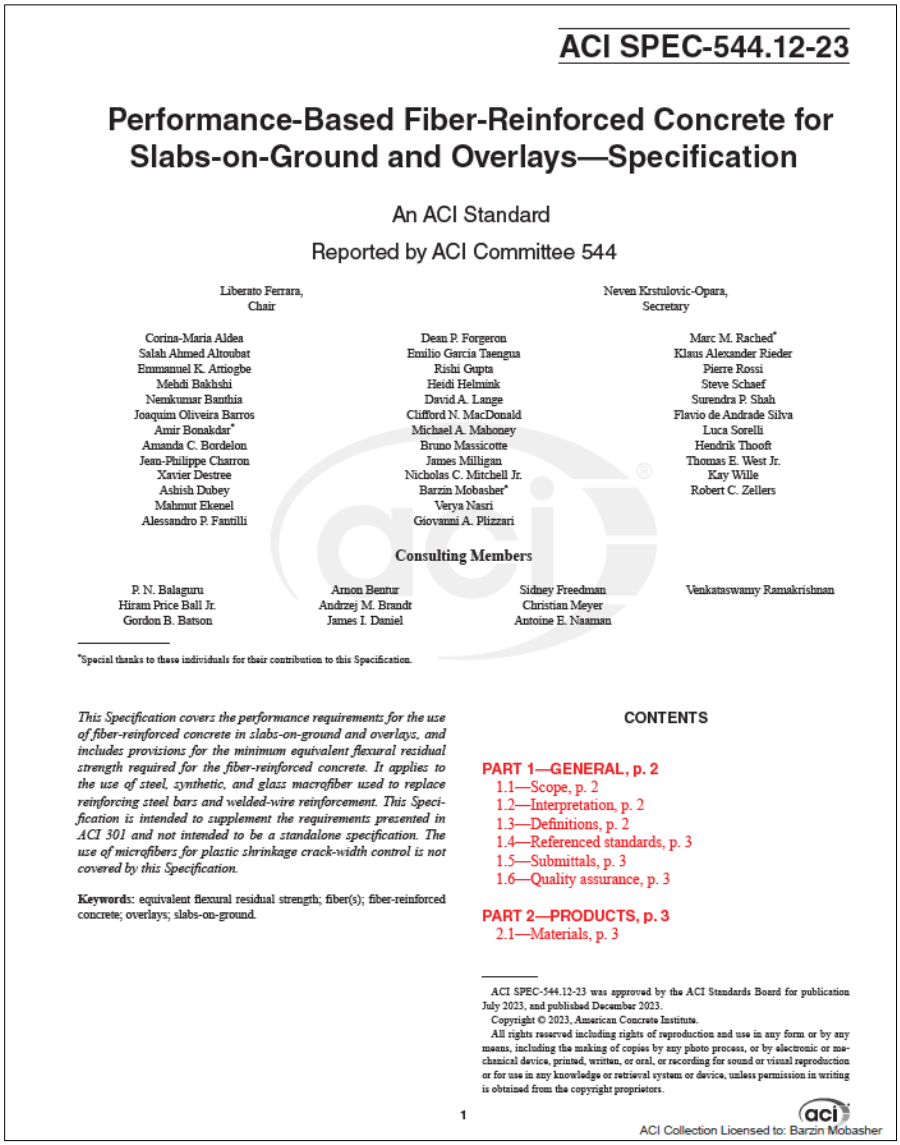

ACI SPEC-544.12-23

Performance-Based Fiber-Reinforced Concrete for Slabs-on-Ground and Overlays—Specification

An ACI Standard

Reported by ACI Committee 544

Liberato Ferrara, Chair

Neven Krstulovic-Opara, Secretary

Corina-Maria Aldea
Salah Ahmed Altoubat
Emmanuel K. Attiogbe
Mehdi Bakhshi
Nemkumar Banthia
Joaquim Oliveira Barros
Amir Bonakdar*
Amanda C. Bordelon
Jean-Philippe Charron
Xavier Destree
Ashish Dubey
Mahmut Ekenel
Alessandro P. Fantilli
Dean P. Forgeron
Emilio Garcia Taengua
Rishi Gupta
Heidi Helmink
David A. Lange
Clifford N. MacDonald
Michael A. Mahoney
Bruno Massicotte
James Milligan
Nicholas C. Mitchell Jr.
Barzin Mobasher*
Verya Nasri
Giovanni A. Plizzari
Marc M. Rached*
Klaus Alexander Rieder
Pierre Rossi
Steve Schaef
Surendra P. Shah
Flavio de Andrade Silva
Luca Sorelli
Hendrik Thooft
Thomas E. West Jr.
Kay Wille
Robert C. Zellers

Consulting Members

P. N. Balaguru
Hiram Price Ball Jr.
Gordon B. Batson
Arnon Bentur
Andrzej M. Brandt
James I. Daniel
Sidney Freedman
Christian Meyer
Antoine E. Naaman
Venkataswamy Ramakrishnan

*Special thanks to these individuals for their contribution to this Specification.

This Specification covers the performance requirements for the use of fiber-reinforced concrete in slabs-on-ground and overlays, and includes provisions for the minimum equivalent flexural residual strength required for the fiber-reinforced concrete. It applies to the use of steel, synthetic, and glass macrofiber used to replace reinforcing steel bars and welded-wire reinforcement. This Specification is intended to supplement the requirements presented in ACI 301 and not intended to be a standalone specification. The use of microfibers for plastic shrinkage crack-width control is not covered by this Specification.

Keywords: equivalent flexural residual strength; fiber(s); fiber-reinforced concrete; overlays; slabs-on-ground.

CONTENTS

PART 1—GENERAL, p. 2
1.1—Scope, p. 2
1.2—Interpretation, p. 2
1.3—Definitions, p. 2
1.4—Referenced standards, p. 3
1.5—Submittals, p. 3
1.6—Quality assurance, p. 3

PART 2—PRODUCTS, p. 3
2.1—Materials, p. 3

ACI SPEC-544.12-23 was approved by the ACI Standards Board for publication July 2023, and published December 2023.

Copyright © 2023, American Concrete Institute.
All rights reserved including rights of reproduction and use in any form or by any means, including the making of copies by any photo process, or by electronic or mechanical device, printed, written, or oral, or recording for sound or visual reproduction or for use in any knowledge or retrieval system or device, unless permission in writing is obtained from the copyright proprietors.

ACI Collection Licensed to: Barzin Mobasher

Figure 67. Title Page for ACI Spec 544.12-23.

The most important aspect of this specification is the minimum residual strength levels required as defined by the standards, as shown in Table 12, which provides an equivalent residual strength value to meet the temperature and shrinkage requirements of steel rebar.

Table 12. ACI 544-12R "Equivalent Flexural Residual Strength for Temperature and Shrinkage Reinforcement Based on ACI 544.4R."

Steel Reinforcement Ratio (%)	Equivalent Flexural Residual Strength, $f^D_{c,150}$ or $f_{c,3}$ (psi)
≤ 0.10	100
0.12	120
0.14	140
0.16	160
0.18	180
0.20	200

Note: For reinforcement ratios greater than 0.2 percent and calculations based on moment capacity, the equivalent flexural strength shall be calculated in accordance with ACI 544.4R.

Listing of All of the ACI Guidelines and Tools Available

- ACI 544.5R-10 "Physical Properties and Durability of Fiber-Reinforced Concrete," Report, ACI Committee, p. 31, (2010)
- ACI 544.6R-15 Report on Design and Construction of Steel Fiber-Reinforced Concrete Elevated Slabs (2015)
- ACI 544.7R-16 Report on Design and Construction of Fiber-Reinforced Precast Concrete Tunnel Segments (2016)
- ACI 544.8R-16: Report on Indirect Method to Obtain Stress-Strain Response of Fiber-Reinforced Concrete, ACI Committee 544 ACI 544.8R (2016)
- ACI 544.9R-17: Report on Measuring Mechanical Properties of Hardened Fiber-Reinforced Concrete, (2017)
- ACI 544.10R-17: Report on Measuring Properties of Fresh Fiber-Reinforced Concrete, (2018)
- ACI 544.4R-18: Report on Structural Design with Fiber-Reinforced Concrete (2018)
- 544.12R-23 Performance-Based Fiber Reinforced Concrete for Slab-on-Ground and Overlay-Specifications (2023)

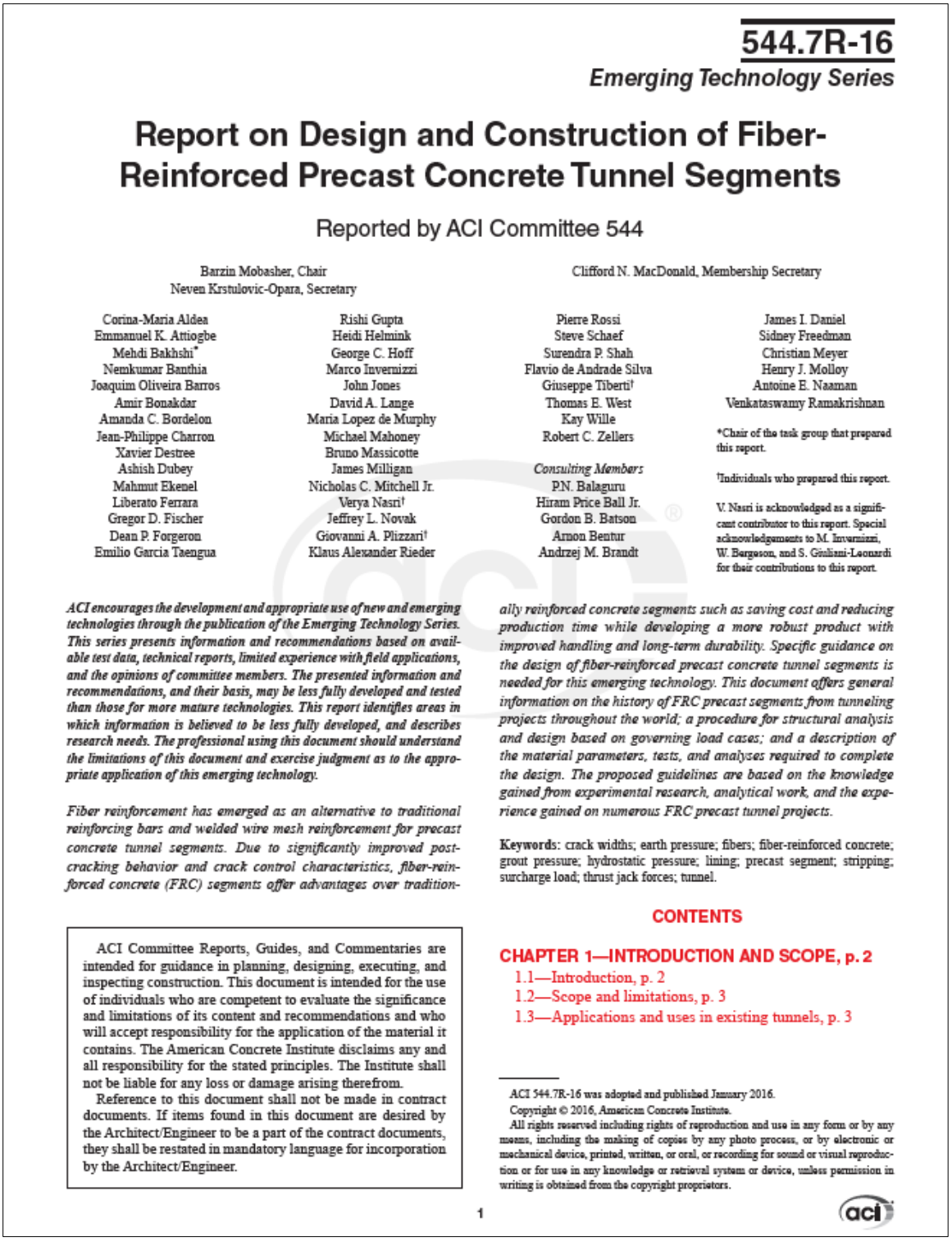

544.7R-16

Emerging Technology Series

Report on Design and Construction of Fiber-Reinforced Precast Concrete Tunnel Segments

Reported by ACI Committee 544

Barzin Mobasher, Chair
Neven Krstulovic-Opara, Secretary

Clifford N. MacDonald, Membership Secretary

Corina-Maria Aldea
Emmanuel K. Attiogbe
Mehdi Bakhshi*
Nemkumar Banthia
Joaquim Oliveira Barros
Amir Bonakdar
Amanda C. Bordelon
Jean-Philippe Charron
Xavier Destree
Ashish Dubey
Mahmut Ekenel
Liberato Ferrara
Gregor D. Fischer
Dean P. Forgeron
Emilio Garcia Taengua
Rishi Gupta
Heidi Helmink
George C. Hoff
Marco Invernizzi
John Jones
David A. Lange
Maria Lopez de Murphy
Michael Mahoney
Bruno Massicotte
James Milligan
Nicholas C. Mitchell Jr.
Verya Nasri†
Jeffrey L. Novak
Giovanni A. Plizzari†
Klaus Alexander Rieder
Pierre Rossi
Steve Schaef
Surendra P. Shah
Flavio de Andrade Silva
Giuseppe Tiberti†
Thomas E. West
Kay Wille
Robert C. Zellers

Consulting Members
P.N. Balaguru
Hiram Price Ball Jr.
Gordon B. Batson
Arnon Bentur
Andrzej M. Brandt
James I. Daniel
Sidney Freedman
Christian Meyer
Henry J. Molloy
Antoine E. Naaman
Venkataswamy Ramakrishnan

*Chair of the task group that prepared this report.

†Individuals who prepared this report.

V. Nasri is acknowledged as a significant contributor to this report. Special acknowledgements to M. Invernizzi, W. Bergeson, and S. Giuliani-Leonardi for their contributions to this report.

ACI encourages the development and appropriate use of new and emerging technologies through the publication of the Emerging Technology Series. This series presents information and recommendations based on available test data, technical reports, limited experience with field applications, and the opinions of committee members. The presented information and recommendations, and their basis, may be less fully developed and tested than those for more mature technologies. This report identifies areas in which information is believed to be less fully developed, and describes research needs. The professional using this document should understand the limitations of this document and exercise judgment as to the appropriate application of this emerging technology.

Fiber reinforcement has emerged as an alternative to traditional reinforcing bars and welded wire mesh reinforcement for precast concrete tunnel segments. Due to significantly improved post-cracking behavior and crack control characteristics, fiber-reinforced concrete (FRC) segments offer advantages over traditionally reinforced concrete segments such as saving cost and reducing production time while developing a more robust product with improved handling and long-term durability. Specific guidance on the design of fiber-reinforced precast concrete tunnel segments is needed for this emerging technology. This document offers general information on the history of FRC precast segments from tunneling projects throughout the world; a procedure for structural analysis and design based on governing load cases; and a description of the material parameters, tests, and analyses required to complete the design. The proposed guidelines are based on the knowledge gained from experimental research, analytical work, and the experience gained on numerous FRC precast tunnel projects.

Keywords: crack widths; earth pressure; fibers; fiber-reinforced concrete; grout pressure; hydrostatic pressure; lining; precast segment; stripping; surcharge load; thrust jack forces; tunnel.

ACI Committee Reports, Guides, and Commentaries are intended for guidance in planning, designing, executing, and inspecting construction. This document is intended for the use of individuals who are competent to evaluate the significance and limitations of its content and recommendations and who will accept responsibility for the application of the material it contains. The American Concrete Institute disclaims any and all responsibility for the stated principles. The Institute shall not be liable for any loss or damage arising therefrom.

Reference to this document shall not be made in contract documents. If items found in this document are desired by the Architect/Engineer to be a part of the contract documents, they shall be restated in mandatory language for incorporation by the Architect/Engineer.

CONTENTS

CHAPTER 1—INTRODUCTION AND SCOPE, p. 2
1.1—Introduction, p. 2
1.2—Scope and limitations, p. 3
1.3—Applications and uses in existing tunnels, p. 3

ACI 544.7R-16 was adopted and published January 2016.

Copyright © 2016, American Concrete Institute.
All rights reserved including rights of reproduction and use in any form or by any means, including the making of copies by any photo process, or by electronic or mechanical device, printed, written, or oral, or recording for sound or visual reproduction or for use in any knowledge or retrieval system or device, unless permission in writing is obtained from the copyright proprietors.

Figure 68. Report on Design and Construction of Fiber-Reinforced Precast Concrete Tunnel Segments.

ACI 544.6R-15

Report on Design and Construction of Steel Fiber-Reinforced Concrete Elevated Slabs

Reported by ACI Committee 544

Barzin Mobasher,*† Chair
Neven Krstulovic-Opara, Secretary

Clifford N. MacDonald, Membership Secretary

Corina-Maria Aldea
Nemkumar Banthia
Joaquim Oliveira Barros*
Gordon B. Batson
Vivek S. Bindiganavile
Peter H. Bischoff
Jean-Philippe Charron
Xavier Destree*
Ashish Dubey
Philip J. Dyer
Mahmut Ekenel
Gregor D. Fischer
Dean P. Forgeron
Antonio Gallovich
Graham T. Gilbert
Vellore S. Gopalaratnam
Antonio J. Guerra
Rishi Gupta
Carol D. Hays
George C. Hoff
Allen J. Hulshizer
Akm Anwarul Islam
John Jones
David A. Lange
Maria Lopez de Murphy
Michael A. Mahoney
Bruno Massicotte
Christian Meyer
Nicholas C. Mitchell Jr.
Gerald H. Morton
Antoine E. Naaman*
Jeffrey L. Novak
Mark E. Patton
Max L. Porter
John H. Pye
Venkataswamy Ramakrishnan
Klaus Alexander Rieder
Pierre Rossi
Surendra P. Shah
Konstantin Sobolev
Jim D. Speakman Sr.‡
Peter C. Tatnall‡
Houssam A. Toutanji
George J. Venta‡
Gary L. Vondran
Kay Wille
Robert Wojtysiak
Carla V. Yland
Robert C. Zellers
Libe Zhang
Ronald F. Zollo

Consulting Members
Ashraf I. Ahmed
Claire G. Ball
Hiram Price Ball Jr.
Leonard W. Bell
Arnon Bentur
Andrzej M. Brandt
Mark A. Bury
Jonas Carlsward
Zhi-Yuan Chen
James I. Daniel
Sidney Freedman
Bob Grace
C. Geoffrey Hampson
Roger L. Lacroix
David R. Lankard
Pritpal S. Mangat
Winston A. Marsden
Henry N. Marsh Jr.
James R. McConaghy
Henry J. Molloy
Dudley R. Morgan
Dirk E. Nemegeer
Michael J. Roach
Morris Schupack‡
Ake Skarendahl
Ben L. Tilsen
Eldon G. Tipping
Jean Francois Trottier

*Members who prepared this report.
†Chair of the task group who drafted this report.
‡Deceased.

Construction of slabs in areas with weak soil conditions has commonly used pile-supported slab structural design so that the adverse effects of soil-structure interaction in terms of differential settlement, cracking, or long-term serviceability problems are avoided. In this application, the construction of slabs on closely spaced pile caps (typical span-depth ratios between 8 and 30) is referred to as elevated ground slabs (EGSs). These slabs may be subjected to moderately high loading, such as concentrated point loading of up to 44 kip (150 kN) and uniformly distributed loadings of 1000 lb/ft² (50 kN/m²). The dynamic loadings may be due to moving loads such as forklifts, travel lifts, and other material handling equipment. Fiber-reinforced concrete (FRC) has been successfully used to address the structural design of these slabs. Based on the knowledge gained, the area has been extended to a construction practice for slabs supported by columns as well. Applications are further extended to multi-story building applications. This report addresses the methodology for analysis, design, and construction of steel FRC (SFRC) slabs supported on piles or columns (also called elevated SFRC [E-SFRC]). Sections of the report address the history, practice, applications, material testing, full-scale testing, and certifications. By compiling the practice and knowledge in the analysis design with FRC materials, the steps in the design approach based on ultimate strength approach using two-way slab mechanisms are presented. The behavior of a two-way system may not require the flexural strength of conventional reinforced concrete (RC) because of redistribution, redundancy, and failure mechanisms.

Methods of construction, curing, and full-scale testing of slabs are also presented. A high dosage of deformed steel fibers (85 to 170

ACI Committee Reports, Guides, and Commentaries are intended for guidance in planning, designing, executing, and inspecting construction. This document is intended for the use of individuals who are competent to evaluate the significance and limitations of its content and recommendations and who will accept responsibility for the application of the information it contains. ACI disclaims any and all responsibility for the stated principles. The Institute shall not be liable for any loss or damage arising there from. Reference to this document shall not be made in contract documents. If items found in this document are desired by the Architect/ Engineer to be a part of the contract documents, they shall be restated in mandatory language for incorporation by the Architect/Engineer.

ACI 544.6R-15 was adopted and published September 2015.

Copyright © 2015, American Concrete Institute.
All rights reserved including rights of reproduction and use in any form or by any means, including the making of copies by any photo process, or by electronic or mechanical device, printed, written, or oral, or recording for sound or visual reproduction or for use in any knowledge or retrieval system or device, unless permission in writing is obtained from the copyright proprietors.

Figure 69. Report on Design and Construction of Steel Fiber-Reinforced Concrete Elevated Slabs.

ACI 544.9R-17

Report on Measuring Mechanical Properties of Hardened Fiber-Reinforced Concrete

Reported by Committee 544

Barzin Mobasher*, Chair
Neven Krstulovic-Opara, Secretary

Clifford N. MacDonald*, Membership Secretary

Corina-Maria Aldea
Emmanuel K. Attiogbe
Mehdi Bakhshi
Nemkumar Banthia
Joaquim Oliveira Barros*
Amir Bonakdar*
Amanda C. Bordelon
Jean-Philippe Charron
Xavier Destree*
Ashish Dubey
Mahmut Ekenel
Liberato Ferrara†
Gregor D. Fischer
Dean P. Forgeron*
Emilio Garcia Taengua
Rishi Gupta
Heidi Helmink
George C. Hoff
Marco Invernizzi
John Jones
David A. Lange
Michael A. Mahoney
Bruno Massicotte
James Milligan
Nicholas C. Mitchell Jr.
Jeffrey L. Novak
Giovanni A. Plizzari
Klaus Alexander Rieder
Pierre Rossi
Steve Schaef
Surendra P. Shah
Flavio de Andrade Silva
Luca Sorelli
Thomas E. West
Kay Wille
Robert C. Zellers

Consulting members

P. N. Balaguru
Hiram Price Ball Jr.
Gordon B. Batson
Arnon Bentur
Andrzej M. Brandt
James I. Daniel
Sidney Freedman
Christian Meyer
Henry J. Molloy
Antoine E. Naaman‡
Venkataswamy Ramakrishnan

*Members of subcommittee who contributed to this report.
†Chair of the subcommittee that developed this report.
‡Consulting members who contributed to this report.

The committee would like to thank H. Aoude and F. Vossoughi for their contributions to this report.

This report provides a synopsis of the existing testing methodologies for the determination of mechanical properties of hardened fiber-reinforced concrete (FRC). This report applies to the mechanical properties of conventionally mixed and placed FRC, including fiber-reinforced self-consolidating concrete (FRSCC), or fiber-reinforced shotcrete (FRS) using steel, glass, polymeric, and natural fibers.

The objective is to enable manufacturers to characterize the mechanical properties of hardened FRC and encourage researchers and testing laboratories to adopt common and unified test methods to build a meaningful database of mechanical properties of hardened FRC materials and products. Test results from the test procedures used in this report are not intended for the design of FRC structures, but to gain a better understanding of factors influencing the determination of their mechanical properties and of FRCs and FRC products.

Keywords: compressive strength; fiber pullout; fiber-reinforced concrete; flexural fatigue resistance; flexural strength; impact resistance; multiaxial behavior; shear and torsion; tensile strength; toughness.

ACI Committee Reports, Guides, and Commentaries are intended for guidance in planning, designing, executing, and inspecting construction. This document is intended for the use of individuals who are competent to evaluate the significance and limitations of its content and recommendations and who will accept responsibility for the application of the material it contains. The American Concrete Institute disclaims any and all responsibility for the stated principles. The Institute shall not be liable for any loss or damage arising therefrom.

Reference to this document shall not be made in contract documents. If items found in this document are desired by the Architect/Engineer to be a part of the contract documents, they shall be restated in mandatory language for incorporation by the Architect/Engineer.

CONTENTS

CHAPTER 1—INTRODUCTION AND SCOPE, p. 2
1.1—Introduction, p. 2
1.2—Scope, p. 2

CHAPTER 2—NOTATION AND DEFINITIONS, p. 2
2.1—Notation, p. 2
2.2—Definitions, p. 3

ACI 544.9R-17 was adopted and published January 2017.

Copyright © 2017, American Concrete Institute.
All rights reserved including rights of reproduction and use in any form or by any means, including the making of copies by any photo process, or by electronic or mechanical device, printed, written, or oral, or recording for sound or visual reproduction or for use in any knowledge or retrieval system or device, unless permission in writing is obtained from the copyright proprietors.

Figure 70. Report on Measuring Mechanical Properties of Hardened Fiber-Reinforced Concrete.



ACI 544.8R-16

Report on Indirect Method to Obtain Stress-Strain Response of Fiber-Reinforced Concrete (FRC)

Reported by ACI Committee 544

Barzin Mobasher[†], Chair
Never Krstulovic-Opara*, Secretary

Clifford N. MacDonald, Membership Secretary

Corina-Maria Aldea
Emmanuel K. Attioglie
Nemkumar Banthia
Joaquim Oliveira Barros*
Gordon B. Batson
Peter H. Bischoff
Jean-Philippe Charron
Xavier Destree
Ashish Dubey
Mahmut Ekenel
Liberato Ferrara
Gregor D. Fischer
Dean P. Forgeron
Antonio Gallovich

Rishi Gupta
George C. Hoff
John Jones
David A. Lange
Maria Lopez de Murphy
Michael A. Mahoney
Bruno Massicotte
Christian Meyer
James Milligan
Nicholas C. Mitchell Jr.
Gerald H. Morton
Antoine E. Naaman*
Jeffrey L. Novak
Giovanni A. Plizzari

Max L. Porter
Venkataswamy Ramakrishnan
Klaus Alexander Rieder
Pierre Rossi
Surendra P. Shah
Flavio de Andrade Silva
Kay Wille
Robert C. Zellers
Lihe Zhang

Consulting Members
P.N. Balaguru
Hiram Price Ball Jr.
Arnon Bentur
Andrzej M. Brandt
James I. Daniel
Sidney Freedman
Melvyn A. Galinat[‡]
Henry J. Malloy
Antoine E. Naaman

*Members of the subcommittee that authored this report.
†Chair of the task group that drafted this report.
‡Deceased.

Development of proper design procedures for fiber reinforced concrete (FRC) materials requires use of material tensile and compressive stress strains that reflect the contribution of fibers to the post-cracking behavior. While uniaxial tension tests provide the most fundamental material properties, conducting closed-loop tension tests are difficult to accomplish; therefore, methods based on indirect measurement of tensile properties using flexural tests are typically used.

This report presents the methodologies that are used for data reduction and presentation of the flexural test results in terms of an equivalent tensile stress-strain response for FRC materials. Existing methods for estimating uniaxial tensile stress-strain response of strain-softening and hardening FRCs from flexural beam-test data are introduced. Different approaches applied to beam tests based on elastic equivalent, curve fitting, or back-calculation of flexural data are introduced. These are divided into two general categories: elastic equivalent approach or inverse analysis method. In the elastic equivalent approach, a summary of available test methods by various code agencies are presented.

Using back-calculation methods, tools based on the finite element method and analytical closed-form solutions are presented. An approach is presented that uses closed-form moment-curvature relationships and obtains load-deflection responses for a beam of three- or four-point loading. The method is used to obtain equivalent parametric tensile stress and strain relationships for a variety of FRC materials. The methods are compared against the available residual strength and also elastically equivalent residual strengths obtained by different specimen geometries.

Results for a range of FRC materials studied show the back-calculated post-peak residual tensile strength is approximately 30 to 37 percent of the elastically equivalent flexural residual strength for specimens with different fiber types and volume fractions.

Keywords: fiber-reinforced concrete; inverse analysis; tensile stress-strain diagram.

ACI Committee Reports, Guides, and Commentaries are intended for guidance in planning, designing, executing, and inspecting construction. This document is intended for the use of individuals who are competent to evaluate the significance and limitations of its content and recommendations and who will accept responsibility for the application of the material it contains. The American Concrete Institute disclaims any and all responsibility for the stated principles. The Institute shall not be liable for any loss or damage arising therefrom.

Reference to this document shall not be made in contract documents. If items found in this document are desired by the Architect/Engineer to be a part of the contract documents, they shall be restated in mandatory language for incorporation by the Architect/Engineer.

ACI 544.8R-16 was adopted and published March 2016.

Copyright © 2016, American Concrete Institute.

All rights reserved including rights of reproduction and use in any form or by any means, including the making of copies by any photo process, or by electronic or mechanical device, printed, written, or oral, or recording for sound or visual reproduction or for use in any knowledge or retrieval system or device, unless permission in writing is obtained from the copyright proprietors.

Figure 71. Report on Indirect Method to Obtain Stress-Strain Response of Fiber-Reinforced Concrete (FRC).

American Concrete Institute
Always advancing

PRC-544.10-21
TechNote

Fiber Effect on Reducing the Permeability of Cracked Concrete Structures—TechNote

Keywords: crack width; durability; fiber; fiber-reinforced concrete; permeability; stress.

Question

Concrete structures are susceptible to cracking during their service life. These cracks become the main route through which liquids and aggressive agents penetrate into and through concrete mass. Does the use of fibers in concrete result in a reduction of crack widths compared to concrete without fibers? Does crack width reduction correlate with maintaining a lower permeability, thus improving the long-term durability of a structure?

Answer

A properly designed concrete with a fiber-reinforcement system has a reduced crack width under service loads. The fibers can cause changes in crack morphology (higher roughness and tortuosity) and increase the likelihood of multiple crack development, crack deflection, and branching. Consequently, ingress of liquid and other aggressive agents is decreased significantly and results in a delay of permeability-related deterioration mechanisms. Therefore, all evidence points to fibers extending the service life of concrete structures.

Introduction

Reinforced concrete structures are designed to withstand stresses caused by external loads (static, cyclic, or dynamic loads), stresses caused by internal and restrained deformations (shrinkage, thermal, and hydraulic gradients), as well as resist chemical and physical degradation mechanisms. Direct observations and testing have clearly revealed that ingress of liquid and aggressive agents into cracked concrete is much larger than in sound concrete. Cracking may allow deep penetration of air, liquid, and aggressive ions, depending on crack size and environmental conditions. These result in issues related to water tightness and reduced corrosion resistance for embedded reinforcing steel. Subsequently, widespread deterioration mechanisms through carbonation, alkali-aggregate reaction (AAR), or chemical attack in aggressive environments may be exacerbated by the presence of cracks (ACI 544.5R).

Discussion

Allowable crack widths—North American (ACI 224R; ACI 224.1R; ACI 224.2R; ACI 318; AASHTO LFRD Bridge Design Specifications; CSA A23.1-2) and European (*fib* Model Code [MC2010]; BS EN 1992-1-1:2004) building codes require that cracks in concrete exposed to weathering be no larger than specified widths to ensure structural and mechanical integrity and durability (Aldea and Shah 2011). Maximum allowable crack widths ranging between 0.006 and 0.015 in. (0.15 and 0.38 mm) are specified in various design codes for most reinforced concrete structures and bridge applications exposed to aggressive environments. ACI 224R, 224.1R, and 224.2R provide information about the cracking mechanisms in concrete. Design recommendations as presented in Table 1 provide allowable crack widths versus exposure conditions in fiber-reinforced concrete, and the use of fibers as a means to control cracking in overlays. More research is needed on concrete permeability to evaluate current limits and determine the maximum allowable width of exposed cracks in structures.

Figure 72. Fiber Effect on Reducing the Permeability of Cracked Concrete Structures.

APPENDIX H: ASTM C1609 Testing Method and Equipment



Figure 73. An Available Testing System for Closed-Loop Testing of FRC Developed by GCTS, Tempe, AZ.

ASTM C1609 Testing Method and Equipment, which can be conducted locally by the equipment developed by GCTS Mechanical Testing Systems of Tempe, Arizona. A significant number of reports and discussions of this test method are available and will be provided upon request.

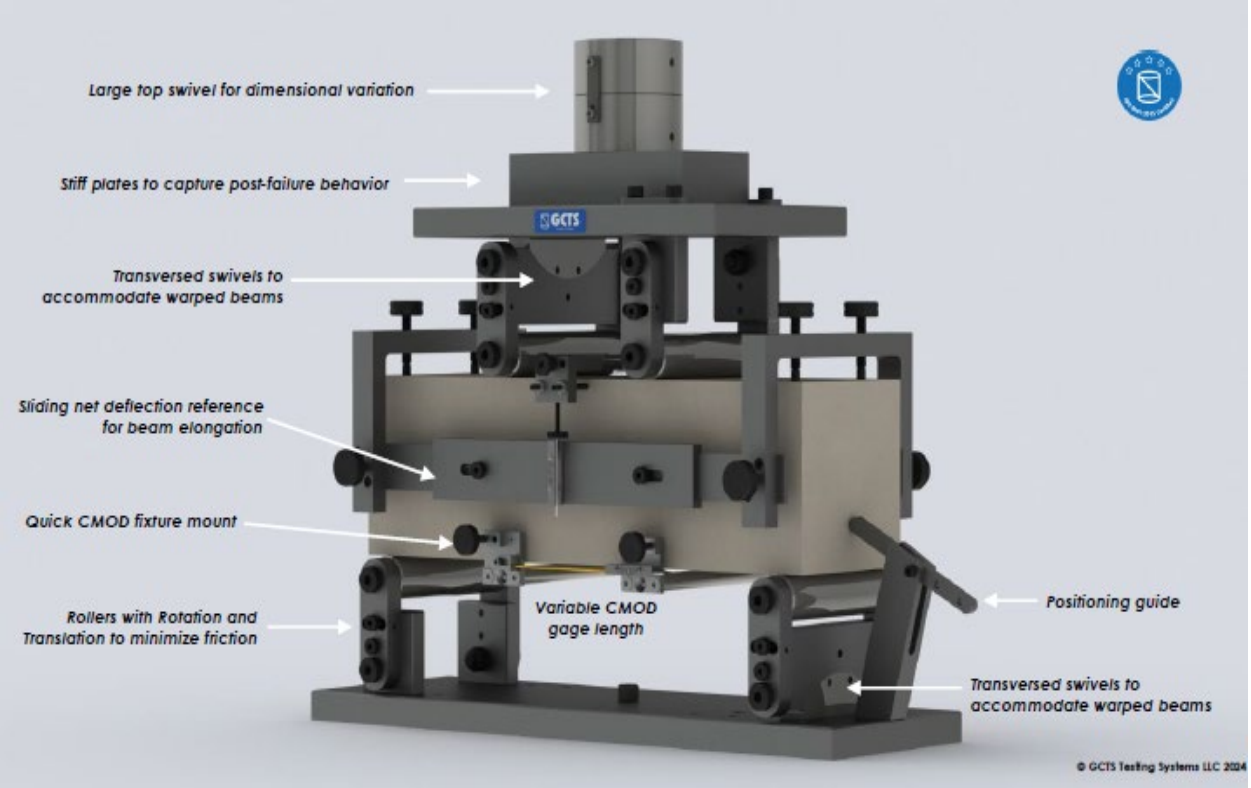

Figure 74. ASTM C1609 Test Setup for Four-Point Bending Test.

Insights to Consider for ASTM C1609: Flexural Testing

The procedure for monotonic flexural testing consisted of load and linear variable differential transformer (LVDT) deflection-controlled phases, as summarized in Table 13. A servo-hydraulic test machine manufactured by MTS Corporation with 22 kips (98 KN) capacity will be used. Parameters computed from the test include stiffness, load at cracking, residual strength, and toughness. The toughness was computed at three deflection limits of L/600, L/300 and L/150, where L is the span of the specimen equivalent to 457 mm (18 in).

Figure 75 shows the test configuration for closed-loop flexural tests. The LVDT was used as the control for displacement-control phases, due to its inherent accuracy in measuring the deflection. The LVDT response is used to control the test during Phases 2 and 3 of the test procedures.

Table 13. Testing Procedure Used in the MTS Station Manager to Control the Test (C1609).

Phase	Control Mode	Loading Rate	Phase Limit
1	Load	50 lb./min (222.41 N/sec)	500 lb. (2224.1 N)
2	LVDT (Deflection)	0.005 in/min (0.127 mm/min)	0.02 in (0.508 mm)
3	Actuator (Deflection)	0.015 in/min (0.381 mm/min)	0.50 in (12.7 mm)

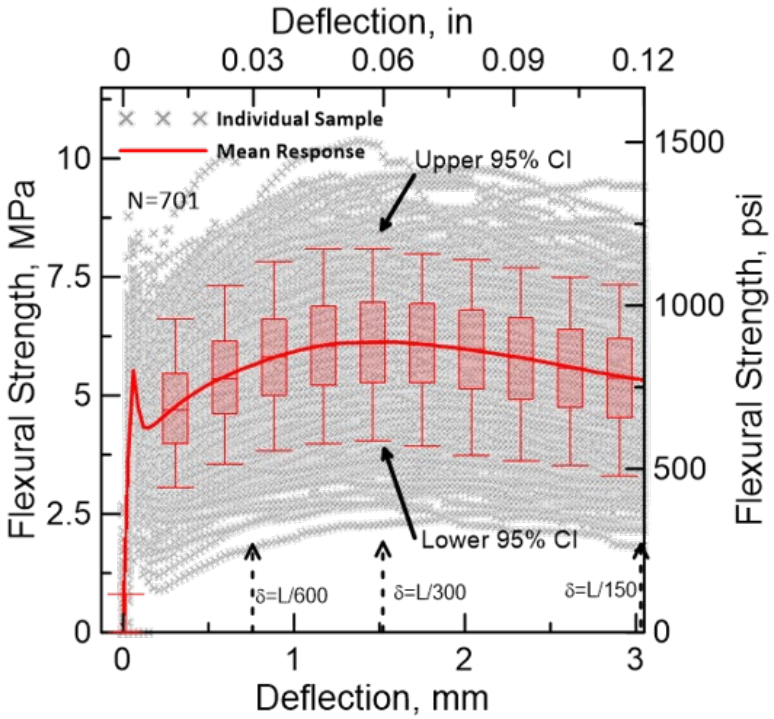

Figure 75. Scatter Plot of All Data with Mean Curve and Box-and-Whisker Plot of Flexural Response of Individual Data for 28-day Specimens [73].

Figure 76 presents the load-deflection response of FRC samples tested in accordance with ASTM C1609, based on 701 specimens. Although the responses cover a wide range, the variation in residual strength shown in the box-and-whisker plots at different deflection levels was not significant across the entire testing range. Data points beyond the whiskers were identified as outliers [73]. Furthermore, no correlation was observed between first crack, f_1, and residual tensile strength, f^D_{150}[74]. This absence of correlation, which is also confirmed when considering other residual strength parameters, indicates that normalizing residual strength with the first-crack flexural strength is meaningless and can lead to ambiguous interpretations.

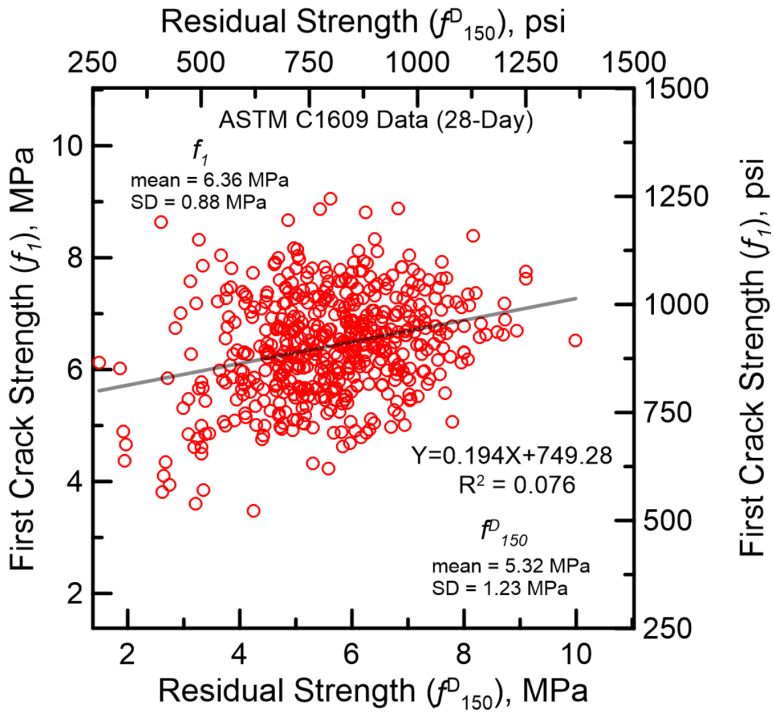

Figure 76. Coefficient Determination Between Residual and First Crack Flexural Strength Parameters [74].

The nominal flexural stress, (f_n) defined by ASTM C1609, can be related to the corresponding average tensile stress, ($\bar{\sigma}_t$). ACI 544.4R recommends that the ratio of these two stress values, ($\bar{\sigma}_t/f_n$) be taken as 0.33. Simulation results from a dataset of 525 beams indicate that the scatter is indeed centered around this 0.33 ratio (refer to Figure 77). This suggests that the residual tensile strength of plain FRC can be reasonably approximated using this relationship of $\bar{\sigma}_t = 0.33 f_n$.

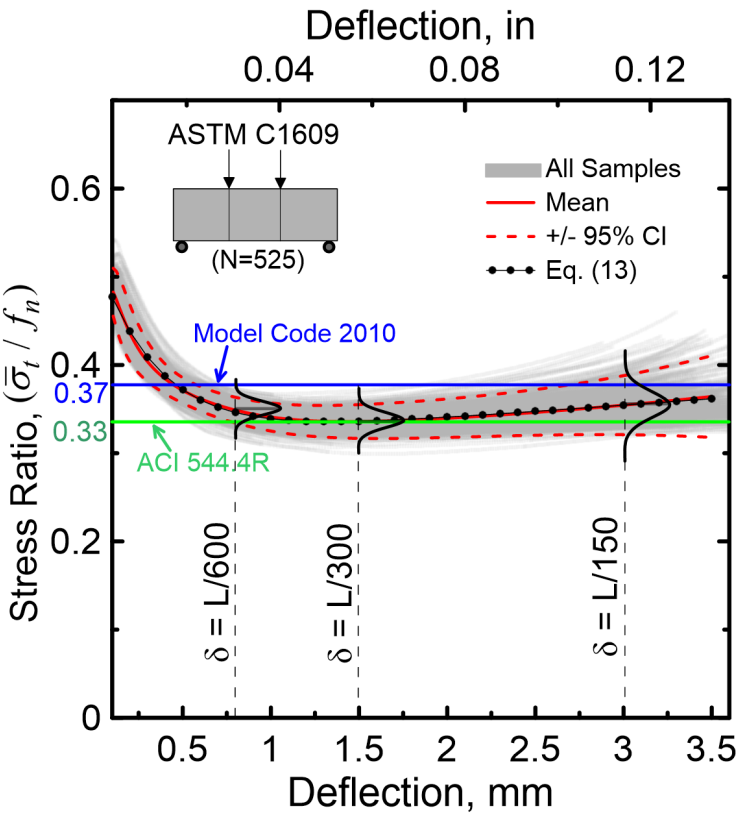

Figure 77. Analysis for Back-Calculated Stress Ratio [74].

APPENDIX I: Tension Stiffening Model for Joint Spacing Design

Fiber Bridging Effect

With the presence of fibers, the load-transfer mechanism from the composite section becomes more complex after cracking. Both conventional reinforcement and fibers govern sharing the tensile load. At crack locations, fibers contribute through fiber bridging mechanisms (refer to Figure 78). The greater residual capacity in the cracked sections allows for more effective resistance to load-induced stresses through the development of shorter effective span lengths between cracks. This enhanced fiber bridging enables the concrete matrix to continue contributing to load resistance after cracking, which improves fatigue resistance under repeated loading cycles.

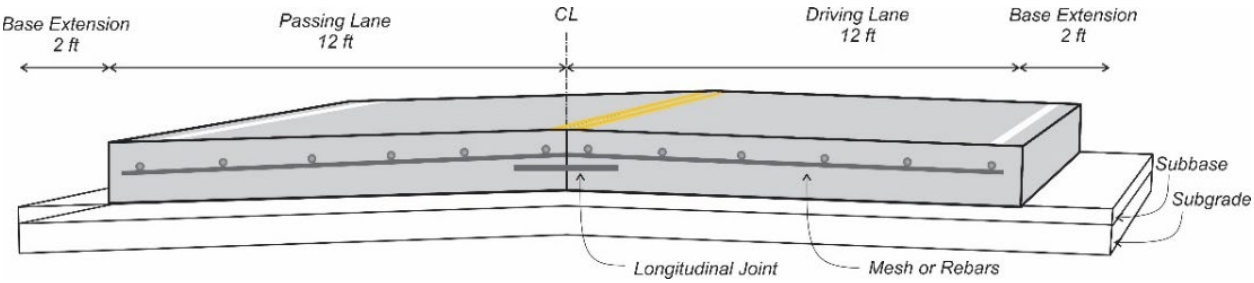

Figure 78. Typical Example of Conventional RC.

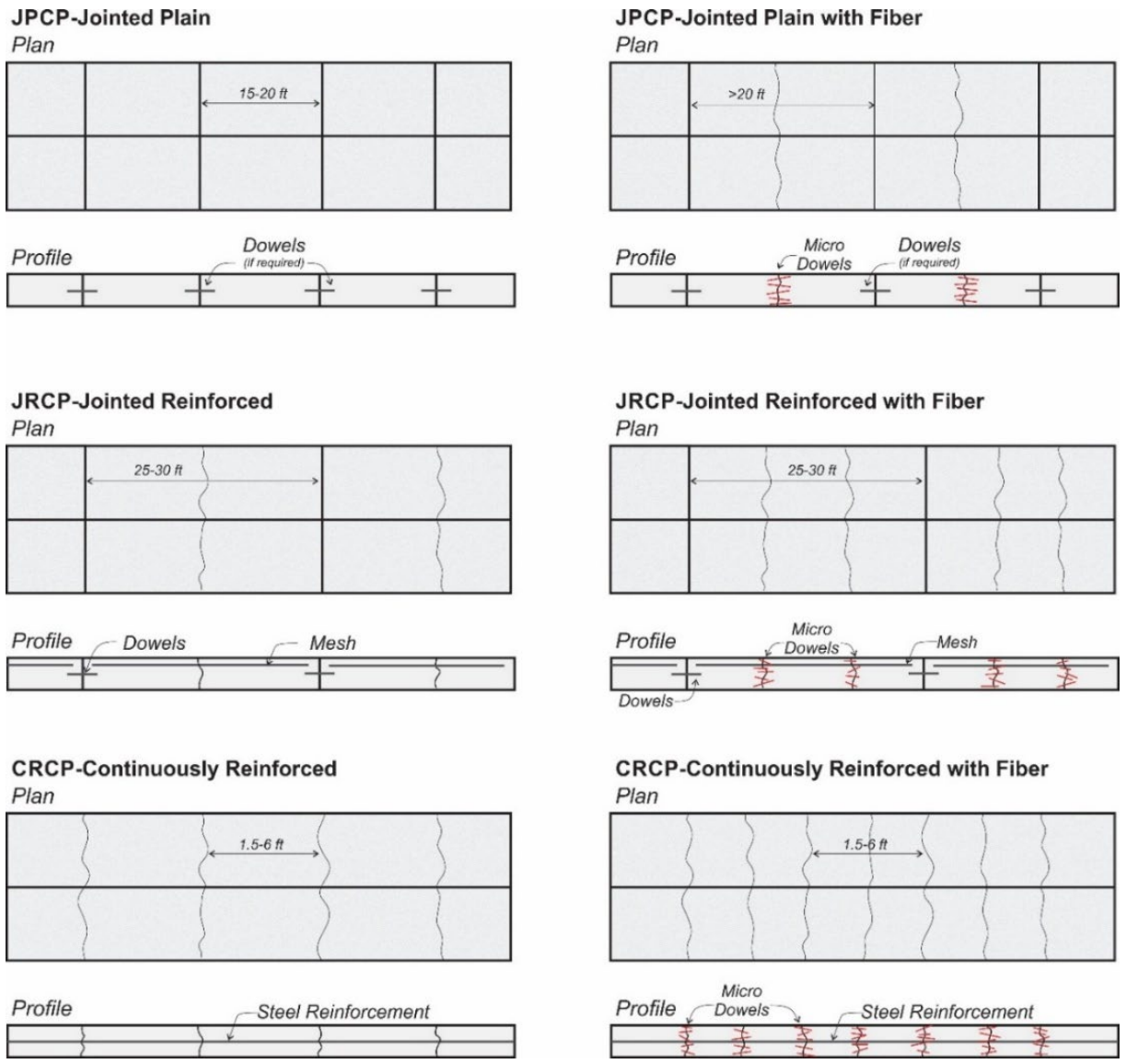

Figure 79. Typical Examples of Hybrid RC.

Tension-Stiffening Modeling of Cement Composite

A finite difference method developed by Soranakom and Mobasher [47,48] was employed to simulate the tension-stiffening behavior in RC in the post-cracking region. The specimen is idealized as a series of one-dimensional segments comprising yarn reinforcement, concrete matrix, and interface elements, as shown in Figure 80. Once the tensile stress in the matrix exceeds the cracking threshold, load transfer is maintained through the yarn, governed by bond-slip. This discrete model divides the total embedded length into nodal segments *n*, allowing for localized analysis of slip, bond stress, and crack spacing. The nodal segments *n*, in the equation, can then be implied as the individual panels in the framework of the pavement. Nodal equilibrium equations are derived with slip as the primary variable, producing a global stiffness matrix [C], nodal slip vector {S}, and external force vector {T} to solve the system iteratively.

$[C]_{n,n}\{S\}_n = \{T\}_n$ **Equation 26**

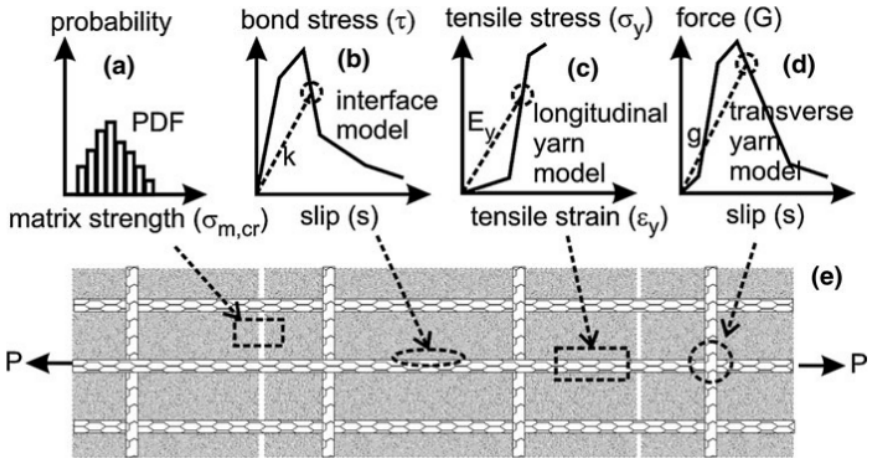

Figure 80. Mechanical Behavior of a Cracked Fabric Reinforced Cement Composite: (a) Matrix Strength for Cracking Criterion, (b) Bond-Slip Model, (c) Longitudinal Yarn Stress-Strain Model, (d) Nonlinear Spring Model Simulating Anchorage Strength at Cross Yarn Junction [48].

To adapt this model for RC incorporating discrete fibers, the same finite difference framework can be utilized by treating the rebar reinforcement as yarn, while explicitly incorporating the fiber bridging mechanism. After the matrix cracks, both the rebar and fiber share the tensile load, transferring it back to the surrounding matrix through bond and bridging actions. Figure 81 illustrates a series of one-dimensional segments composed of the reinforcing bar, bond interface, concrete matrix, and fiber bridging elements.

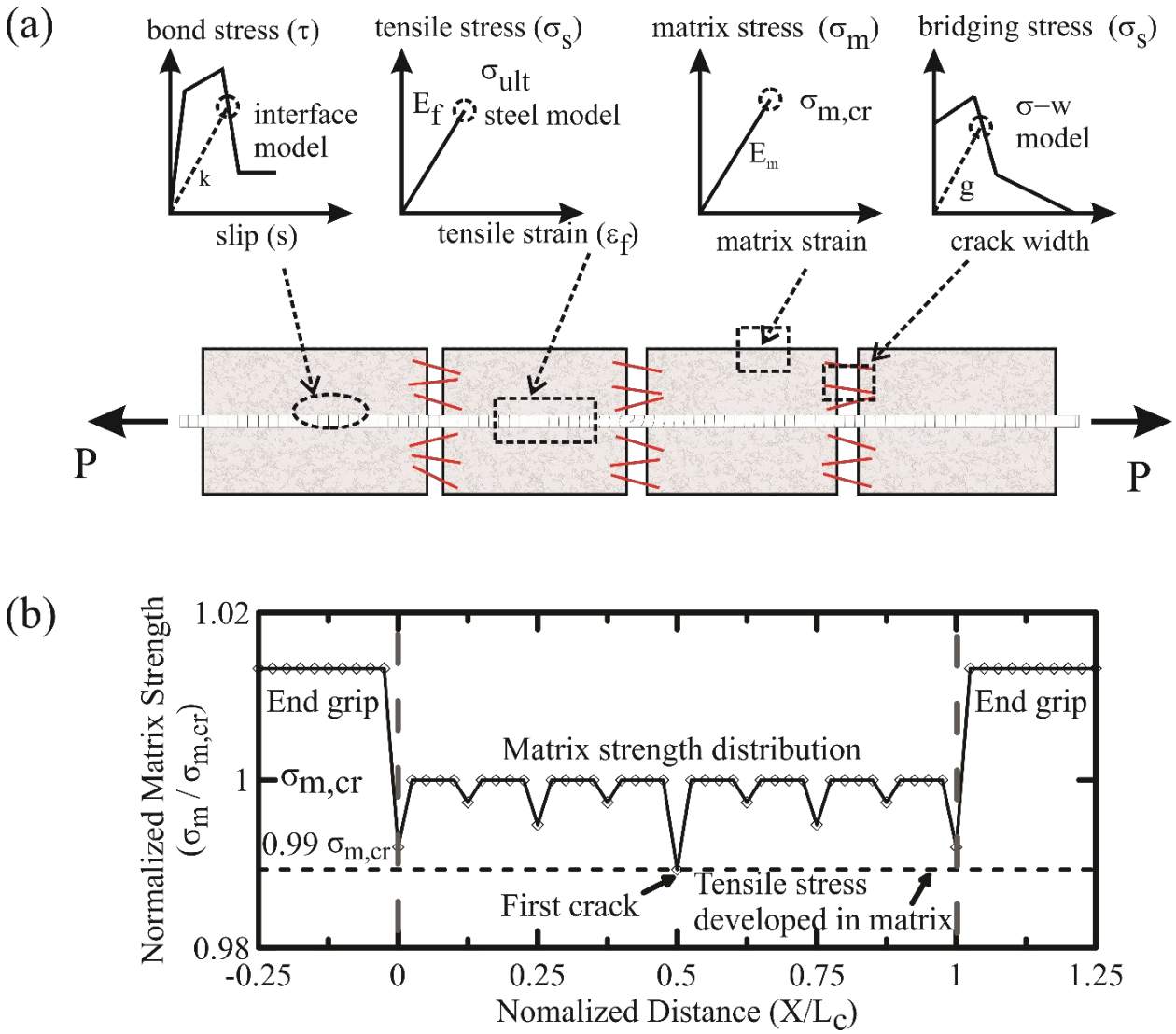

Figure 81. (a) Cracking Mechanisms Including Matrix Cracking, Fiber Bridging in Terms of Stress-Crack Width Relation, Interface Bonding Stress-Slip Model and Tensile Stress-Strain Relationship of Longitudinal Reinforcement; (b) Stress Distribution in Matrix at Cracked State.

References

[1] Folliard, Kevin, David Sutfin, Ryan A Turner, and David P. Whitney. 2006. “Fiber in Continuously Reinforced Concrete Pavements.” Texas Department of Transportation.

[2] Kosaka, Takashi, Yoshifumi Nishiumi, Toshimichi Ichinomiya, and Kimio Saito. 2019. Development and serviceability of a highway bridge deck using ultra-high performance fiber-reinforced concrete.” Civil Engineering Design 1 (2019) 54–63. https://doi.org/10.1002/cend.201900002.

[3] Hasani, Mahmoud, Fereidoon Moghadas Nejad, Jafar Sobhani, and Mahdi Chini. 2020. “Mechanical and durability properties of fiber reinforced concrete overlay: Experimental results and numerical simulation.” Construction and Building Materials 268 (2021). https://doi.org/10.1016/j.conbuildmat.2020.121083.

[4] Roesler, Jeffery R., Amanda Bordelon, Alexander S. Brand, Armen N. Amerkhanian. 2018. “Fiber Reinforced Concrete for Pavement and Overlays.” Federal Highway Administration National Concrete Consortium.

[5] Isla, F., B. Luccioni, G. Ruano, M.C. Torrijos, F. Morea, G. Giaccio, R. Zerbino. 2015. “Mechanical response of fiber reinforced concrete overlays over asphalt concrete substrate: Experimental results and numerical simulation.” Construction and Building Materials 93 (2015) 1022–1033. https://doi.org/10.1016/j.conbuildmat.2015.05.050.

[6] Concrete industrial ground floors : a guide to design and construction, The Concrete Society, 2016.

[7] A.B. Folorunsho, S. Kim, C. Park, A Review on the Performance of Fibers on Restrained Plastic Shrinkage Cracks, Buildings 14 (2024). https://doi.org/10.3390/buildings14082477.

[8] 3-D Micromechanical Damage Models, Fiber Pullout Models and Fracture Toughness of Discontinuous Steel Fiber Reinforced Cementitious Composites, 2008.

[9] Mechanistic-Empirical Pavement Design Guide - A Manual of Practice (2nd Edition), American Association of State Highway and Transportation Officials (AASHTO), 2015.

[10] 2024 AASHTOWare Pavement ME Design (PMED) , (n.d.). https://me-design.com/MEDesign/ (accessed May 4, 2025).

[11] D. Timm, W. Barrett, Analysis of The 2002 Design Guide of Rigid Pavement (ALDOT Project 930-554), (2005).

[12] Y. Chen, R.L. Lytton, Development of a New Faulting Model in Jointed Concrete Pavement using LTPP Data, Transp Res Rec 2673 (2019) 407–417. https://doi.org/10.1177/0361198119838988.

[13] P. Taylor, Concrete Pavement Distress Assessments and Solutions: Identification, Causes, Prevention & Repair (NCPTC), 2018. http://www.cptechcenter.org/.

[14] E. J. Yoder, M. W. Witczak, Principles of Pavement Design, 2nd Edition, 1991.

[15]A. Celik Ozyildirim, Standard Title Page-Report on Federally Funded Project Title and Subtitle 5. Report Date High-Performance Fiber-Reinforced Concrete in a Bridge Deck December 2005 6. Performing Organization Code, 2000.

[16]ACI. Committee, 544.4R-18: Guide for Design with Fiber-Reinforced Concrete, n.d.

[17]C. Reinforcing Steel Institute, CONTINUOUSLY REINFORCED CONCRETE PAVEMENT MANUAL Guidelines for Design, Construction, Maintenance, and Rehabilitation, 2016.

[18]J. Eggers, P.E.T. Rupnow, C. Abadie, Flexural Strength and Fatigue of Steel Fiber Reinforced Concrete (SFRC) (2004 Hale Boggs Deck), n.d. www.ltrc.lsu.edu.

[19]S.J. Stephen, R. Gettu, Fatigue fracture of fibre reinforced concrete in flexure, Materials and Structures/Materiaux et Constructions 53 (2020). https://doi.org/10.1617/s11527-020-01488-7.

[20]S. Cho, A.C. Bordelon, M.O. Kim, Effects of Macro Fibers on Crack Opening Reduction in Fiber Reinforced Concrete Overlays, Polymers (Basel) 16 (2024). https://doi.org/10.3390/polym16162282.

[21]C. Pleesudjai, C.A.S. Oliveira, D.L. Araujo, D. Patel, M.A.S. de Andrade, R.T. Filho, B. Mobasher, Efficiency of hybrid reinforced concrete beams with low reinforcement ratios, Mater Struct 58 (2025) 218. https://doi.org/10.1617/s11527-025-02736-4.

[22]fib - federation internationale du beton, fib Model code for concrete structures 2010, Ernst & Sohn (2013).

[23]M.A. Mooney, H. Zheng, C.J. Naito, S.E. Quiel, J. Ouyang, J. Wisniewski, Precast Concrete Segmental Liners for Large Diameter Road Tunnels-Laboratory Testing, n.d.

[24]A. Akkari, Evaluation of a Polyvinyl Alcohol Fiber Reinforced Engineered Cementitious Composite for a Thin-Bonded Pavement Overlay, 2011. http://www.lrrb.org/pdf/201111.pdf.

[25]A. Harapin, M. Jurišić, N. Bebek, M. Sunara, Long-Term Effects in Structures: Background and Recent Developments, Applied Sciences (Switzerland) 14 (2024). https://doi.org/10.3390/app14062352.

[26]M. Bakhshi, Characterization and Modeling of Moisture Flow through hydrating Cement- Based Materials under Early-Age Drying and Shrinkage Conditions, 2011.

[27]M. Bakhshi, B. Mobasher, Experimental observations of early-age drying of Portland cement paste under low-pressure conditions, Cem Concr Compos 33 (2011) 474–484. https://doi.org/10.1016/j.cemconcomp.2011.01.009.

[28]V. Gribniak, G. Kaklauskas, D. Bacinskas, W.P. Sung, A. Sokolov, D. Ulbinas, Investigation of shrinkage of concrete mixtures used for bridge construction in Lithuania, Baltic Journal of Road and Bridge Engineering 6 (2011) 77–83. https://doi.org/10.3846/bjrbe.2011.10.

[29]M. Bakhshi, B. Mobasher, M. Zenouzi, Model for Early-Age Rate of Evaporation of Cement-Based Materials, J Eng Mech 138 (2012) 1372–1380. https://doi.org/10.1061/(ASCE)EM.1943-7889.0000435.

[30]T. Rahmani, B. Kiani, M. Bakhshi, M. Shekarchizadeh, Application of Different Fibers to Reduce Plastic Shrinkage Cracking of Concrete, in: 2012: pp. 635–642. https://doi.org/10.1007/978-94-007-4566-7_62.

[31]N. Concrete Pavement Technology Center, Fiber-Reinforced Concrete for Pavement Overlays: Technical Overview Final Report Sponsored by Federal Highway Administration Technology Transfer Concrete Consortium (TTCC) Pooled Fund TPF-5(313) (Part of Intrans Project 15-532), 2019. www.intrans.iastate.edu.

[32]S.K. Nayar, R. Gettu, Mechanistic-empirical design of fibre reinforced concrete (FRC) pavements using inelastic analysis, (2046). https://doi.org/10.1007/s12046-019-1255-1S.

[33]P. By, J. Roesler, A. Bordelon, M. Beyer, D. Wang, DESIGN AND CONCRETE MATERIAL REQUIREMENTS FOR ULTRA-THIN WHITETOPPING Design and Concrete Material Requirements for Ultra-Thin Whitetopping Illinois Center for Transportation, (2008).

[34]B. Belletti, R. Cerioni, A. Meda, G. Plizzari, Design Aspects on Steel Fiber-Reinforced Concrete Pavements, (n.d.). https://doi.org/10.1061/ASCE0899-1561200820:9599.

[35]AASHTO Guide: Design of Pavement Structures, (1993).

[36]ADOT, ARIZONA DEPARTMENT OF TRANSPORTATION PAVEMENT DESIGN MANUAL, 2017.

[37]H.M. Westergaard, Stresses in concrete pavements computed by theoretical analysis, Public Roads (1926).

[38]G.G. Meyerhof, Load-carrying capacity of concrete pavements, Journal of the Soil Mechanics and Foundations Division 88 (1962) 89–116.

[39]M. Bakhshi, B. Mobasher, Experimental observations of early-age drying of Portland cement paste under low-pressure conditions, Cem Concr Compos 33 (2011) 474–484. https://doi.org/10.1016/j.cemconcomp.2011.01.009.

[40]C. Soranakom, B. Mobasher, Modeling of tension stiffening in reinforced cement composites: Part I. Theoretical modeling, Materials and Structures/Materiaux et Constructions 43 (2010) 1217–1230. https://doi.org/10.1617/s11527-010-9594-8.

[41]C. Soranakom, B. Mobasher, Correlation of tensile and flexural responses of strain softening and strain hardening cement composites, Cem Concr Compos 30 (2008) 465–477. https://doi.org/10.1016/j.cemconcomp.2008.01.007.

[42]X. Destrée, Y. Yao, B. Mobasher, Sequential Cracking and Their Openings in Steel-Fiber-Reinforced Joint-Free Concrete Slabs, Journal of Materials in Civil Engineering 28 (2016). https://doi.org/10.1061/(asce)mt.1943-5533.0001377.

[43]X. Destrée, Y. Yao, B. Mobasher, M. Asce, Sequential Cracking aTheir Openings in Steel-Fiber-Reinforced Joint-Free Concrete Slabs, 28 (2016) 1–11. https://doi.org/10.1061/(ASCE)MT.1943-5533.0001377.

[44]C. Pleesudjai, D.D. Patel, B. Mobasher, Generalized Nonlinear Moment-Curvature Model for Serviceability-Based Design of Hybrid Reinforced Concrete, Journal of Structural Engineering 149 (2023). https://doi.org/10.1061/JSENDH.STENG-12235.

[45]B. Mobasher, Y. Yao, C. Soranakom, Analytical solutions for flexural design of hybrid steel fiber reinforced concrete beams, Eng Struct 100 (2015) 164–177. https://doi.org/10.1016/j.engstruct.2015.06.006.

[46]A. Bentur, K. Kovler, Evaluation of early age cracking characteristics in cementitious systems, 2003.

[47]C. Soranakom, B. Mobasher, Geometrical and mechanical aspects of fabric bonding and pullout in cement composites, Materials and Structures/Materiaux et Constructions 42 (2009) 765–777. https://doi.org/10.1617/s11527-008-9422-6.

[48]C. Soranakom, B. Mobasher, Modeling of tension stiffening in reinforced cement composites: Part I. Theoretical modeling, Mater Struct 43 (2010) 1217–1230. https://doi.org/10.1617/s11527-010-9594-8.

[49]J. Veselý, V. Šmilauer, P. Pánek, Finite element analysis of concrete pavement subjected to thermal loading, 14th Conference of Civil and Environmental Engineering for PhD Students and Young Scientists: Young Scientist 2022 (Ys22) 2887 (2023) 020010. https://doi.org/10.1063/5.0158610.

[50]Y. Qin, J.E. Hiller, Modeling temperature distribution in rigid pavement slabs: Impact of air temperature, Construction and Building Materials 25 (2011) 3753–3761. https://doi.org/10.1016/j.conbuildmat.2011.04.015.

[51]S.C. Park, K.I. Lee, S.H. Baek, S.J. Kim, S.M. Kim, Behavior and Early-Age Performance of Continuously Reinforced Concrete Bus Pad, Materials 18 (2025) 1–28. https://doi.org/10.3390/ma18133143.

[52]M.Y. Darestani, D.P. Thambiratnam, D. Baweja, A. Nataatmadja, Dynamic Response of Concrete Pavements under Vehicular Loads, (2006) 59–66. https://doi.org/10.2749/222137806796169164.

[53]K. Folliard, D. Sutfin, R. Turner, D.P. Whitney, Fiber in Continuously Reinforced Concrete Pavements, n.d. www.ntis.gov.

[54]J. Roesler, A. Bordelon, M. Beyer, D. Wang, Design and Concrete Material Requirements for Ultra-Thin Whitetopping Illinois Center for Transportation, (2008).

[55]A. Celik Ozyildirim, High-Performance Fiber-Reinforced Concrete in a Bridge Deck, 2005.

[56]A.C. Birely, P. Park, J.A. Mcmahon, X. Shi, Y. Rew, SPR-705: Fiber-Reinforced Concrete for the Improved Performance of Transportation Infrastructure, 2018.

[57]K. Amini, P.E. Pavan Vaddey, F. Benjamin, P.E. Birch, P.E. David Corr, Fiber Reinforced Concrete for Bridge Deck Overlays, 2023. https://www.modot.org/research-publications.

[58]A. Sakulneya, C. Anderson, J. Castro-Perez, J. Roesler, Performance and Design of Continuously Reinforced Concrete Pavements, Rantoul, 2024. https://doi.org/10.36501/0197-9191/24-011.

[59]G. Griffiths, N. Thom, Concrete pavement design guidance notes, CRC Press, 2000.

[60]A. Committee, Design of slabs-on-ground, in: American Concrete Institute, 2010.

[61]G.G. Meyerhof, Bearing capacity of floating ice sheets, Transactions of the American Society of Civil Engineers 127 (1962) 524–557.

[62]P.K. Juhasz, P. Schaul, Design of Industrial Floors—TR34 and Finite Element Analysis (Part 2), J. Civ. Eng. Archit 13 (2019) 512–522.

[63]J. Roesler, G. Paulino, C. Gaedicke, A. Bordelon, K. Park, Fracture behavior of functionally graded concrete materials for rigid pavements, Transp Res Rec (2007) 40–49. https://doi.org/10.3141/2037-04.

[64]Fick Gary, Jerod Gross, Mark B. Snyder, Dale Harrington, Jeffery Roesler, Tom Cackler, Guide to Concrete Overlays, 2021. https://cptechcenter.org/.

[65]J. Roesler, A. Bordelon, A. Amirkhanian, P. Taylor, S. Tritsch, J. Gross, D. Harrington, Benefit and Application of Fiber Reinforcement in Concrete Pavement Acknowledgements TTCC/Fiber Reinforced Concrete OverlayProject Reinforced Concrete for Pavement Technical Advisory Committee National Concrete Consortium National Concrete Pavement Technology Center (Iowa State), n.d. http://www.cptechcenter.org/technical.

[66]S.A. Altoubat, J.R. Roesler, D.A. Lange, K.A. Rieder, Simplified method for concrete pavement design with discrete structural fibers, Construction and Building Materials 22 (2008) 384–393. https://doi.org/10.1016/j.conbuildmat.2006.08.008.

[67]J. Roesler, Effect of Macrofibers on Behavior and Performance of Concrete Slabs and Overlays, n.d.

[68]A. Bordelon, J. Roesler, Design with fiber reinforcement for thin concrete overlays bonded to asphalt, J Transp Eng 138 (2012) 430–435. https://doi.org/10.1061/(ASCE)TE.1943-5436.0000339.

[69]P. By, J. Roesler, A. Bordelon, M. Beyer, D. Wang, DESIGN AND CONCRETE MATERIAL REQUIREMENTS FOR ULTRA-THIN WHITETOPPING Design and Concrete Material Requirements for Ultra-Thin Whitetopping Illinois Center for Transportation, (2008).

[70]D. Patel, C. Pleesudjai, M. Bakhshi, V. Nasri, B. Mobasher, Back-calculation of mechanical properties of fiber-reinforced concrete in tunnel lining segments, Structural Concrete (2025). https://doi.org/10.1002/suco.70052.

[71]C. Soranakom, B. Mobasher, Closed-Form Moment-Curvature Expressions for Homogenized Fiber-Reinforced Concrete, ACI Mater J 104 (n.d.). https://doi.org/10.14359/18824.

[72]A.C. 544, ACI 544.8R-16: Report on Indirect Method to Obtain Stress-Strain Response of Fiber-Reinforced Concrete (FRC), (2016) 22.

[73]C. Pleesudjai, D. Patel, K.A.W. Gaona, M. Bakhshi, V. Nasri, B. Mobasher, Statistical Process Control of Fiber-Reinforced Concrete Precast Tunnel Segments, ACI Mater J 121 (2024). https://doi.org/10.14359/51740373.

[74]D. Patel, C. Pleesudjai, M. Bakhshi, V. Nasri, B. Mobasher, Back-calculation of mechanical properties of fiber-reinforced concrete in tunnel lining segments, Structural Concrete (2025). https://doi.org/10.1002/suco.70052.